APPLICATION OF IMAGE ENHANCEMENT ALGORITHMS TO IMPROVE THE VISIBILITY AND CLASSIFICATION OF MICROCALCIFICATIONS IN MAMMOGRAMS

A THESIS SUBMITTED TO
THE GRADUATE SCHOOL OF NATURAL AND APPLIED SCIENCES
OF
MIDDLE EAST TECHNICAL UNIVERSITY

BY

CANSU AKBAY

IN PARTIAL FULFILLMENT OF THE REQUIREMENTS
FOR
THE DEGREE OF MASTER OF SCIENCE
IN
BIOMEDICAL ENGINEERING

JANUARY 2015

Approval of the thesis:

APPLICATION OF IMAGE ENHANCEMENT ALGORITHMS TO IMPROVE THE VISIBILITY AND CLASSIFICATION OF MICROCALCIFICATIONS IN MAMMOGRAMS

submitted by **CANSU AKBAY** in partial fulfillment of the requirements for the degree of **Master of Science in Biomedical Engineering Department, Middle East Technical University** by,

Prof. Dr. Gülbin Dural Ünver
Dean, Graduate School of **Natural and Applied Sciences** _____

Prof. Dr. Hakan Işık Tarman
Head of Department, **Biomedical Engineering** _____

Prof. Dr. Nevzat Güneri Gençer
Supervisor, **Electrical and Electronics Eng. Dept., METU** _____

Dr. Gülay Gençer
Co-supervisor, **Radiology Dept., Dr Nafiz Köfez Sincan Devlet Hastanesi** _____

Examining Committee Members:

Prof. Dr. Gözde Bozdağı Akar
Electrical and Electonics Engineering Dept., METU _____

Prof. Dr. Nevzat Güneri Gençer
Biomedical Engineering Dept., METU _____

Assoc. Prof. Dr. Yeşim Doğrusöz Serinağaoğlu
Biomedical Engineering Dept., METU _____

Assoc. Prof. Dr. Ilkay Parnas Ulusoy
Biomedical Engineering Dept., METU _____

Assist. Prof. Dr. Fatih Kamışlı
Electrical and Electonics Engineering Dept., METU _____

Date: _____

I hereby declare that all information in this document has been obtained and presented in accordance with academic rules and ethical conduct. I also declare that, as required by these rules and conduct, I have fully cited and referenced all material and results that are not original to this work.

Name, Last Name: CANSU AKBAY

Signature :

ABSTRACT

APPLICATION OF IMAGE ENHANCEMENT ALGORITHMS TO IMPROVE THE VISIBILITY AND CLASSIFICATION OF MICROCALCIFICATIONS IN MAMMOGRAMS

Cansu Akbay,
M.S., Department of Biomedical Engineering
Supervisor : Prof. Dr. Nevzat Güneri Gençer
Co-Supervisor : Dr. Gülay Gençer

January 2015, 98 pages

Breast cancer is the second leading cause of cancer deaths for women. Mammography is the most effective technology presently available for breast cancer screening, despite the fact that there are still some limitations of the imaging technique, such as insufficient resolution, low local contrast and noise combined with the subtle nature of the usual radiographic findings. One of the most important radiographic findings associated to the existence of breast cancer is the clustered microcalcifications. Especially, it has been shown that some characteristics concerning the clustering parameters of microcalcifications are of great diagnostic value. However, the mentioned limitations of mammography make the detection and interpretation of microcalcifications a complicated task. The main purpose of this thesis is to develop Computer Aided Diagnosis (CAD) system in order to increase the efficiency of the mammographic screening process. The system may provide automated detection of microcalcification clusters leading a considerable decrease in misdiagnosis rates. To make microcalcifications more visible than their surrounding tissues, image enhancement on mammograms is required. There are many contrast enhancement algorithms that can be employed for the same purpose. However, by contrast enhancement it is expected to reduce overlap between tonal values that belongs to microcalcifications and their surrounding tissues instead of stretching the histogram of an image. The algorithms based on multiresolution analysis such as wavelet transform, contourlet

transform and the detail enhancement on local frequency algorithms are considered to achieve this purpose. In this study, these algorithms have been implemented on clinical data and their performances are compared by using quantitative methods and evaluated under supervision of radiologists. To observe the efficiency of enhancement on classification of microcalcification clusters, selected regions from original images and images enhanced by using 2 enhancement methods chosen by a radiologist are used. To classify microcalcification clusters as benign and suspicious, features are extracted by using texture analysis. For classification the Support Vector Machine (SVM) is employed. As a result, best classification is obtained by features obtained from Gabor filter banks and enhanced images with a detail enhancement method with using mean and standart deviation by 77 % truth rate .(the area under the ROC curve is 0.81) .

Keywords: Computer aided diagnosis, microcalcification clusters, image enhancement, detail enhancement, multiresolution analysis, feature extraction, Support Vector Machine

ÖZ

MİKROKALSİFİKASYON KÜMELERİNİN MAMOGRAFİ GÖRÜNTÜLERİ ÜZERİNDE GÖRÜNÜRLÜĞÜNÜN ARTTIRILMASI VE SINIFLANDIRILMASI İÇİN GÖRÜNTÜ İŞLEME ALGORİTMALARININ UYGULANMASI

Cansu Akbay,
Yüksek Lisans, Biyomedikal Mühendisliği Bölümü
Tez Yöneticisi : Prof. Dr. Nevzat Güneri Gençer
Ortak Tez Yöneticisi : Dr. Gülay Gençer

Ocak 2015 , 98 sayfa

Meme kanseri, kadınlarda akciğer kanserinden sonra en çok ölümle sonuçlanan ikinci kanser türüdür. Günümüzde meme kanserinin teşhisinde en etkin görüntüleme yöntemi mamografidir. Yetersiz çözünürlük, düşük sınırlı kontrast ve ihmal edilemeyecek boyutta gürültü gibi kısıtlamaların olması tanı koymada mamografinin etkinliğini azaltmaktadır. Meme kanserinin varlığının saptanmasına yönelik en önemli radyolojik bulgulardan birisi, kümelenmiş mikrokalsifikasyonlardır. Mamografide bahsi geçen kısıtlamalar, mikrokalsifikasyonların tespit edilmesi ve yorumlanması açısından sorun oluşturmaktadır. Tezin temel amacı, bilgisayar destekli tanı sistemi geliştirerek, mamografik görüntüleme işleminin etkinliğini arttırmaktır. Sistem, mikrokalsifikasyon kümelerinin otomatik olarak belirlenmesiyle, yanlış tanı oranında önemli azalmayı sağlayabilir. Mikrokalsifikasyonların, etraflarındaki dokulara göre daha görünür hale gelmesi için, mamografi görüntüleri üzerinde görüntü iyileştirme yapılması gereklidir. Bu amaçla bir çok kontrast iyileştirme algoritması vardır. Ancak, kontrast iyileştirme yöntemleriyle, görüntüye ait histogramın genişletilmesi yerine mikrokalsifikasyonlara ait gri seviye değerleri ile etrafındaki dokulara ait gri seviye değerleri arasındaki çakışma azaltılmaktır. Bu çalışmada, bu amacı sağlayan algoritmalar klinik veriler üzerine uygulanmış ve performansları yeni nicel yöntemler kullanılarak karşılaştırılmıştır, aynı zamanda radyologlar tarafından değerlendirilmiştir. Yapı-

lan görüntü iyileştirmenin mikrokalsikasyon kümelerinin sınıflandırılmasında etkisini gözlemlemek amacıyla orjinal görüntüler ve radyolog tarafından seçilen 2 methot ile iyileştirilen görüntüler kulllanılmıştır. Mikrokalsifikasyon kümelerinin 'iyi huylu' ve 'şüpheli' olarak sınıflandırılması için, doku analizi ile özellik çıkarımı gerçekleştirilmiştir. Sınıflandırma için destek vektör makinesi (DVM) kullanılmıştır. Sonuç olarak ortalama ve standartma sapma kullanılarak yapılan detay iyileştirme metodundan elde edilen görüntülere Gabor filtrelerinin uygulanmasıyla elde edilen özniteliklerin, diğer özniteliklere göre sınıflandırma için daha iyi performans gösterdiği gözlemlenmiştir. Gabor filterinden elde edilen özniteliklere DVM uygulanmasıyla mikrokalsikasyon kümeleri yüzde 77 doğruluk oranıyla iyi huylu ve kötü huylu olarak sınıflandırılmıştır (ROC'un altında kalan alan 0.81 olarak bulunmuştur.).

Anahtar Kelimeler: Bilgisayar destekli tanı, mikrokalsifikasyon kümeleri, görüntü iyileştirme, detay iyileştirme, çoklu çözünürlük analizi, öznitelik çıkarma, destek vektör makinesi

To those who suffered from breast cancer

ACKNOWLEDGMENTS

To begin with, I would like to express my sincere thanks to my supervisor Prof. Nevzat Güneri Gençer for his guidance and for his effort to motivate me thought my study. I would like to thank Dr. Gülay Gençer, who is the originator of this thesis, for a chance to introduce me the world of radiology and her time devoted me.

Further, I wish to thank to Prof. Dr. Gözde Bozdağı Akar and Assoc. Prof. Dr. Ilkay Parnas Ulusoy for their recommendations and helps. I also express my sincere thanks to Arif Ergün Turan and Muhammed Yeşilkaya for sharing their knowledge with me.

I would like to thank all doctors and clinical stuffs of mammography department of Yıldırım Beyazıt Eğitim ve Araştırma Hastanesi and radiology department of Dr Nafiz Körez Sincan Devlet Hastanesi for availability to study with real clinical data.

I am greatful to my lab mates Reyhan Zengin, Mürsel Karadaş, Damla Alptekin, Mahsa Keykhali and Azadeh Kamali and my special group of friends Ekin Kantar, Gülce Bal, Öykü Çobanoğlu, Ferah Çoğun and others for their supports whenever I needed in many numerous ways.

Last but not least, I am indebted to my family, especially my brother Can, for their endless love, patience and encouragement thought the thesis.

TABLE OF CONTENTS

LIST OF TABLES

TABLES

LIST OF FIGURES

FIGURES

LIST OF ABBREVIATIONS

AMBE	Absolute Mean Brightness Error
AMHE	Adaptively Modified Histogram Equalization
BI-RADS	Breast Imaging Reporting and Data System
BTH	Black Top Hat Transformation
CAD	Computer Aided Diagnosis
CC	Cranio Caudal
CDF	Cumulative Density Function
CLAHE	Contrast Limited Adaptively Histogram Equalization
CT	Contourlet Transform
DCIS	Ductal Carcinoma in situ
DDSM	Digital Database for Screening Mammography
DFB	Directional Filter Bank
DFT	Discrete Fourier Transform
DICOM	Digital Imaging and Communications in Medicine
DSM	Distribution Separation Measure
DWT	Discrete Wavelet Transform
EME	Measure of Enhancement
FDA	Food and Drug Administration
FLDA	Fisher Linear Discriminant Analysis
FOS	First Order Statistics
GA	Genetic Algorithm
GLCM	Gray level Co-occurrence matrix
GRNN	General Regression Neural Network
HE	Histogram Equalization
HM	Histogram Modification
IR	Infrared
LP	Laplacian Pyramid
MATLAB	Matrix Laboratory

MCs	Microcalcifications
MIAS	Mammography Image Analysis Society
MIL	Multi Intance Learning
MLO	Medio Lateral Oblique
MRI	Magnetic Resonance Imaging
MSE	Mean Square Error
NN	Neural Networks
NSCT	NonSubsampled Contourlet Transform
NSDFB	NonSubsampled Directional Filter Bank
PCA	Principal Component Analysis
PDF	Probability Density Function
PDFB	Pyramidal Directional Filter Bank
PGM	Portable Gray Map
PSNR	Peak-Signal-to-Noise Ratio
QMFs	Quadrature Mirror Filters
RBF	Radial Basis Function
ROC	Receiving Operational Curve
ROI	Region of Interest
SFS	Sequential Forward Search
SNR	Signal-to-Noise Ratio
SSIM	Structural Similarity Image Quality Index
TBC	Target to Background Contrast Enhancement Measure
TBCE	Target to Background Contrast Enhancement Measure Based on Entropy
THT	Top Hot Transformation
UIQI	Universal Image Quality Index
US	Ultrasound
WTH	White Top Hat Transformation

CHAPTER 1

INTRODUCTION

Breast cancer is a cancer type which developed in breast tissue. Early diagnosis of breast cancer is important for its treatment. Breast cancer can be explored by self examination, clinical breast examination and breast screening via medical imaging such as mammography, ultrasound (US), magnetic resonance imaging (MRI), and scintimammography. Among these imaging techniques, mammography is more crucial to diagnose breast cancer in the early stages. However there are limitations of mammography to detect abnormalities related to breast cancer. These limitations are mainly due to low contrast in the mammogram images, i.e., the small differences between X ray attenuation of normal and cancerous tissues, in dense breasts.

1.1 Scope of the Thesis

The main goal of this thesis is to develop a Computer Aided Diagnosis (CAD) software to make microcalcification clusters more identifiable on mammogram images and to generate features used to classify benign and suspicious clusters of microcalcifications. For this purpose, several image enhancement algorithms on both spatial domain (histogram modeling, morphological operators) and frequency domain (detail enhancement based on frequency, multiresoltion analysis etc.) are implemented on region of interest (ROI) of real mammogram images which include microcalcification clusters. To evaluate the performance of the enhancement algorithms, quantitative measures are implemented and assessment of radiologists is considered. According to assessment of the radiologist, 2 suitable enhancement methods are chosen to ob-

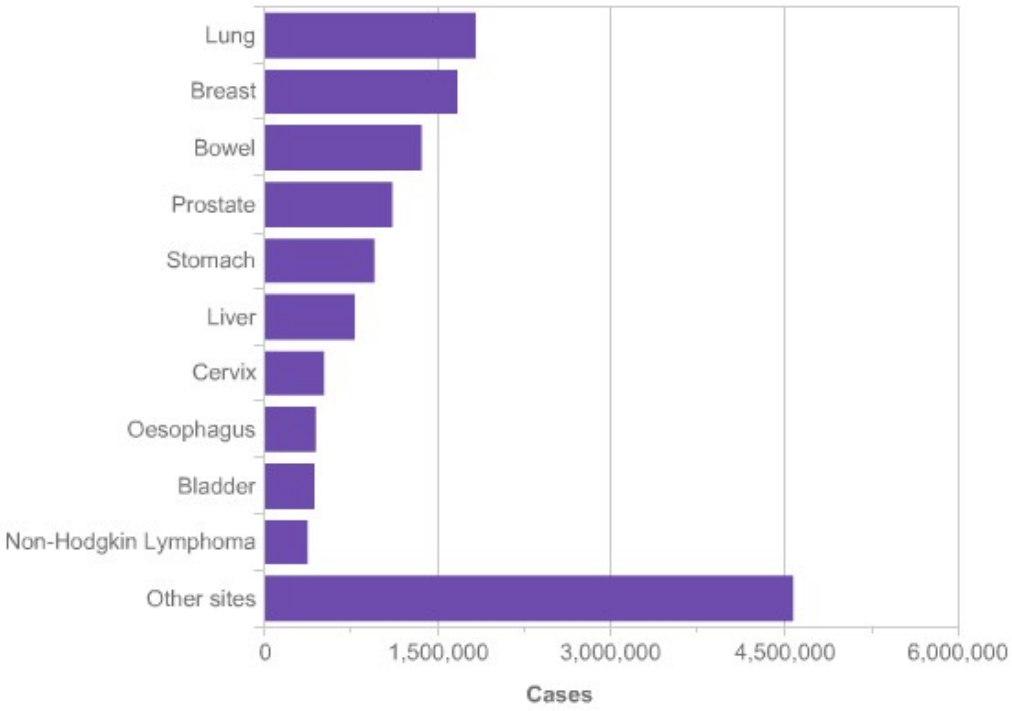

Figure 1.1: The 10 Most Commonly Diagnosed Cancers, World, 2012 Estimates [2]

serve efficiency of enhancement on classification .

Feature extraction is applied to depict properties of microcalcification clusters for classification. In this thesis, features are extracted from texture.

Following feature extraction, a classification process is employed and performance of the classification algorithm is evaluated. To decide which features best describe microcalcifications as benign or suspicious, necessary proceedings are applied.

Finally the results of CAD is compared with the existing biopsy reports that belong to patients whose mammogram images are used in thesis.

All applications are implemented on MATLAB.

There are a number of studies in the literature which aimed to develop CAD for detection and classification of microcalcifications. They are mentioned in section 2.5. Apart from these studies, it is considered that mammogram images are similar to the infrared (IR) images according to their gray levels and visual appearance. The contrast and detail enhancement methods used for the IR images are applied on real

mammogram images obtained from radiology departments of hospitals and radiological diagnosis is compared with the pathological diagnosis.

1.2 Databases Used in Thesis

List of databases used in CAD studies are given Table 1.1. Among these databases Digital Databases Screening Mammography (DDSM) and Mini-MIAS (Mammographic Image Analysis Society) are available on websites in [11] and [12].

Table 1.1: List of Databases for used in several CAD Studies [1]

Mammographic Image Analysis Society (MIAS)	An organization of UK research groups which has generated a digital mammogram database. The database contains 322 digitized films and includes radiologist opinions about locations of any abnormalities and their classification (malignant or not).
Washington University Digital Mammography Database	This database contains digitally acquired images of proven breast pathology. Each case consists of a single scout image of a breast lesion obtained during the course of stereotactic core needle biopsy. Cases are organized according to lesion histopathology.
Digital Database for Screening Mammography (DDSM)	Database produced as a collaboration between the Massachusetts General Hospital, the Sandia National Laboratories, and the University of South Florida Computer Science and Engineering Department. The database contains approximately 2,500 studies. Images containing suspicious areas have associated information about locations and types of suspicious region.
Nijmegen Digital Mammogram Database	Database is composed of 40 images provided by the Department of Radiology, University Hospital Nijmegen. All mammograms show one or more microcalcification clusters.
UCSF/LLNL Digital Mammogram Library	Database consists of a 12-volume CD library of digitized mammograms featuring microcalcifications. It was developed by Lawrence Livermore National Laboratories (LLNL) and the University of California at San Fransisco (UCSF) Radiology Department.

DDSM consists of digitalized film screen mammograms that belong to 2620 patients. There are 4 views (right MLO, left MLO, right CC, left CC) for each patient. DDSM includes ground truth and other information such as, age of the patient, digitalization information, etc. It has been prepared for the researchers in the CAD field. To access these database, a permission is required and to read the images, special software tools are used [13].

Mini-MIAS database consists of 322 digitalized mammogram images in MLO (Media

Lateral Oblique). Size of these images is 1024×1024 pixels. The format of images is '.pgm', they are 8 bit grayscale images. Images are labeled as B (benign) and M (malignant) acording to the radiological findings by the experts. Information about lesions such as mass are also available. 33 images which include calcifications from mini-MIAS data set are used in this thesis for an experiment.

In this thesis 70 CR images obtained from the radiology department of Yıldırım Beyazıt Eğitim ve Araştırma Hastanesi and 8 CR images obtained from Radiology department of Sincan Devlet Hastanesi are used. All images are in DICOM format and 16 bit gray scale images. Totaly 70 regions are selected for processing.

1.3 Thesis Organization

This thesis consists of 7 chapters. It is organized as follows :

In chapter 2, brief information about breast cancer is provided. The abnormalities that can be visible on mammograms, advantages and limitations of mammography to detect breast cancer are discussed. Definition of computer aided diagnosis and benefits of using it for breast cancer diagnosis are discussed.

Chapter 3 deals with the existing image enhancement methods that needs for making microcalcifications more visible compared to their surrounding tissues. The methods chosen for this purpose are explained and the results of their implementations are given.

Chapter 4 intends to give quantitative image enhancement performance measures. The results for the chosen enhancement method are shown.

Chapter 5, the methods used for feature extraction, dimension reduction of feature vector, classification with Support Vector Machines(SVM) are presented.

Chapter 6 consists of the results of classification with SVM by using different types of features.

Chapter 7 consists of the conclusion of this study and presents prospective future works.

CHAPTER 2

BACKGROUND

2.1 Mammography

Mammography is a special type of X ray imaging for breast that uses low amplitude and high current X ray . The breast is compressed between two plates.The bottom plate is film plate and the upper plate is subjected to X ray source. Figure 2.1 illustrates basis part of typical mammography device and screening of right breast.

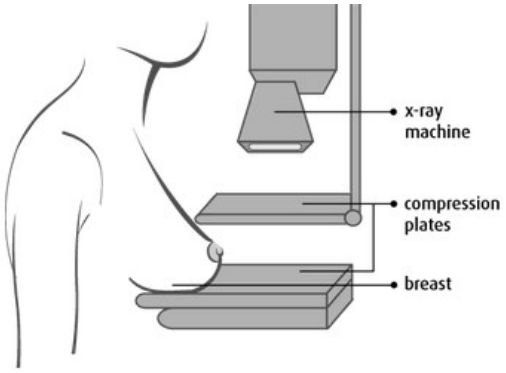

Figure 2.1: Mammography Screening [3]

There are two mammographic views according to position of plates and angle of X ray:medio lateral oblique (MLO) and cranio caudal(CC). In the CC view, the breast is compressed from the top to the bottom. X ray tube is located on the top. In the MLO view, the breast compressed between plates with an angle (standard angle is 90 degree).

Quality of a medical image is important for efficiency of diagnosis. In mammography, it is important to catch small details like microcalcifications, which may be first sign of the breast cancer. To identify them, images with a high spatial resolution is necessary. As the difference between X-ray attenuation of normal and cancerous tissues are quite small, it is difficult to detect microcalcification clusters in some cases. The breasts of younger woman contains more glands and ligaments resulting in dense breast tissue. In heterogeneously dense breast, it is difficult to detect cancerous tissue on mammogram, since the fibrograndular tissue may hide the abnormalities. With aging, the breast tissue become fattier and has fewer glands. In this case, it is more easier to detect cancer related tissues on mammogram images.

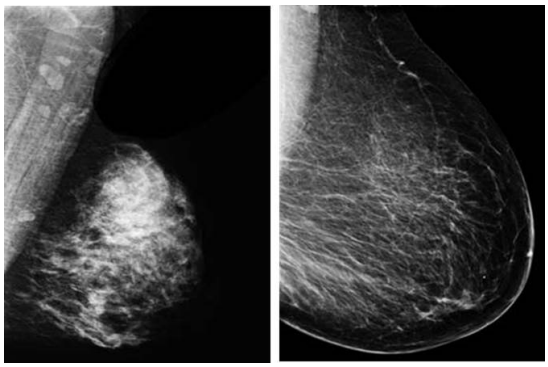

Figure 2.2: Left:Heteregenously dense breast tissue Right:Fatty breast Tissue

2.2 Important Findings in Mammography

Important findings for breast cancer are listed below:([14])

a-) Masses
b) Calcifications
c-) Architectural Distortion
d-) Asymmetries (asymmetry, global asymmetry, focal asymmetry, developing asymmetry)
e-) Intramammary lymph node
f-) Skin lesion

g-) Solitary dilated duct

Among these abnormalities, intramammary lymph node, skin lesion and solitary dilated duct are rarely significant.

2.3 Breast Imaging Reporting and Data System (BI-RADS)

BI-RADS is a tool published by American College of Radiology to define mammogram findings and results.

Table 2.1: BI-RADS categories and their indications.

BI-RADS Category	
BI-RADS 0	Need additional image evaluation
BI-RADS 1	Normal
BI-RADS 2	Benign Findings
BI-RADS 3	Probably Benign Finding /Short Interval Follow-Up Suggested
BI-RADS 4	Suspicious Abnormality /Biopsy Should Be Considered
BI-RADS 5	Highly Suggestive of Malignancy - /Appropriate Action Should Be Taken
BI-RADS 6	Malignant diagnosis has already been done

2.4 Microcalcifications (MCs)

Calcifications are small calcium deposits. Although most of calcifications are benign, they can be earlier sign of the breast cancer. Non palpable ductal carcinoma in situ (DCIS) and infiltrating carcinoma are diagnosed based on microcalcification clusters. Microcalcifications that have higher probability of malignancy depends on their cluster distribution, size, shape and association with other abnormalities, such as mass and architectural distortion. In some cases they occur in the lesion (tumor or parenchymal distortion). If they are found suspicious by radiologist, generally biopsy is required.

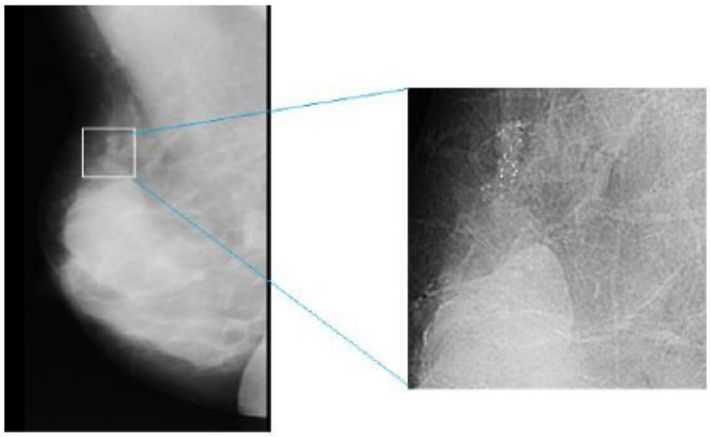

Figure 2.3: Mammogram image in MLO view and clustered microcalcification in ROI

Very coarse calcifications are often considered as benign. The more smaller calcifications are suspicious for malignancy. Most malignant microcalcifications are less than 0.5 mm. Pleomorphic, microcalcifications with irregular shape, linearly branching, punctate and amorphous calcifications tend to be malignant. Generally, 5 or more microcalcifications within 1 cm^2 area are suspicious. However, microcalcifications less than five in a group can be malignant rarely.

2.5 Computer Aided Diagnosis (CAD) for Microcalcifications

CAD is a computer based set of image processing and pattern recognition algorithms that provides information about existence of suspicious findings and/or their probability of being benign or malignant.

General CAD models for mammogram images starts with preprocessing step to obtain better visual appearance and make the interested regions more detectable. Preprocessing includes noise reduction or contrast enhancement. As the size of microcalcifications is small, it is difficult to distinguish them from noises. For microcalcification detection, noise reduction is not prepared if there is no significant noise.

As a second step of CAD, image segmentation algorithms are implemented. Local

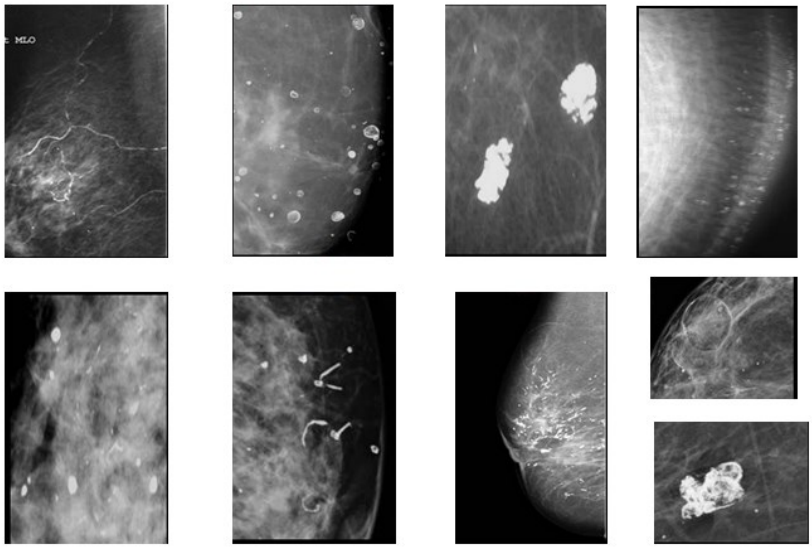

Figure 2.4: Mammography images of benign calcifications:(from left to right) vascular, lucent centered, popcorn, skin, round, suture, large-rod like, eggshell, dysthropic [4]

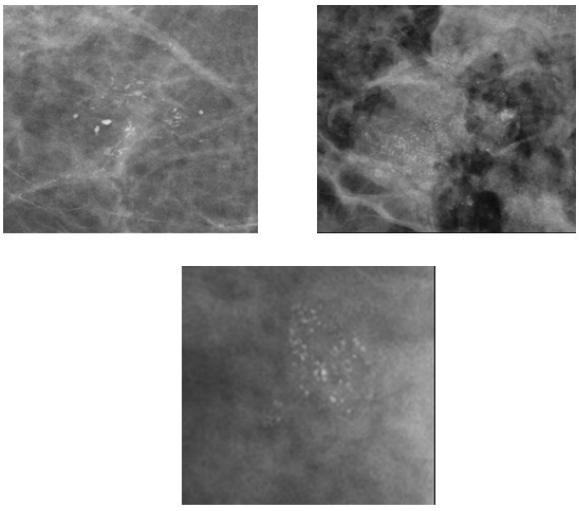

Figure 2.5: Mammography images of malignant calcifications: [4]

thresholding is a primitive segmentation method which works well if and only if the contrast between microcalcifications and other breast regions is quite high. Other common approach is region growing. Bankman et al proposed an active contours models for segmentation of microcalcifications [15]. Shanmugavadivu et al. developed a segmentation algorithm based on Grab Cut segmentation unified with k means clustering for segmentation of a lesion with microcalcifications [16]. Jumaat et al implemented several Snakes algorithms and compared them for boundary segmentation of microcalcifications [17]. Duarte et al. used mathematical morphology operators and Otsu's method for segmentation [18]. All studies mentioned for segmentation of microcalcifications are not a part of the CAD for microcalcification detection. They only aimed to provide detection of microcalcifications automatically. There is no segmentation stage in CAD developed in this thesis.

Feature extraction is the following step for detection and/or classification of MCs. For feature extraction, some of existing features are textural based features ([19]), wavelet or multiresolution based features [20], [21], shape related features([22]). Soltanian Zadeh et al used genetic algorithm (GA) to compare different types of texture features and impacts on classification of MCs. [23]

Final step for CAD is detection or classification of MCs. Studies ([24], [23], [25], [26], [27], [28], [21], [29], [30], [31], [32]) aimed to develop CAD for microcalcifications on mammogram are listed in Table 2.2. Used databases, number of data and feature types are various and affect the performance of the detection or/and classification.

To evaluate performance of detection or/and classification, the receiving operational curve (ROC) is used. A ROC curve is a plot of the true positive rate (sensitivity) versus true negative rate versus false positive rate (1-specificity). The true positive rate is the probability of successful diagnosis of all malignant microcalcifications. The false positive rate is the probability of diagnosis of benign microcalcifications as malignant. In CAD, ROC is used to compare the first diagnostic findings about illness obtained from imaging systems and final diagnosis after biopsy. ROC is used for evaluation of the performance of classification operations. The area under the ROC, A_z shows the performance of classification operation and the value of its changes

between 0 and 1. When it equals to 1, it means that the ideal classification is achieved. [33]

Desired CADx for this thesis is given Figure 2.6

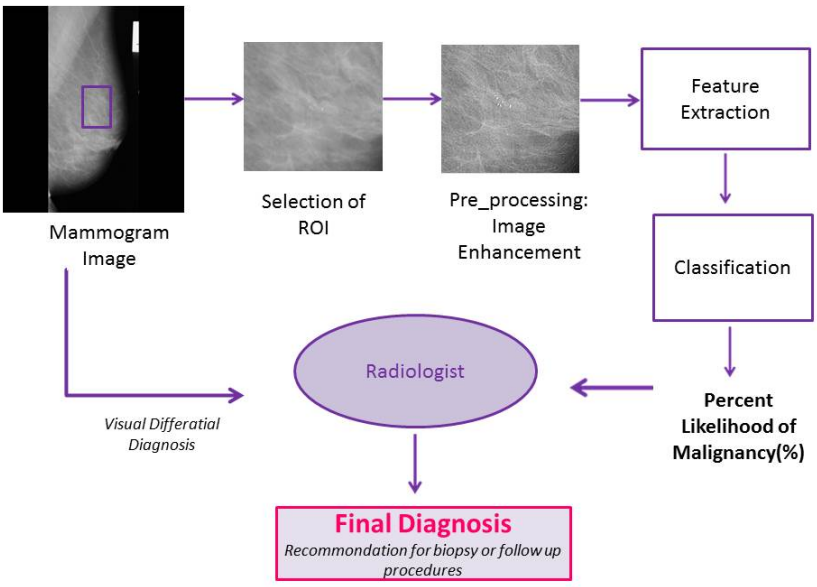

Figure 2.6: Schematic Distribution of a CAD System

Table 2.2: Previous CAD Studies for Detection / Classification Of Microcalcifications

Study	CAD	Method	Features	Database	# of samples	Az Value
H.K Fu et al (2005)	Detection& Classification	GRNN vs SVM	61 features (textural(44), spatial(15)& spectral domains(2)) After SFS , 11 features for SVM 25 features for GRNN	Nijmegen dataset	7531 features 6234 normal tissue 1117 MCs	0.98 for SVM 0.978 for GRNN
Zhang et al. (2012)	Detection	MIL	5 features Area, mean intensity, ecentricity, major axis length, degree	DDSM	40 MCa 990 normal	0.8618 Bag-KI_SVM
Nikita et al (2011)	Classification	SVM	23 features (top ranked features) BIRADS, GLCM	DDSM	1715 882 benign 833 malignant	0.82
Jasmine et al(2012)	Classification	SVM	100 features(after dimension reduction) NSCT _energy	Mini_MIAS	?	0.90
Soltanian Zadeh et al (2004)	Classification	Genetic algorithm	Multiwavelet /wavelet features Haralick features(GLCM) Shape features	Nijmegen database	103 MC cluster 29 bening 74 malignant	0.84-0.89
P.Kuş,İ.Karagöz (2013)	Detection	SVM	5 features Kurtosis, Skewness, Entropy, Energy	Mini_MIAS	57 ROI 21 malignant 11 benign 25 normal	0.94
Nayakama et al. (2004)	Classification	The Bayes Theorem	5 histological features	?	58 35 malignant 23 benign	0.96
Manoharan et al.(2010)	Classification	SVM	Jacobi Momments 'S' features	?	16 benign 19 malignant	0.84
Hadjiski (2006) Et al	Classification	Both LDA & SVM	64 GLCM 20 morphological 20 run length statistics(RLS) Average of 7 features for SVM	Specific data for them	175 51 malignat 124 benign	0.82+_0.03 for SVM 0.83±0.03 for LDA
Arikidis et al.(2006)	Detection& Classification	FLDA	Eigen image features in the wavelet domain(36 features)	DDSM	54 regions 46 malignat 8 benign	TP=0.69
Yu et al.(2006)	Classification	Back projection NN vs Bayesian Classifier	Wavelet coefficients & Markov Random Field	Mini_MIAS	20 images containing 25 areas of MCs	Sensitvity 0.92 Fp/image 0.75

CHAPTER 3

IMAGE ENHANCEMENT METHODS

The main idea of image enhancement is to provide better visual perception in a subjective way. The expectations from image enhancement are to eliminate noise, to enhance weak edges or features in an image while remaining strong edges or features. To make microcalcification clusters more visible than their surrounding tissues, image enhancement is required. The existing image enhancement methods considered for this purpose are shown in Figure 3.1 and the methods chosen for our study are discussed.

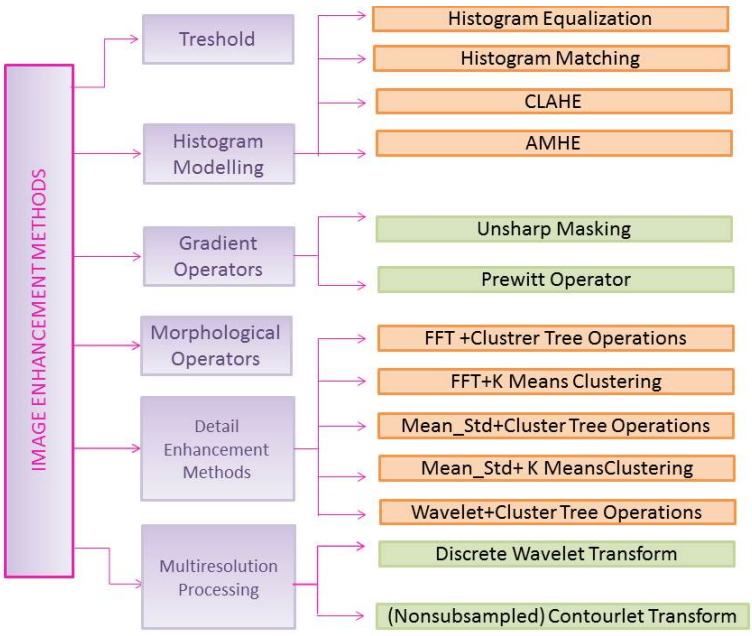

Figure 3.1: Distribution of some existing image enhancement methods

3.1 Thresholding

Thresholding is easy to implement in both spatial domain and frequency domain. It is applied accompanied by other image processing applications for different purposes. Image thresholding can be defined as a primitive image segmentation method. If the gray level intensity of the region of interest is separable from its background, image thresholding can be applied to segment and to obtain the preferred features. However, since mammography image has low contrast, it is difficult to identify gray levels that belong to pixels which represent microcalcifications. Another application of thresholding is noise attenuation. In both spatial domain and frequency domain, noises are detectable by thresholding. The values lower than the assigned threshold value T are considered as noise. The best example for using thresholding in noise attenuation is multilevel thresholding in the frequency domain [34].

$$g(x,y) = \begin{cases} 0, & f(x,y) \leq T \\ f(x,y), & f(x,y) \geq T \end{cases} \tag{3.1}$$

In this thesis, thresholding is used for image enhancement integrated with other image enhancement methods. Thresholding is also used in quality performance metrics explained in Chapter 4.

3.2 Histogram Modeling

Histogram of an image with gray levels in range [1 L-1] represents number of pixels for each gray level. By looking histogram of an image, information about contrast of an image and noise information (such as salt and pepper noise) are obtained. Contrast enhancement methods based on histogram modeling are implemented on spatial domain, so they have less computational cost compared to frequency domain applications. They provide high contrast image with a wide dynamic range of the intensity scale. In this section, contrast enhancement methods based on histogram modeling are discussed. Histogram modeling methods are not eligible for our study, since the frequency of gray levels that belongs to large objects and background become higher,

small details disappear.

3.2.1 Histogram Equalization

Histogram equalization [HE] is a nonlinear operation that makes the number of gray levels to reach approximately equal and obtain a uniform histogram. It provides an increase on dynamic range of gray levels. Local histogram equalization is more effective than global histogram equation. However, the drawback of local histogram equalization is the blocking effect.

Pixel frequency serves how many times a gray level is seen in the image and it is denoted as 'probability density function (pdf)'. The pdf is calculated by equation (3.2). In this equation p_k denotes how many times a gray level k is seen in an image with depth m, and p denotes the total number of pixels in the image.

$$pdf(k)\frac{p_k}{p}, 0 \leqslant k \leqslant 2^m - 1 \tag{3.2}$$

Histogram equalization uses a transform function k' to make the probability of each pixel value same.

$$cdf(k) = \sum_{i=1}^{k} pdf(k) \tag{3.3}$$

$$k' = (2^n - 1)cdf(k) \tag{3.4}$$

where cdf denotes the cumulative density function. In some cases histogram equalization brings about over increase on dynamic range that causes unnatural appearance and visual artifacts occur [35].

3.2.2 Histogram Matching

Histogram matching is another histogram based contrast enhancement method which maps gray levels of original image into desirable level. Each gray intensity value of input image is denoted by k and those of the desirable output image denotes by z. Histogram matching is processed by the following steps [36]:

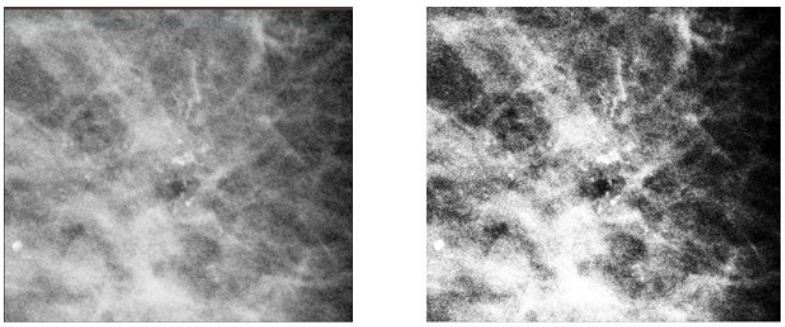

Figure 3.2: Contrast Enhancement by Using Histogram Equalization:(a) A ROI of DICOM Image,(b) Result of enhancement with HE

- Probability density function (pdf) and cumulative density function (cdf) of the input image is calculated to define a transform function T:

$$pdf_{input}(k) = \frac{p_k}{p}, 0 \leqslant k \leqslant 2^m - 1 \tag{3.5}$$

$$cdf_{input}(k) = \sum_{i=1}^{k} pdf(k), 0 \leqslant k \leqslant 2^m - 1 \tag{3.6}$$

- The transformation function T for the input image is calculated by using the cdf of the input images:

$$T(k) = (2^{m-1} cdf_{input}(k)) \tag{3.7}$$

- pdf and cdf is calculated for the desirable intensity values of the output image:

$$pdf_{output}(z) = \frac{p_z}{p}, 0 \leqslant z \leqslant 2^n - 1 \tag{3.8}$$

$$cdf_{output}(k) = \sum_{i=1}^{z} pdf(k), 0 \leqslant z \leqslant 2^n - 1 \tag{3.9}$$

- The transformation function G for the input image is calculated by using the cdf of input images:

$$G(z) = (2^{n-1} cdf_{output}(z)) \tag{3.10}$$

- Finally, to obtain the output image, inverse transform of G function is applied on transform function T.

$$z = G^{'}(T(k)) \tag{3.11}$$

Figure 3.3 shows implementation of histogram matching on interested region of image mdb219 from mini-MIAS database. The brightness of the output image is quite high that may cause a loss in clinical findings.

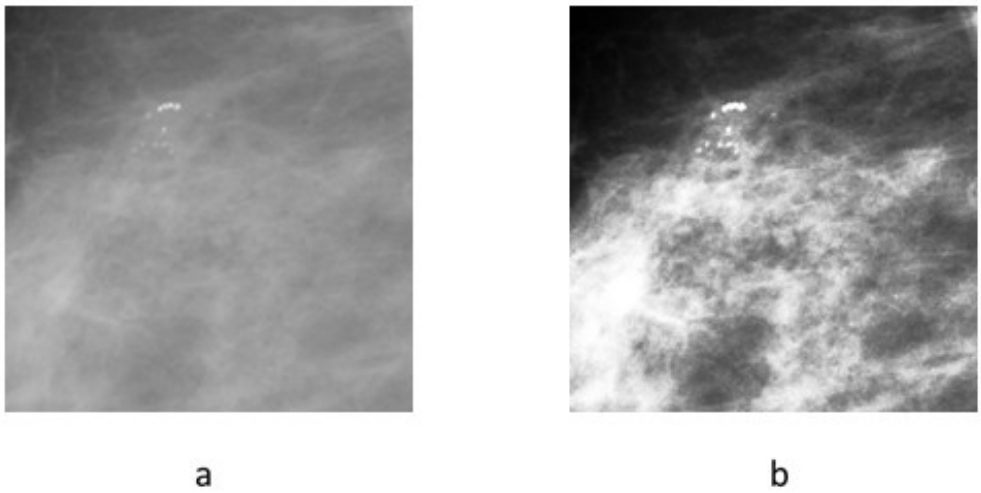

Figure 3.3: Contrast Enhancement by Using HM:(a) A ROI of MIAS Image mdb219, (b) Result of enhancement with AM.

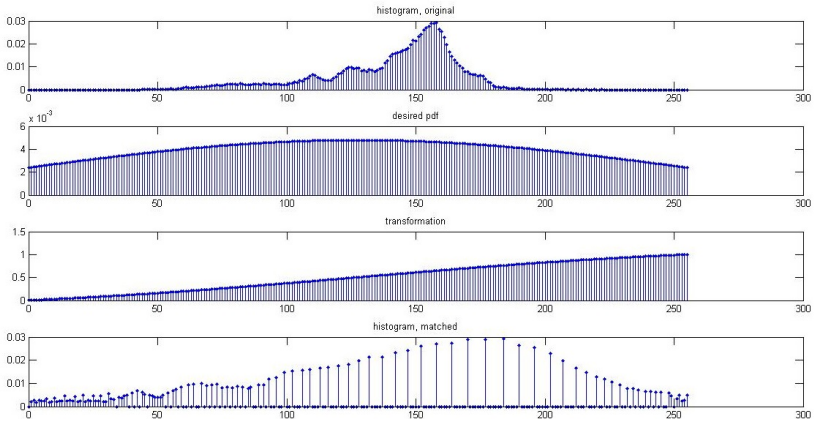

Figure 3.4: Contrast Enhancement by Using HM:(a) Histogram of a ROI of MIAS Image mdb219. (b) Desired gray level density distribution. (c) Gray level distribution of the transform function. (d) Histogram of enhanced image by HM.

3.2.3 Adaptively Modified Histogram Equalization

Adaptively Modified Histogram Equalization (AMHE) is based on modification of pdf before equalization of histogram [5].

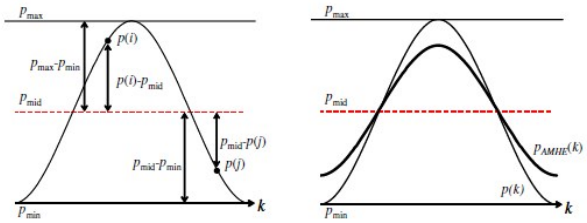

Figure 3.5: Left:Original PDF, Right:Modified PDF [5].

$$pdf_{AMHE}(k) = \begin{cases} pdf_{mid} + \alpha \frac{(pdf(k) - pdf_{mid})^2}{pdf_{max} - pdf_{mid}}, & pdf(k) > pdf_{mid} \\ pdf_{mid} + \alpha \frac{(pdf_{mid} - pdf(k))^2}{pdf_{mid} - pdf_{min}}, & \text{Otherwise} \end{cases} \tag{3.12}$$

where pdf_{mid} is the average of the maximum pdf value pdf_{max} and minimum pdf value pdf_{min} and α is the contrast enhancement rate. Calculation of α is follows:

- The image is divided into 2 sub images:upper and lower according to pdf
- The brightness of each sub images (X_{up} and X_{low}) are calculated:

$$X_{low} = \frac{\sum_{k=0}^{X_m} kpdf(k)}{\sum_{X_m+1}^{L-1} pdf(k)} \tag{3.13}$$

$$X_{up} = \frac{\sum_{X_m+1}^{L-1} kpdf(k)}{\sum_{X_m+1}^{L-1} pdf(k)} \tag{3.14}$$

  whereX_m is the mean brightness of the whole image.

- α is calculated according to these brightness:

$$\alpha = \begin{cases} \frac{X_m - X_{low}}{X_{up} - X_{low}}, & \text{if} 0 \leq k \leq X_m \\ \frac{X_{up} - X_m}{X_{up} - X_{low}}, & \text{if} X_m \leq k \leq (L-1) \end{cases} \tag{3.15}$$

$$cdf_{AMHE}(k) = \sum_{i=1}^{k} pdf_{AMHE}(k) \tag{3.16}$$

The value of pdf_{AMHE} should be positive. It is set to 0 in case its value is negative.

The new value of each gray level intensity k is modified by calculating the cdf according to new pdf:

$$cdf_{AMHE}(k) = \sum_{i=1}^{k} pdf_{AMHE}(i) \tag{3.17}$$

$$cdf_{AMHE}(k) = \frac{cdf_{AMHE}(k)}{cdf_{AMHE}(L-1)}(L-1) \tag{3.18}$$

where L is the maximum intensity value.

Results of implementation AMHE for contrast enhancement of a mammogram image is given in Figure 3.6. AMHE causes painting effect on the output image and small details, such as microcalcifications, are invisible.

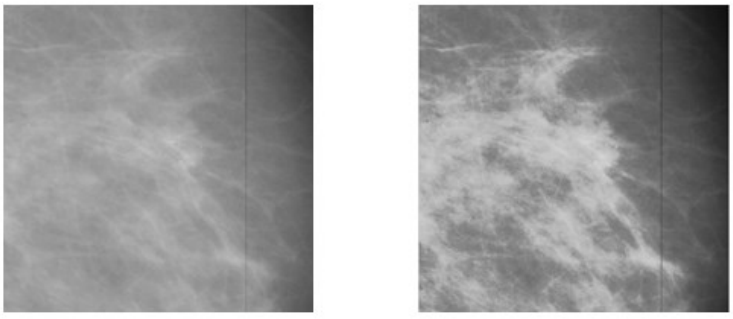

a b

Figure 3.6: Contrast Enhancement by Using AMHE:(a) A ROI of MIAS Image mdb238, (b) Result of enhancement with AMHE.

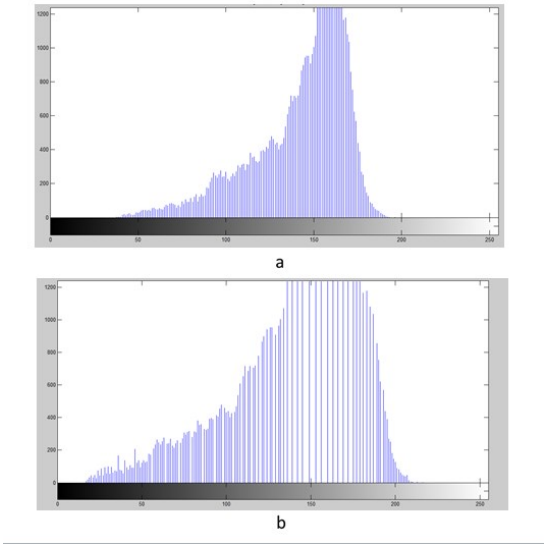

Figure 3.7: Change in Histogram:(a) Histogram of the ROI of MIAS Image mdb238, (b) Histogram of Enhanced Image by AMHE.

3.2.4 Contrast Limited Adaptive Histogram Equalization

The methods for contrast enhancement mentioned before are direct methods which means that they try to find a mapping function obtained from histogram of the image and to scale the histogram according to it. As they do not use specific regions on image to improve the contrast, over enhancement occurs and details on bright and darker regions are lost. To eliminate this problem, contrast limited adaptive histogram equalization can be preferred. The algorithm of CLAHE is clipping the pixel frequencies on histogram which are greater than defined threshold value. As shown in Figure 3.8, the excess part of the histogram pdf, the part over the threshold, is redistributed among all histogram bins [37].

3.3 Gradient Operators

In this section, the gradient operators used in this thesis are explained. These operators are not sufficient for image enhancement individually. Their implementation with the other methods is expressed in the related parts of the thesis.

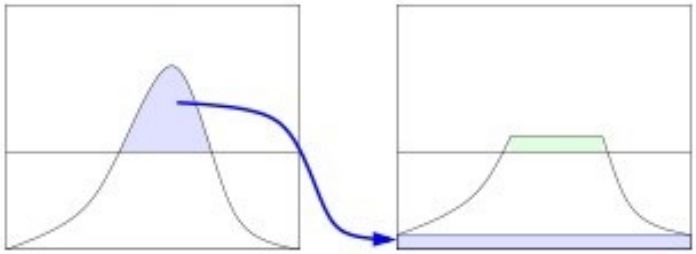

Figure 3.8: CLAHE threshold and redistribution of excess bins.

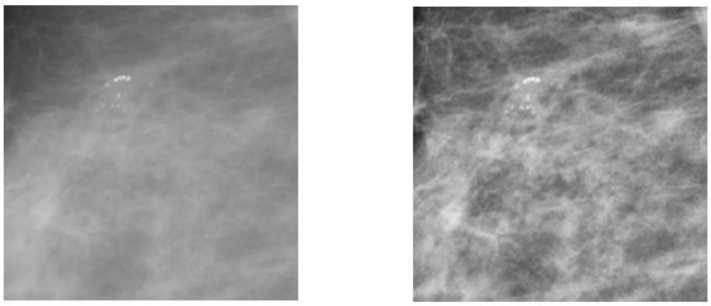

Figure 3.9: Contrast Enhancement by Using CLAHE:(a) A ROI of MIAS Image mdb219,(b) Result of enhacement with CLAHE.

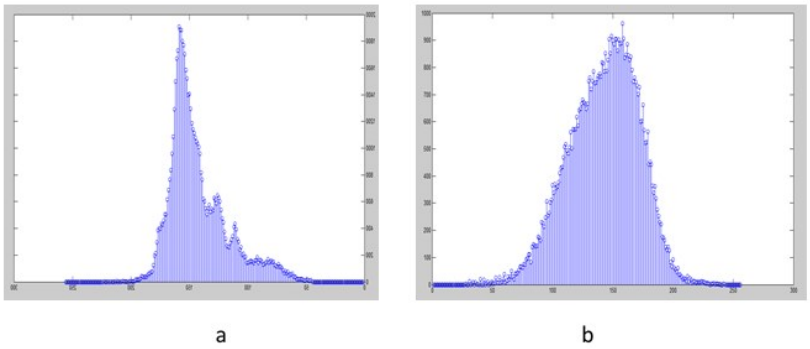

Figure 3.10: Change in Histogram:(a) Histogram of the ROI of MIAS Image mdb219, (b) Histogram of Enhanced Image by CLAHE.

3.3.1 Unsharp Masking

The unsharp filter, by definition, is a simple sharpening operator which enhances edges and other high frequency components in an image via a procedure that subtracts an unsharp or smoothed version from the original image. The implementation of unsharp masking starts with convolution of the original image with unsharp mask kernels. These kernels consist of 8 edge directional kernels defined as sharpening filter given Figure 3.11. After convolution with these kernels, the resultant image which has low frequency response is subtracted from the original image. Thus high pass filtered image is obtained. This high pass filtered image is amplified by production with an adaptively selected weight value. Finally the result of this production is added to the original image. These sequential operations contribute to reduce low frequency information and amplify high frequency details [38]. In this thesis unsharp masking was used with DWT to make more sharply reconstructed images from the selected wavelet coefficients. More details about this image enhancement application is given section 3.5.1.

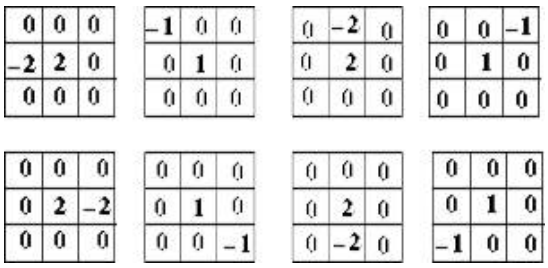

Figure 3.11: Unsharp Masks

3.3.2 Prewitt Operator

Prewitt operator is one of the edge detection algorithms which detects both horizontal and vertical edges. It uses 2 convolution kernels given Figure 3.13. It is expected, from an image enhancement process, to improve the detectability of important image details or objects by human or computer. Prewitt operator provides boundaries

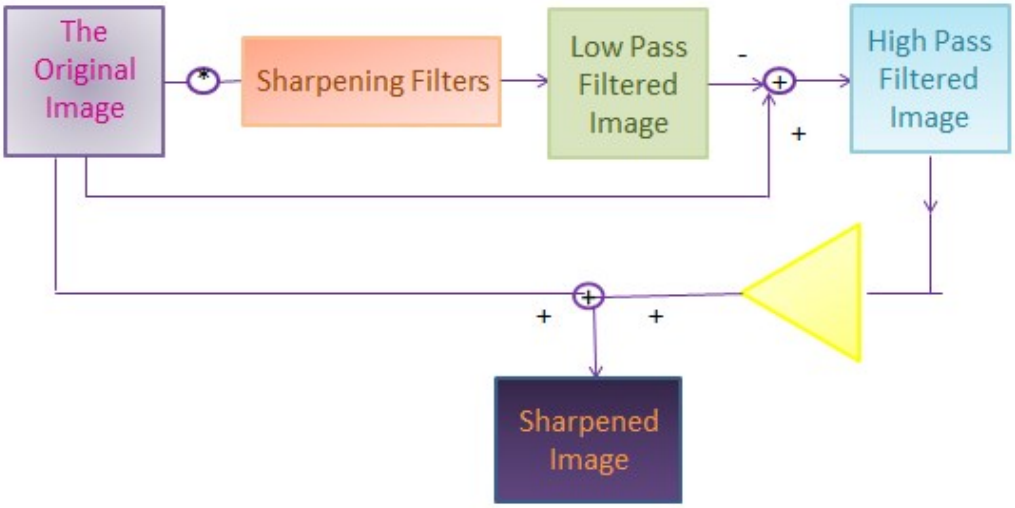

Figure 3.12: Unsharp Masking Procedures.

of these details or objects that contribute to an enhanced image with better visual characteristics when it is used with image enhancement applications [39].

-1	0	1
-1	0	1
-1	0	1

Vertical

-1	-1	-1
0	0	0
1	1	1

Horizontal

Figure 3.13: Masks Used By Prewitt Operator.

In this thesis, Prewitt filter is implemented in image enhancement together with Non-subsampled Contourlet Transform (NSCT) explained in section 3.5.3.

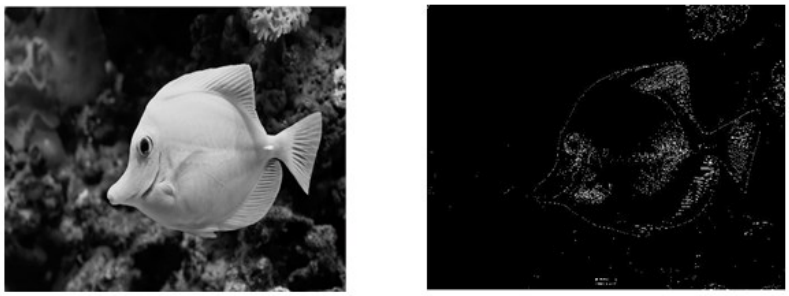

Figure 3.14: (a) Image of yellow fish (b) Edge detected image obtained by applying the Prewitt operator.

3.4 Morphological Operators

Morphological operators are cited in image processing applications such as target detection. It is based on structural analysis of an image and consist of dilation and erosion operations. Dilation operation increases bright regions while decreasing dark regions. Erosion operation is similarly increases dark regions and decreases bright regions. To implement these operations, two parameters are required: an image and a predefined processing operator, structural element (B) which is smaller than an image. The results of morphological operations are changed with size and shape of SE.

Top hot operation is a very successful and effective method for detection of dim targets in the infrared images [40]. It is based on opening and closing operations which are the combination of erosion operation represented by $(f \ominus B)$ and dilation operation represented by $(f \oplus B)$.

$$(f \oplus B)(x, y) = max_{i,j}(f(x - i, y - j) + B(i, j) \tag{3.19}$$

$$(f \ominus B)(x, y) = min_{i,j}(f(x + i, y + j) - B(i, j) \tag{3.20}$$

Figure 3.15 illustrates how opening operation works. Suppose that A is a object in the image and B is a structural element which has a ball shape. B is transverses edge of

the object. First, it is placed inside the object, the object shrinks. Then, it transverses the outside of the resulting object. The object grows, but small branches removed in the last step will not be removed. Formulation of the opening operation is given equation 3.21.

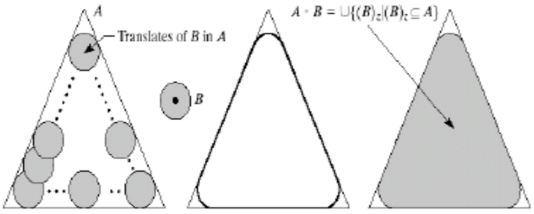

Figure 3.15: Opening Operation.

$$(f \circ B)(x, y) = (f \ominus B) \oplus B \tag{3.21}$$

Figure 3.16 visualizes the closing operation. In the closing operation, a dilation of an object grows the object and fill the gaps. If we erode the result after dilation with the rotated structure element, the objects will keep their structure and form, but small holes filled by dilation will not appear. Objects merged by the dilation will not be separated again. This operation can close gaps between two structures without growing the size of the structures like that dilation. Formulation of the closing operation is given equation 3.22.

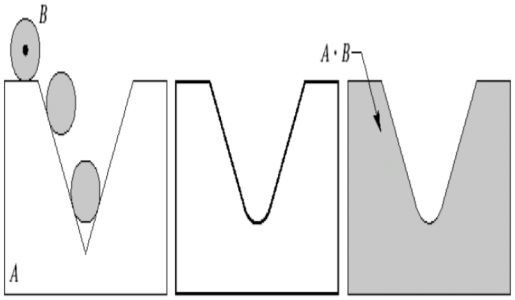

Figure 3.16: Closing Operation.

$$(f \bullet B)(x,y) = (f \oplus B) \ominus B \tag{3.22}$$

Accordingly, while opening operation smooths bright small regions of the image, closing operation eliminates dark small regions.

THT processes in 2 ways: white top hat (WTH) transformation and black top hat (BTH) transformation.The WTH transformation is defined as the difference between the input image and its opening by a structuring element. The BTH transformation is defined as the difference between the closing and the input image. WTH transformation finds out bright regions. As microcalcifications have brighter than other tissues in the breast, WHT is considered for the detection of microcalcifications.

$$WTH(x,y) = f(x,y) - (f \circ B)(x,y) \tag{3.23}$$

$$BTH(x,y) = (f \bullet B)(x,y) - f(x,y) \tag{3.24}$$

The results of application of WHT with different sizes of the structural elements are given in Figures 3.17 and 3.18. In Figure 3.17, microcalcifications are in the lesion. When the size of disk is small the microcalcifications are visible but the lesion disappears. By increasing the size of structural element, there is approximately no change between the original and transformed image. Although WHT makes dim targets more visible, there is a clinical finding loss, so it is not preferred for image enhancement in this study.

3.5 Detail Enhancement Methods

Detail enhancement is based on increasing the contrast between the target and its background. To determine target region and its background, clustering operation based on the frequency characteristics is used. It is believed that the frequency characteristics of microcalcification clusters are different from their surrounding tissues in view of their sharp edges. The algorithm of detail enhancement starts with division of an image of size $M \times N$ into blocks of size $B_1 \times B_2$. Then, the discrete Fourier trans-

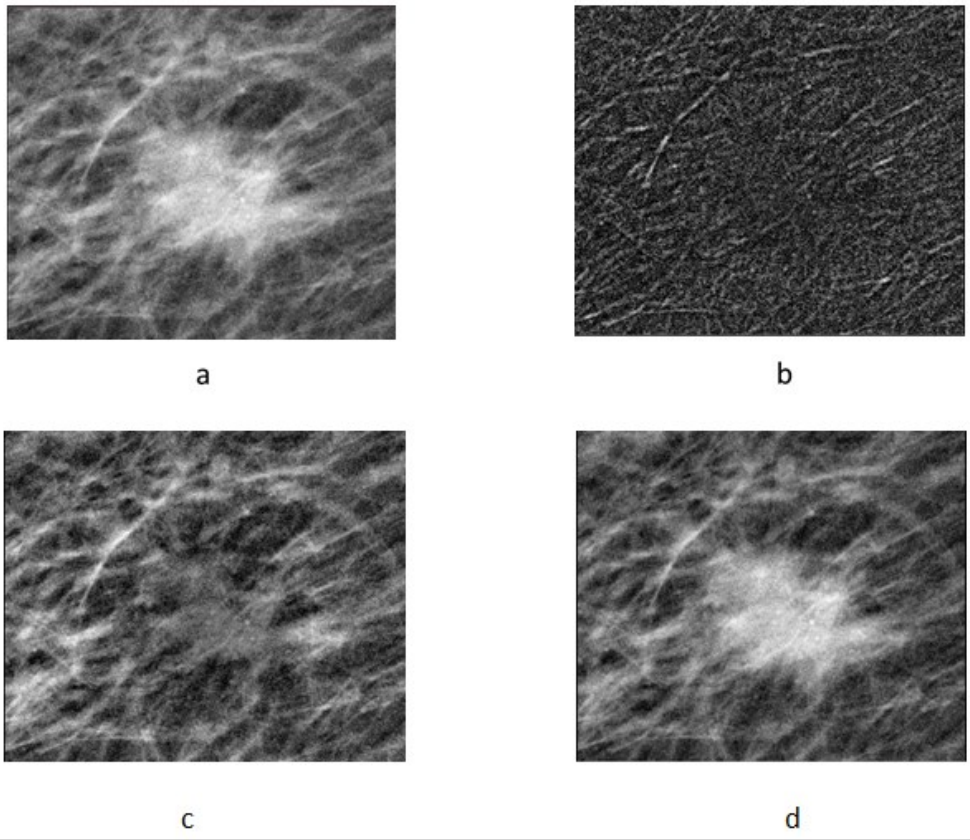

Figure 3.17: (a) ROI of DICOM Image. (b) Application of THT disk=5. (c) Application Of THT disk=50. (d) Application Of THT disk=100.

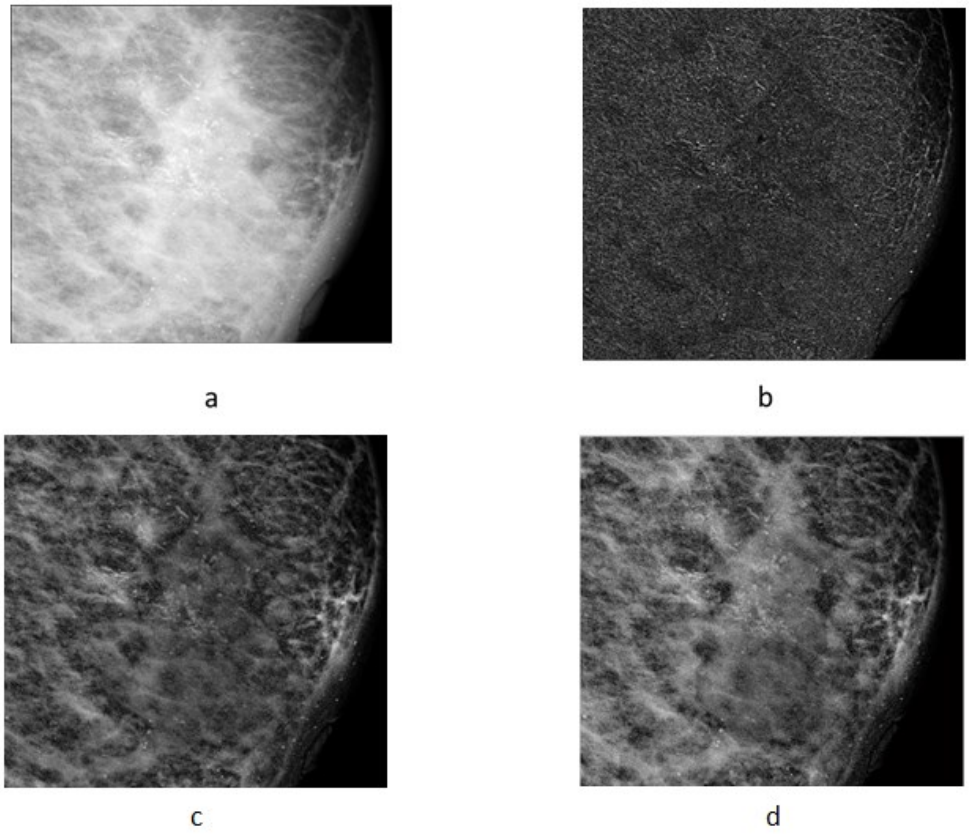

Figure 3.18: (a) ROI of DICOM Image (b) Application Of THT disk=5. (c) Application Of THT disk=50. (d)Application Of THT disk=100.

form (DFT) of each block is computed to obtain frequency information. To decrease the cost of the DFT operation, the length of data is diminished by half, $B_1B_2/2$.

$$F_i(u,v) = \frac{1}{B_1B_2}\sum_{x=0}^{B_1-1}\sum_{y=0}^{B_2-1} I_i(x,y)e^{-2j\pi(ux/B_1)+(uy/B_2)}. \tag{3.25}$$

The results of the DFT operation, F_i , is used in cluster tree operation to label each block as target or background. Before clustering operation F_i which is 2D data is converted to 1D data, V_i, achieved using the zigzag scanning. By converting 2D data to 1D, the zero frequency component is shifted to the center of spectrum [36]. The clustering operation begins with calculating the distance d between each block,V_i

$$d_{ab}^2 = (V_a - V_b)(V_a - V_b)^T \tag{3.26}$$

In equation 3.20, V_a represents block a and V_b represents block b and d_{ab}^2 represents Euclidean distance between block a and block b. If the distance d is very small between the 2 blocks, these blocks are grouped in same clusters. In the next step, cluster centers are obtained by averaging the blocksV_i which belong to the same cluster. To make cluster ($C_j(n)$) normalized ($\overline{(CC_j(n))}$), median filtering and the energy of each cluster(TE_j) are used. The window size for median filtering is chosen as 3.

$$TE_j = \sum_{n=1}^{B_1B_2/2} [CC_j(n)]^2 \tag{3.27}$$

$$\overline{(CC_j(n))} = \frac{[CC_j(n-1)]^2 + [CC_j(n)]^2 + [CC_j(n+1)]^2}{TE_j} \tag{3.28}$$

In the following step, the weights of each cluster center are calculated as given in equation 3.28.

$$w_j = \sum_{n=1}^{B_1B_2/2} \overline{(CC_j(n))}n \tag{3.29}$$

The weight value of each cluster is used to determine the target and the background regions. If the cluster has high cluster center weight, the blocks in the cluster are considered as target region. If the cluster has a low cluster center weight, the blocks

in the cluster are considered as background region. Up to now, the labeling of target and background regions is performed. For enhancement the high frequency and mid-frequency coefficients of the blocks are multiplied by gain value which is computed by using weight value of the corresponding blocks. The matrix that consists of these gain values is called the gain matrix. Each gain value is construct by computation of the distance between a single pixel of the block and all block centers. The distance equation is given in equation 3.31. x_c, y_c are the center coordinates of the block centers. BW_k represents the weight value of the k^{th} block. The total number of blocks is b.

$$BW(k) = w_j, kthblock \in cluster_j \tag{3.30}$$

$$D_k(x,y) = \frac{1}{\sqrt{(BW_k(x_c) - x)^2 + (BW_k(y_c) - y)^2} + \in} \tag{3.31}$$

$$G(x,y) = \sum_{k=1}^{b} \frac{D_k(x,y)}{\sum_{l=1}^{b} D_l(x,y)} \tag{3.32}$$

There are two gain matrices: one of them is for mid frequency image, G_{mid} and the other one is for high frequency image, G_{high}. Calculation of G_{mid} and G_{high} is given in equations (3.33) and (3.34), respectively. G_{min} and G_{max} represents the minimum and maximum values of the gain matrix. α_{mid}, α_{high}, β_{mid} and β_{high} are constants. β_{mid} and β_{high} avoid enhanced image from being saturated [41].

$$G_{mid}(x,y) = \frac{(G(x,y) - G_{min})\alpha_{mid}}{(G_{max} - G_{min})} + \beta_{mid} \tag{3.33}$$

$$G_{high}(x,y) = \frac{(G(x,y) - G_{min})\alpha_{high}}{(G_{max} - G_{min})} + \beta_{high} \tag{3.34}$$

In the final step, the enhanced image is reconstructed by using the gain matrices and low frequency, midfrequency and high frequency components of the original image. To obtain the low frequency image I_{low}, 25×25 averaging filter is applied on the original image. Similarly, the high frequency image I_{high} is obtained by applying

5×5 averaging filter on the original image. The midfrequency image is subtraction of high frequency image and low frequency image from the original image.

$$I_{enh}(x,y) = I_{low}(x,y) + G_{mid}(x,y)I_{mid}(x,y) + G_{high}(x,y)I_{high}(x,y) \quad (3.35)$$

As it is explained above, detail enhancement uses frequency information and clustering operation to label target and background regions. To get frequency information, DFT of the image blocks are calculated. The clustering operation is implemented on these Fourier coefficients. The gain values which are used to reconstruct the enhanced image are obtained according to the clustering operation. The complexity of these operations are quite high. A.E.Turan has made some modifications on these image enhancement methods to reduce these complexity and increase the performance in his master thesis [36]. These modifications and their implementations on our study is discussed in the following parts of the thesis.

3.5.1 Modifications on Using FFT

The first modification is based on using mean and standard deviation of each block instead of the Fourier coefficients. Computation of mean and standard deviation is less complex than the FFT. To calculate the distance matrix, the distance between mean and the standard deviation of each blocks is used. The computation of the gain matrix is changed due to the fact that the length of distance matrix is decreased to 2. The new equations for calculating the gain matrix are given below:

$$TE_j = \sum_{n=1}^{2} [CC_j(n)]^2 \quad (3.36)$$

$$\overline{(CC_j(n))} = \frac{[CC_j(n)]^2}{TE_j} \quad (3.37)$$

$$w_j = \sum_{n=1}^{2} \overline{(CC_j(n))} n \quad (3.38)$$

The other modification is to use the wavelet transform coefficients of each blocks instead of the DFT coefficients. 2D discrete wavelet transform is explained in Section 3.5.1. The usage of the DWT does not provide less complexity. However, when it is compared to FFT, the DWT gives directional frequency information. It is considered that the frequency distribution on each direction (horizontal, vertical and diagonal) increases the performance of clustering. Microcalcifications have point like appearances. They have different frequency characteristics in whole directions compared to their surrounding tissues.

3.5.2 Modifications on Using Clustering Tree Operations

This modification is based on the use of k-means clustering instead of hierarchical cluster tree operation. K-Means algorithm is an unsupervised clustering algorithm that classifies the input data points into multiple classes based on their distance from each other. One of the applications of it is image segmentation.

The procedure of the k-means clustering is given as follows [42] :

1. Assign the cluster centers $v_i, i = 1, 2..., c$ by selecting c blocks among whole blocks randomly.

$$v_i = \frac{1}{|A_i|} \sum_{z_k \in A_i} z_k \tag{3.39}$$

where A_i is the number of blocks corresponding to the ith cluster, z_k is the data point
2. Assign $u_{ik}, i = 1, 2, ..c$ and k=1,2,...N by using equation (3.40)

$$U = u_{ik} \begin{cases} 1, & \text{if } \|z_k - v_i\|^2 \leq |z_k - v_j\|^2 \\ 0, & \text{Otherwise} \end{cases} \tag{3.40}$$

where $\|z_k - v_i\|^2$ is a distance measure between (?) z_k and the cluster center v_i
3. Compute the function J given equation 3.41.

$$J(z, u, v) = \sum_{i=1}^{c} \sum_{k=1}^{N} \mu_{ik} |z_k - v_i\|^2 \tag{3.41}$$

Clustering is ended in case J has merged .
4. Update the cluster center v_i by using equation (3.33), return to step 2.

In our study c is chosen 3 to cluster the region except breast (black background), microcalcification region and other tissues. Enhancement by using detail enhancement and its modifications are implemented by dividing the input image into 16 blocks. Chosen α_{mid}, α_{high}, β_{mid} and β_{high} coefficients for MIAS and DICOM Images are given in Table 3.1. The results of these enhancement for MIAS image mdb 223 is given Figure 3.20.

Table 3.1: Chosen Coefficients of Detail Enhancement Methods for MIAS and DICOM images

Coefficients	**For MIAS**	**For DICOM**
α_{mid}	0.5	2
α_{high}	4	4
β_{mid}	0.5	0.1
β_{high}	0.5	0.1

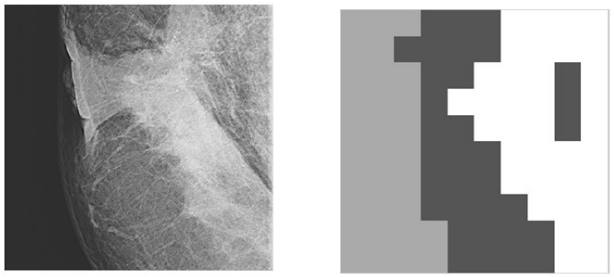

Figure 3.19: (a) A ROI of DICOM Image. (b) Clustering Distribution.

3.6 Multiresolution Analysis

Most of the existing image enhancement methods use frequency information of an image to distinguish noise, weak and strong edges. However it is difficult to identify noises, since they correspond to similar frequency information with weak edges. The property of noises that they do not have any geometrical information can be used to

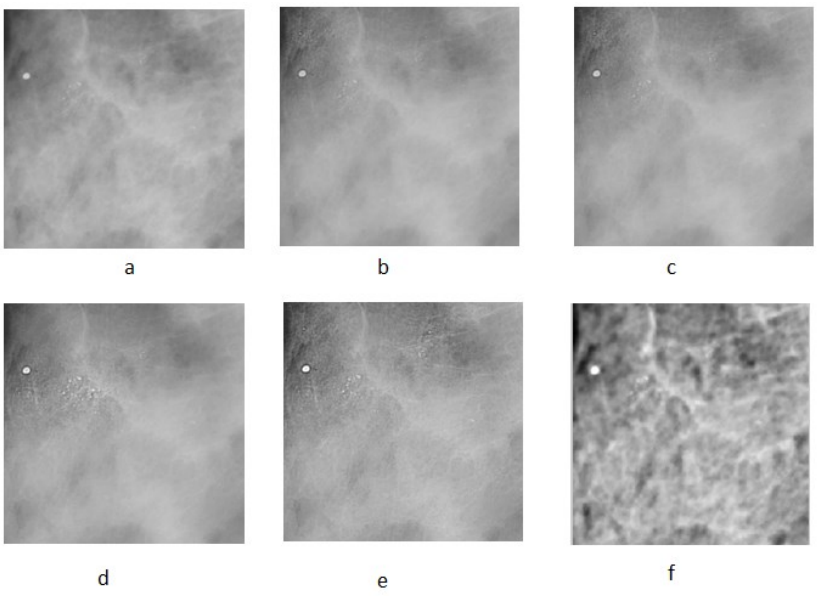

Figure 3.20: Output Images of Enhancement Methods:(a) A ROI of MIAS Image mdb 223 (b) Enhanced image with FFT (c) Enhanced image with mean and standart deviation (d) Enhanced image with discrete wavelet transform (e) Enhanced Image with k means clustering (f) Enhanced Image with k means clustering and mean /standart deviation.

distinguish weak edges from noises. In this thesis, there is no denoising approach since microcalcifications are small in size. To identify the background which corresponds to weak edges and microcalcifications which corresponds to strong edges, geometrical information is obtained by multiresolution analysis. Multiresolution analysis, which was discovered with wavelet transform in 1980s maps a signal or an image into a set of coefficients.

3.6.1 Discrete Wavelet Transform

The wavelet transform is a mathematical microscope that points out image details [21]. Firstly, an input image is decomposed into low and high frequency components by convolution and downsampling operations. These operations are performed by using high pass filters H_0 and low pass filter H_1. These filters with downsampling operators are called quadrature mirror filters (QMFs). The result of low pass filter is called approximation (LL) and results of high pass filter gives detail coeffi-

cients LH, HL, HH. Decomposition process is iterated only on approximation and detail coefficients are remained. Decomposition of image into second level produces a shrinkage on the size of the approximation (LL).This means that quarter of original image size pixels are not contained in the approximation band [43]. It is considered that microcalcifications correspond to the highest frequencies. The detection of microcalcifications is accomplished by setting the wavelet coefficient LL in last level of decomposition to zero in order to eliminate the image background information before the reconstruction of the image. The reconstructed mammogram is expected to contain only high-frequency components, including the microcalcifications [44]. To create more shaper image, after reconstruction of wavelet coefficients by eliminating low frequency band of last level of decomposition, unsharp masking is applied. The drawback of the unsharp masking is that it creates a white frame surrounding the image.

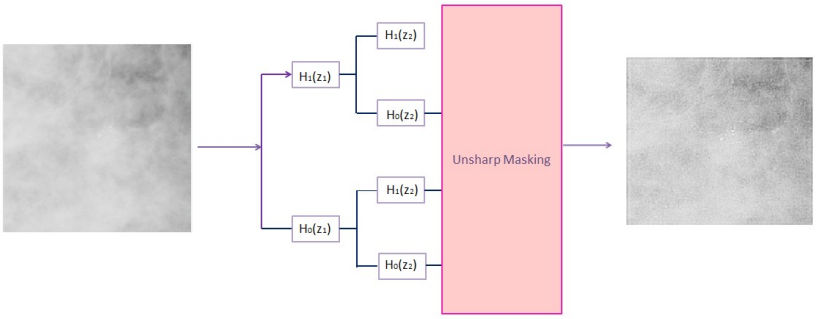

Figure 3.21: Schematic distribution of enhancement by using DWT and Unsharp Masking.

3.6.2 Contourlet Transform

The contourlet transform (CT) which was proposed by Do and Vetterli [45] provides directional multiresolution image presentation. For multiresolution it employs Laplacian pyramids (LP) which is an alternative method to the wavelet decomposition. The process of LP is listed below:

1.Extraction of coarse approximation of the image by low pass filtering and down-

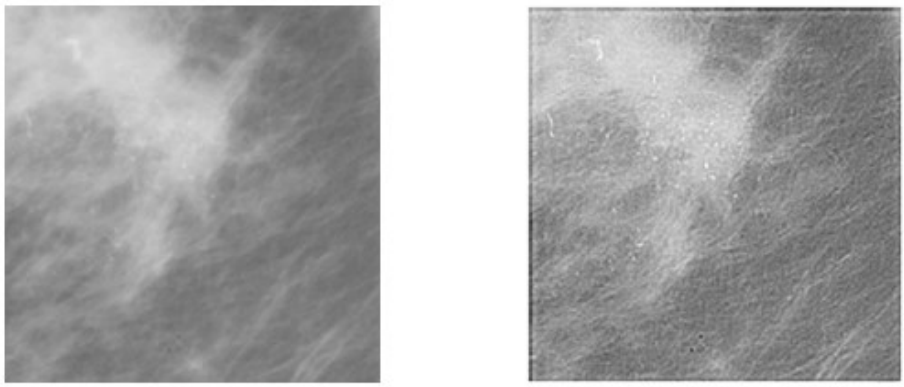

Figure 3.22: Contrast Enhancement by Using DWT:(a) A ROI of MIAS Image mdb209. (b) Result of enhacement with DWT.

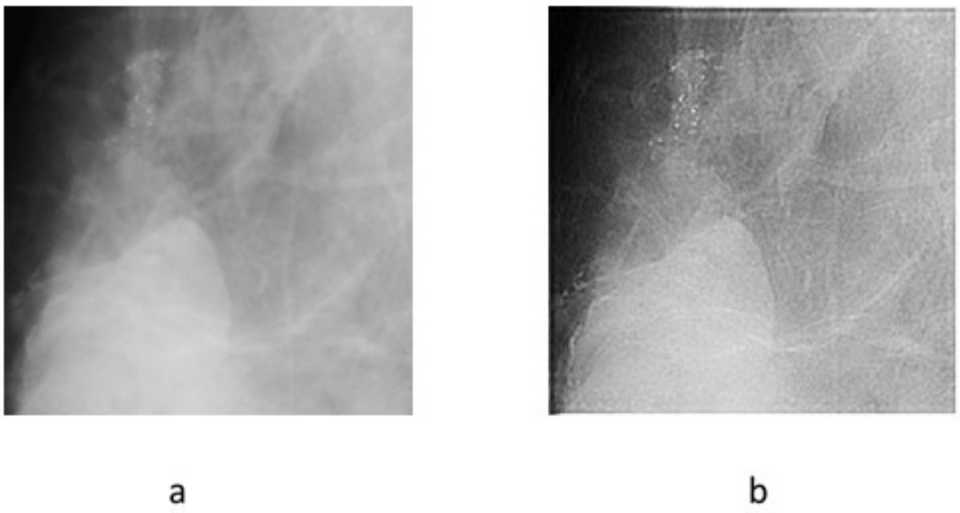

Figure 3.23: Contrast Enhancement by Using DWT:(a)A ROI of MIAS Image mdb241. (b) Result of image enhacement with DWT.

sampling,

2.Prediction of the image by upsampling and high pass filtering,

3. Calculation of the prediction error by subtracting the predicted image from the original image. This process is iterated on the coarse version [6].

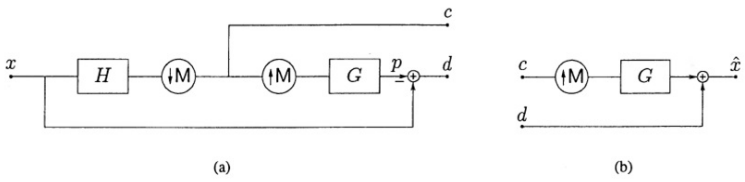

Figure 3.24: Schematic Distribution Of the Laplacian Pyramid (a) Analysis: The output c is a coarse aproximation and the output d is the difference between the original image x and the prediction p (b) Synthesis [6].

Directional decomposition of an image is based on decomposing image into subbands. These subbands give directional information or energy along each dimension. Thus, directional decomposition is used in many image processing applications such as target detection, denoising, enhancement, texture analysis, etc. To attain directional decomposition, directional filter bank (DFB) is applied on each pyramidal level obtained from LP. The combination of DFB with LP is called pyramidal directional filter bank which is shown in Figure 3.26 (PDFB) [46].

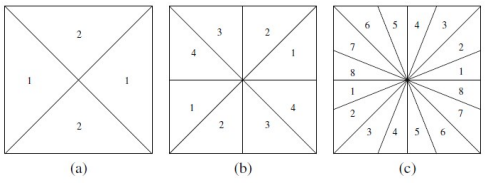

Figure 3.25: Directional Filter Bank Spectrum Partition (a) l=1 provides 2 subbands. (b) l=2 provides 4 subbands. (c) l=3 provides 8 subbands [7].

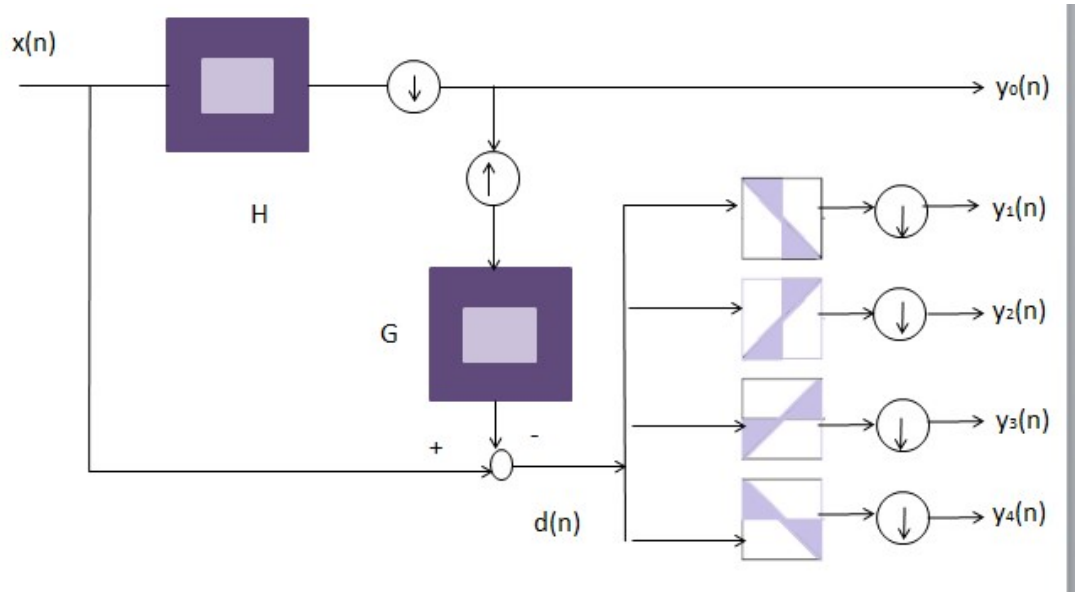

Figure 3.26: Analysis Part of Contourlet Transform By Using Four Directional Filter Bank.

3.6.3 Image Enhancement by Using NSCT

As there is no downsampling and upsampling operations in NSCT, it is shift invariant which means that each pixel of the subbands obtained from NSCT corresponds to that of the original image in the same location [47]. Nonsubsampled pyramids are employed for multiscale decomposition in NSCT. The nonsubsampled pyramids consists of two channel filter bank: one of them is high pass filter and the other one is low pass filter. There is no downsampling and upsampling operations used with these filters. Thus, the nonsubsampled filters are not similar to LP [47].

The frequency response of the building block of nonsubsampled pyramid is shown in Figure 3.27. To iterate multiscale decomposition the nonsubsampled filter banks are applied following upsampling operation by 2.

For directional decomposition in NSCT, the nonsubsampled directional filter banks are employed. NSDFB consists of 2 channel filter banks without any sampling operation.

In Figure 3.29 , $y_{i,j}$ represents each subband, where i denotes the decomposition level and j denotes the direction. NSCT is used to create a function f for subbands which

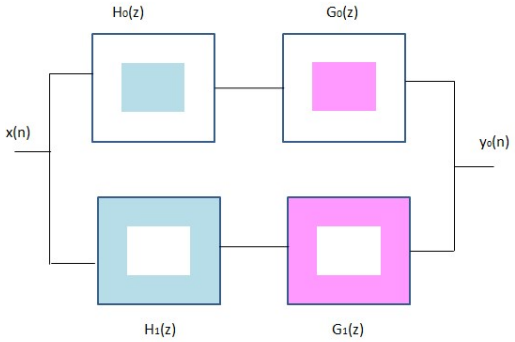

Figure 3.27: Frequency response of the building block of nonsubsampled pyramid.

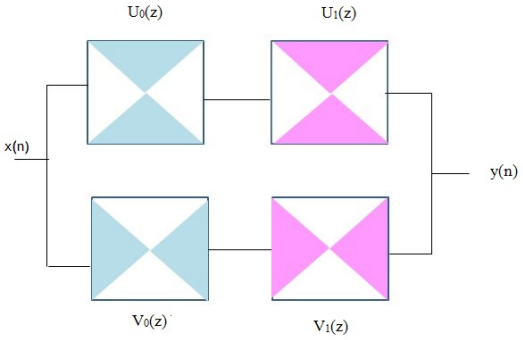

Figure 3.28: Frequency response of the building block of the nonsubsampled directional filter bank.

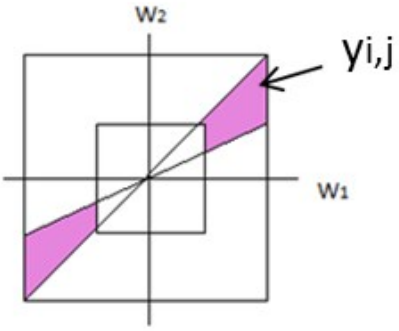

Figure 3.29: Decomposition levels and directions in the frequency domain.

indicates the features of interest. This f function creates enhanced subbands y' to reconstruct an enhanced image.

$$y'_{i,j} = f(y_{i,j}) \tag{3.42}$$

The f function used for enhancement of the directional subbands is given in equation (3.36). W_1 and W_2 are the weight factors to enhance directional subbands corresponding the surrounding tissue of microcalcification and microcalcifications, respectively. $b_{i,j}$ denotes a binary image which holds edges of the subbands. $(n1, n2)$ are the coordinates of the pixels. By implementation of edge detection methods $b_{i,j}$ can be obtained. In our study a Prewitt operator that explained in Section 3.3.2 was chosen to get $b_{i,j}$ and a threshold $T_{i,j}$ is calculated for each subbands. The appropriate value for $T_{i,j}$ is chosen $3\sigma_{i,j}$ for both MIAS data and DICOM images in our study. $\sigma_{i,j}$ is the standard deviation of the related subband $y_{i,j}$. The weight factor W_1 is assigned $3\sigma_{i,j}$ for MIAS images and $6\sigma_{i,j}$ for DICOM images, while the weight factor W_2 is assigned $4\sigma_{i,j}$ for MIAS images and $12\sigma_{i,j}$ for DICOM images. W_1 should be smaller than W_2 since multiplication of W_2 and each subband corresponding to microcalcifications makes microcalcifications more visible. After enhancement of subbands, the enhanced image is reconstructed from enhanced subbands y' [48].

$$f(y_{i,j}) = \begin{cases} W_1 y_{i,j}(n1, n2), & \text{if } b_{i,j}(n1, n2) = 0 \\ W_2 y_{i,j}(n1, n2), & \text{if } b_{i,j}(n1, n2) = 1 \end{cases} \tag{3.43}$$

To implement NSCT for decomposion of the image into subbands Nonsubsampled Contourlet Toolbox [49] in MATLAB is used.

The results of enhancement using NSCT is given below.

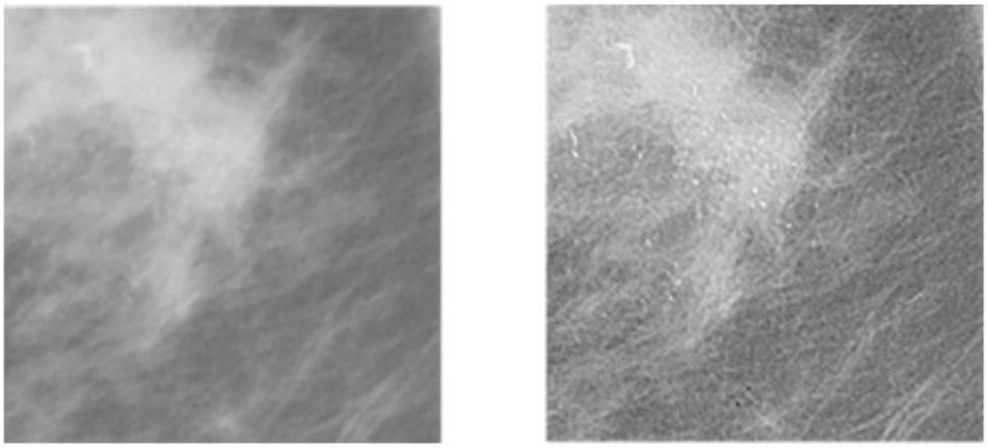

Figure 3.30: Contrast Enhancement by using NSCT: (a) A ROI of MIAS Image mdb209. (b) Result of enhacement with NSCT.

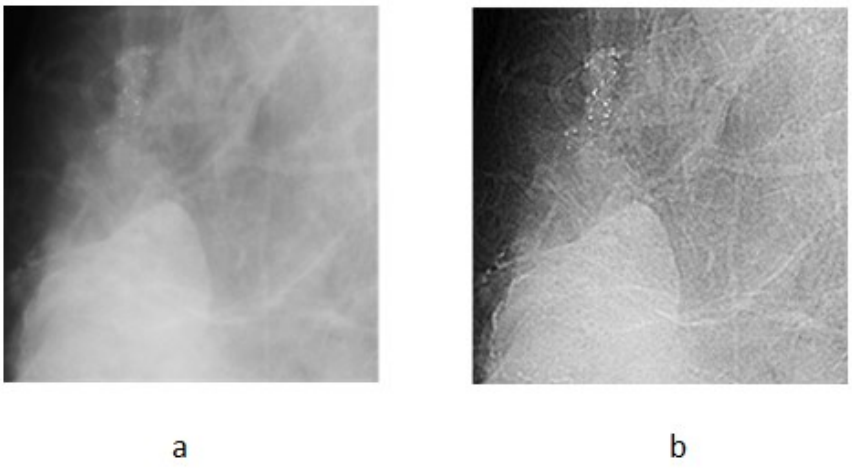

Figure 3.31: Contrast Enhancement by using NSCT: (a) A ROI of MIAS Image mdb241. (b) Result of enhancement with NSCT

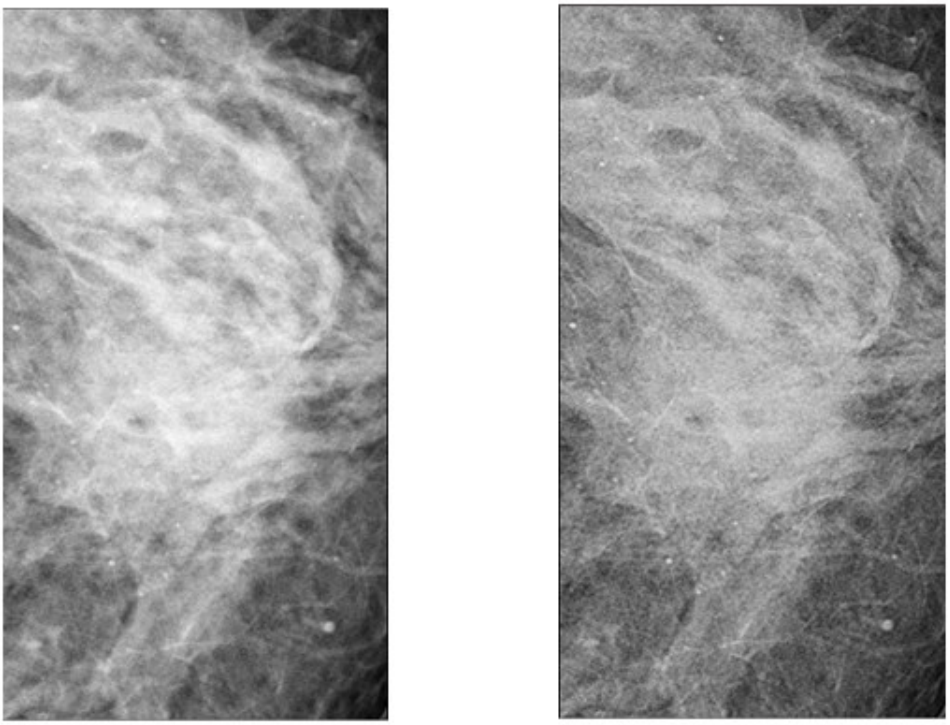

Figure 3.32: Contrast Enhancement by using NSCT: (a) A ROI of DICOM Image (b) Result of enhancement with NSCT.

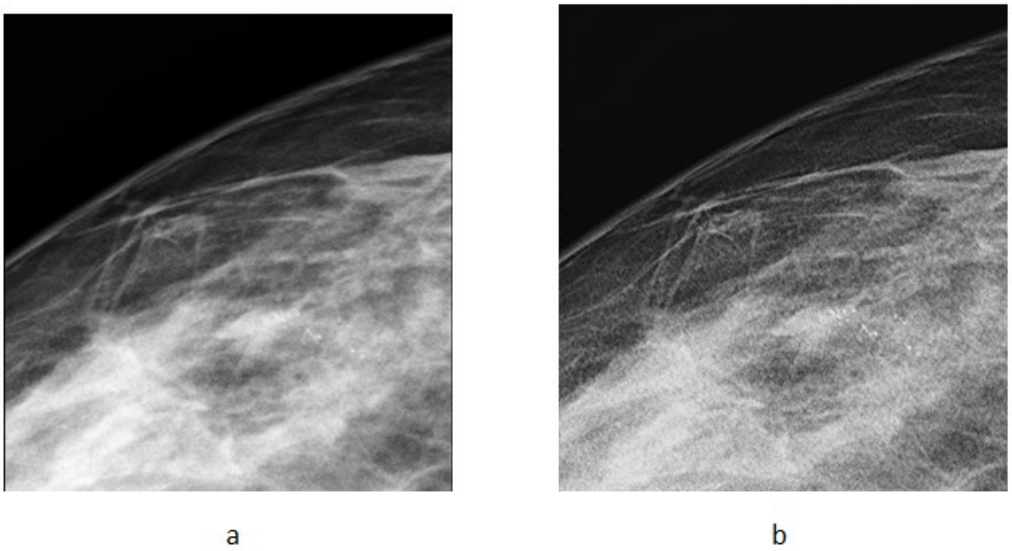

Figure 3.33: Contrast Enhancement by using NSCT: (a) A ROI of DICOM Image. (b) Result of enhancement with NSCT.

CHAPTER 4

PERFORMANCE EVALUATION FOR IMAGE ENHANCEMENT

After image enhancement operation, the visual appearance of image will be changed. This change is remarkable by human vision, but decision of whether the performance of enhancement is satisfactory or not is critical, especially for medical images, to avoid misdiagnosis. Subjective evaluation varies from person to person, therefore quantitative measures must be used for evaluation. The change in the original image is observed by looking at the change in histogram. However, since it is unclear which gray level intensity belongs to target and its background, change in histogram does not give meaningful information about the enhancement performance. Classical measures used to measure the quality of the image mean square error (MSE), signal-to-noise-ratio (SNR) and peak-signal-to-noise-ratio (PSNR). They are not completely enough for evaluation without visual perception. Absolute mean brightness error (AMBE) and the measure of enhancement (EME) are other quantitative measures [50]. AMBE evaluates changes in brightness of the image by calculating the absolute difference between input and output images. These measures are not suitable for our study. Several measures used for image quality descriptions are given in the following sections of this chapter.

4.1 Metrics of Mammogram Contrast Enhancement

Singh and Bovis introduced three metrics to evaluate the quality of contrast between target (microcalcifications in our study) and the background (surrounding tissues in

our study). These metrics measure how the distribution of gray levels that belongs to target and background regions are separated after image enhancement operations. The image statistics, such as mean, standard deviation and entropy of the distribution of each gray level, are used in the calculation of these metrics, and are explained in the following sections [8].

4.1.1 Distribution Separation Measure(DSM)

As the mammogram images have low contrast, the density of gray levels that belongs to microcalcifications overlaps with that of their surrounding tissues. It is expected, from a good enhancement method, to reduce this overlap as shown in Figure 4.1. DSM is a quantitative metric which shows separation of distributions of gray levels on both original and enhanced mammogram images. DSM is formulated by equation (4.1). μ_{ucalE} and μ_{ucalO} represent the mean of microcalcifications on the enhanced and original images, respectively. In the same way, $\mu_{utissueE}$ and $\mu_{utissueO}$ represent the mean of the surrounding tissues of the original and enhances images, respectively. DSM value should be greater than 0 and the highest DSM value indicates the best enhancement.

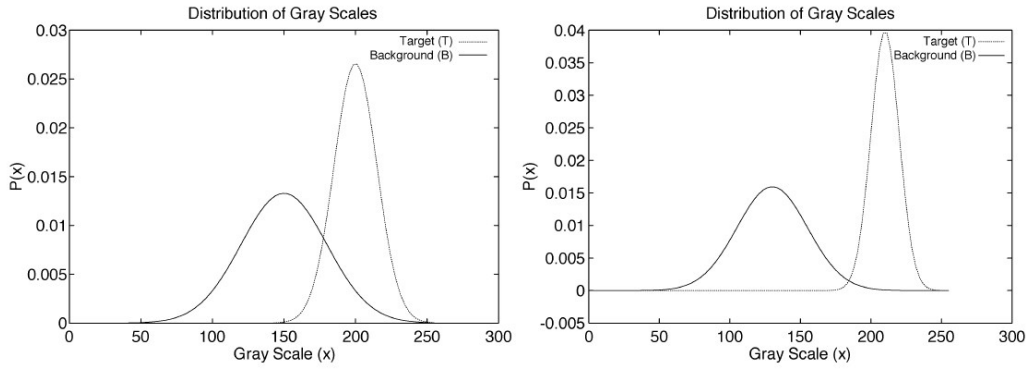

Figure 4.1: Distribution overlap between the background B and target T before and after enhancement [8].

$$DSM = |\mu_{ucalE} - \mu_{utissueE}| - |\mu_{ucalO} - \mu_{utissueO}| \tag{4.1}$$

4.1.2 Target to Background Contrast Enhancement Measure (TBC)

A good enhancement maximizes the difference between the mean gray levels that correspond to microcalcifications and their surrounding tissues. The homogeneity of each microcalcification is increased, since their boundaries and localizations become more clear. Target to Background Contrast Enhancement Measure (TBC) is a quality metric based on the ratio of the mean and standard deviation values of microcalcifications and other regions, on both original and enhanced images. Standard deviation is a measure of homogeneity. TBC is defined as:

$$TBC = \frac{\frac{\mu_{ucalE}}{\mu_{utissueE}} - \frac{\mu_{calO}}{\mu_{utissueO}}}{\frac{\sigma_{ucalE}}{\sigma_{ucalO}}} \tag{4.2}$$

TBC value should be grater than zero for an expected image enhancement.

4.1.3 Target to Background Contrast Enhancement Measure Based on Entropy(TBCE)

TBCE compares the homogeneity of distributions of gray levels that uses the ratio of entropy instead of standard deviation. Equation (4.3) defines TBCE. In that expression, ε_{ucalE} and ε_{ucalO} indicate the entropy of the enhanced and original images, respectively.

$$TBCE = \frac{\frac{\mu_{ucalE}}{\mu_{utissueE}} - \frac{\mu_{calO}}{\mu_{utissueO}}}{\frac{\varepsilon_{ucalE}}{\varepsilon_{ucalO}}} \tag{4.3}$$

By combination of these three measures , a single quantitative value D is obtained to evaluate the performance of the image enhancement methods. To calculate D , the measures are normalized between 0 and 1. Following , D is calculated by :

$$D = \sqrt{(1 - DSM)^2 + (1 - TBC)^2 + (1 - TBCE)^2} \tag{4.4}$$

The smallest value of D denotes the best enhancement method.

4.2 Relative Entropy Analysis

Entropy is a statistical measure of randomness of the intensity of pixels in image. It is defined as follows:

$$Entropy = -\sum_{i=1}^{K} pdf(i) log_2(pdf(i)) \tag{4.5}$$

where $pdf(i)$ represents the probability density function of i^{th} gray level and K is the maximum intensity value in the image. When the pdf of each intensity values are equal, in other words if an image has uniform gray level distribution, the maximum entropy value is obtained [51].

Entropy does not give information about the performance of enhancement method. It just shows a change in the gray level distribution of the image. To compare the probability distributions of input and enhanced images, relative entropy function is introduced:

$$Relative\ Entropy = \sum_{i=1}^{K} pdf_{org}(i) log_2(\frac{pdf_{org}(i)}{pdf_{enh}(i)}) \tag{4.6}$$

It is approximately equal to 0, when the distributions of the original and enhanced images are similar. When the probability density functions are replaced the value of the relative entropy will change [52].

4.3 Mutual Information Analysis

Mutual information is an image quality measure, alternative to the relative entropy function, based on the relationship between the entropy of the original and enhanced images. The relative entropy is a non symmetric function, whereas mutual information analysis provides a symmetric function. It is formulated by

$$I(x:y) = \sum_{x,y} pdf_x(x) log2(\frac{pdf_{xy}(x,y)}{pdf_x pdf_y}) \tag{4.7}$$

where pdf_{xy} represents joint distribution of two images [52].

4.4 Intensity Contrast Calculated with GLCM

Intensity contrast was proposed by Chen to estimate the difference between the local contrast of the original and enhanced images [53]. Contrast is a measure of intensity contrast between a pixel and its adjacent pixels and it is defined as:

$$Con = \sum_{i=1}^{K} |i-j|^2 p_{ij} \tag{4.8}$$

In this equation, K represents the maximum intensity value and p_{ij} represents the gray level co-occurance matrix (GLCM). GLCM is 2D matrix that shows how often a pixel with the intensity (gray-level) value i occurs in a specific spatial relationship to a pixel with the value j and it is calculated as

$$p_{i,j} = \sum_{i=0}^{M-1} \sum_{j=0}^{N-1} \begin{cases} 1, & \text{if } I(x,y) = i \text{ and } I((x+\Delta x),(y+\Delta y)) = j \\ 0, & \text{Otherwise} \end{cases} \tag{4.9}$$

A higher contrast value is desired for good enhancement.

4.5 Discrete Entropy Calculated with GLCM

Another image quality metrics proposed by Chen is discrete entropy calculation using GLCM instead of using pdf. $Entropy$ measures the impermanence of elements of the GLCM.

$$Entropy = -\sum_{i=1}^{k} p_{ij} log_2(p_{ij}), 0 \leq (j) \leq (k) \tag{4.10}$$

The highest value for discrete entropy indicates a best enhancement.

4.6 Structural Similarity Image Quality Index(SSIM)

The structural similarity is a state of art method to compare similarity between two images [54]. The SSIM measurement system is based on three independent comparisons between input image x and output image y: luminance ($L(x,y)$), contrast ($c(x,y)$), and structural ($s(x,y)$). Similarity measure (S) is a function luminance,

contrast and structure comparisons:

$$S(x,y) = f((l(x,y), c(x,y), s(x,y) \tag{4.11}$$

S is symmetric, i.e., ($S(x,y) = S(y,x)$), and its value is less than or equal to 1. It is equal to 1 when $x = y$.

The luminance comparison is obtained using the following expression:

$$L(x,y) = \frac{2\mu_x\mu_y + C1}{\mu_x^2 + \mu_y^2 + C1} \tag{4.12}$$

whereμ_x μ_y denote the mean values of the input image x and output image y, respectively. C1 is a constant that inhibits division by 0, in case, $\mu_x^2 + \mu_y^2 = 0$:

$$C1 = (K_1 L)^2, K_1 \leqslant (1), L = \text{maximum intensity value} \tag{4.13}$$

The contrast comparison is similar to the luminance comparison. It uses standard deviations of x and y instead of mean values:

$$C(x,y) = \frac{2\sigma_x\sigma_y + C2}{\sigma_x^2 + \sigma_y^2 + C2} \tag{4.14}$$

C2 is a constant and is calculated as follows:

$$C2 = (K_2 L)^2, K_2 \leqslant (1), L = \text{maximum intensity value} \tag{4.15}$$

The structural comparison $s(x,y)$ is defined as:

$$s(x,y) = \frac{\sigma_{xy} + C3}{\sigma_x\sigma_y + C3} \tag{4.16}$$

Here, σ_{xy} is a correlation coefficient that corresponds to the cosine angle between $x - \mu_x$ and $y - \mu_y$ and it is defined as:

$$\sigma_{xy} = \frac{1}{n-1}\sum_i\sum_j (I_x(i,j) - \mu_x)(I_y(i,j) - \mu_y) \tag{4.17}$$

The constant C3 is chosen half of C2, i.e.,

$$C3 = \frac{C2}{2} \tag{4.18}$$

After calculating these three comparison values, SSIM is calculated by their combination. α, β and γ are constants with positive values that are used to set the importance

of the comparison components. In this study, they are set to 1. The $SSIM$ is defined as follows:

$$SSIM(x,y) = [I(x,y)]^{\alpha}[C(x,y)]^{\beta}[S(x,y)]^{\gamma} \tag{4.19}$$

Normalized with respect to pixel sizes, $SSIM$ can be written as:

$$SSIM(x,y) = \frac{1}{MN}\sum_{x=0}^{M}\sum_{y=0}^{N} SSIM(x,y) \tag{4.20}$$

When the constants C1 and C2 are set to 0, the similarity matrix is called the "universal quality index" and is defined as

$$UIQI = \frac{\sigma_{xy}}{\sigma_x\sigma_y}\frac{2\mu_x\mu_y}{\mu_x^2+\mu_y^2}\frac{2\sigma_x\sigma y}{\sigma_x^2+\sigma_y^2} \tag{4.21}$$

where μ_x, σ_x, $\sigma_{x,y}$ parameters used in the calculation of $SSIM$ are the local statistics. A window with a predetermined size is shifted on each image and these parameters are calculated in the window. To obtain the final value of $SSIM$, the average of these local values are calculated. Equation (4.21) represents a final equation for evaluating the overall image quality.

$$SSIM(x,y) = \frac{1}{M}\sum_{j}^{M} SSIM(x_j y_j) \tag{4.22}$$

While M denotes the number of windows, x_j and y_j denote the j^{th} local window.

The quality metrics are calculated for enhanced images with detail enhancement methods, DWT and NSCT.

4.7 Image Enhancement Results and Their Comparison By Using Quality Metric

To calculate the mammogram contrast enhancement metrics, special processes are required. Firstly, the ROI with microcalcification clusters is chosen. Then to obtain a list of coordinates for each pixel that belongs a microcalcification, binary segmentation is performed by thresholding. Figure 4.2 depicts binary segmentation by thresholding of ROI MIAS image mdb 209. Mean and standard deviation of all pixels in the ROI (except the pixels in the list of pixels of microcalcification), and for all pixels

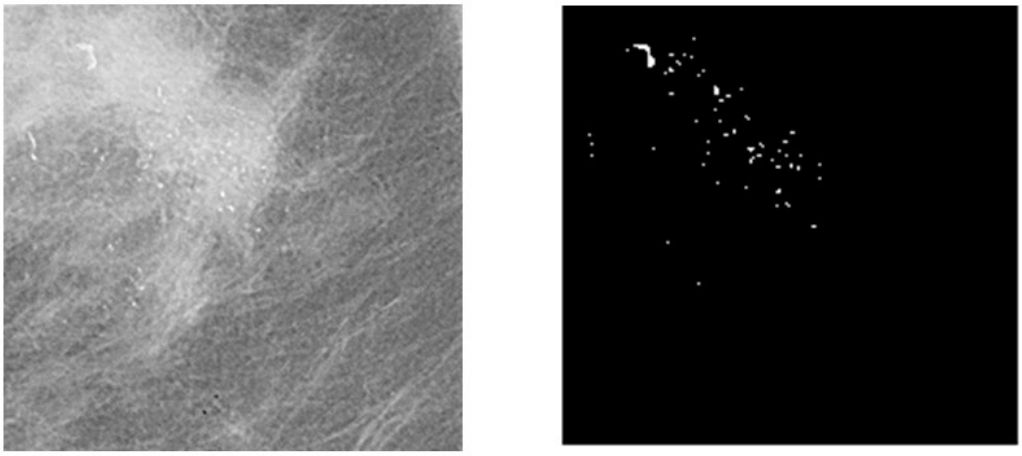

Figure 4.2: Binary Segmentation By Tresholding.

in the list of microcalcification are calculated. These mean and standard deviations are used to obtain the quality metrics: DSM, TBC, and TBCE.

For this study, detail enhancement methods and enhancement methods based on multiresolution analysis are preferred. Both types of enhancement methods are based on identification of the region with microcalcification cluster and determining the specific coefficients to amplify them. Detail enhancement methods are local enhancement methods and enhancement methods based on multiresolution analysis are global methods. It is considered that local enhancement methods provides better enhancement results compared to global approaches. Among detail enhancement methods, DWT provides geometrical information compared to DFT. Wavelet coefficients obtained by DWT achieve to detect point-like objects such as microcalcifications.

The abbreviations of used enhancement methods and their explanations are:
EWFFT——->Detail enhancement by using FFT and hierarchical clustering
EWMStd——>Detail enhancement by using mean/standard deviation and hierarchical clustering
EWDWT——->Detail enhancement by using DWT and hierarchical clustering
EWKM———>Detail enhancement by using FFT and k means clustering
EWMStdKM—->Detail enhancement by using mean/standard deviation and k means clustering
EWDWTUM—>Enhancement by using DWT and unsharp masking

EWNSCT——>Enhancement by using NSCT.

Figures 4.3-4.4 show the results of image enhancement methods on MIAS images mdb252 and mdb241, respectively. Figures 4.5-4.6 show the results of image enhancement methods on 2 DICOM images. Tables 4.2- 4.3 present the mean and standard deviations of quality measures calculated for each enhanced MIAS images and 30 of 70 DICOM images, respectively. The best mean values of enhancement methods are highlighted by pink and minimum standard deviations are highlighted by blue. High values of standard deviations are related to density of breast tissue and distribution of microcalcification . For fatty breasts, the differences between intensity values of microcalcifications and their surrounding tissues is higher than those of dense breasts. Calculated quality measures also varies from grouped microcalcifications to diffused microcalcifications. It is observed that, detail enhancement by using k means clustering(EWKM) outperforms to other enhancement methods which are compared with the given quality measures for MIAS images. For DICOM images, quality measures calculated for enhancement method by using NSCT gives the best results compared to other enhancement methods.

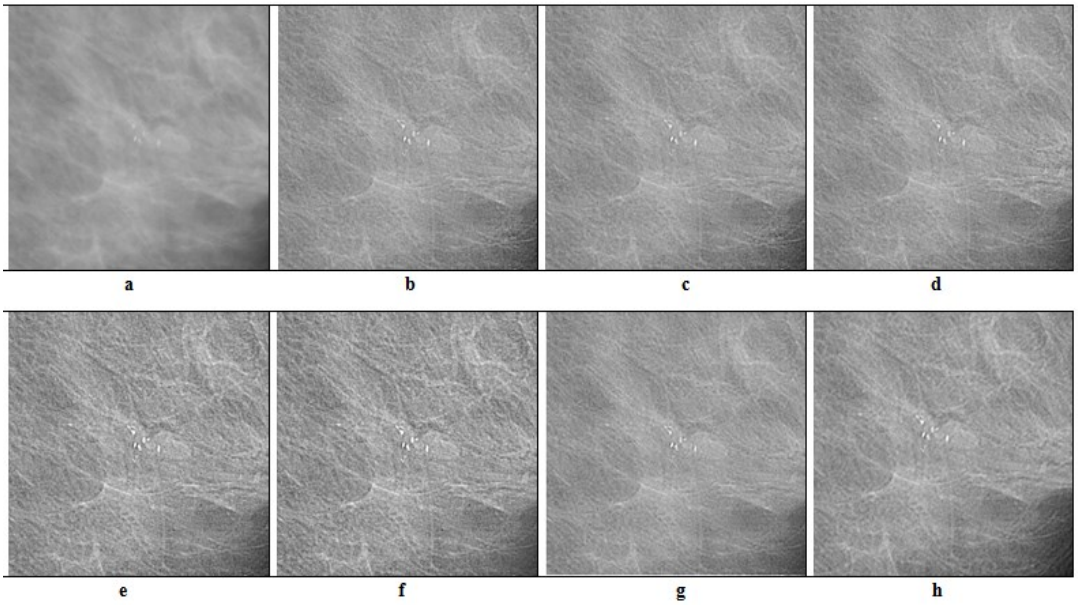

Figure 4.3: Output Images of Enhancement Methods: (a) Original Image (mdb252), (b) Enhanced Image with EWFFT (c) Enhanced Image with EWMStd, (d) Enhanced Image with EWDWT, (e) Enhanced Image with EWKM, (f) Enhanced Image with EWKMMStd, (g) Enhanced Image with EWDWTUM, (h) Enhanced Image with EWNSCT.

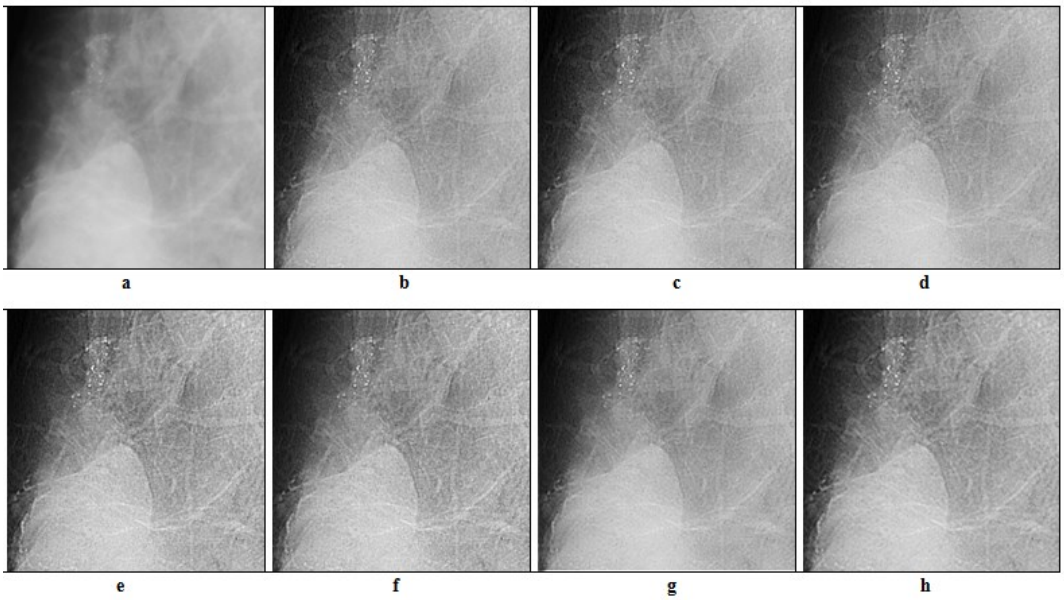

Figure 4.4: Output Images of Enhancement Methods: (a) Original Image (mdb241), (b) Enhanced Image with EWFFT (c) Enhanced Image with EWMStd, (d) Enhanced Image with EWDWT, (e) Enhanced Image with EWKM, (f) Enhanced Image with EWKMMStd, (g) Enhanced Image with EWDWTUM, (h) Enhanced Image with EWNSCT.

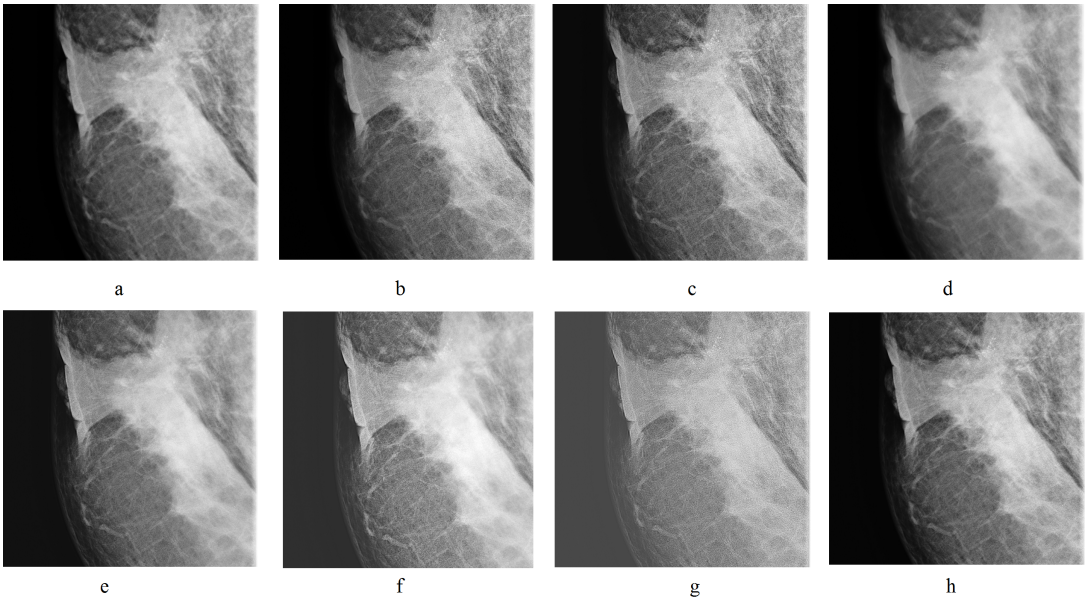

Figure 4.5: Output Images of Enhancement Methods: (a) Original Image (DICOM), (b) Enhanced Image with EWDFT (c) Enhanced Image with EWMStd, (d) Enhanced Image with EWDWT, (e) Enhanced Image with EWKM, (f) Enhanced Image with EWMStdKM, (g) Enhanced Image with EWDWTUM, (h) Enhanced Image with EWNSCT.

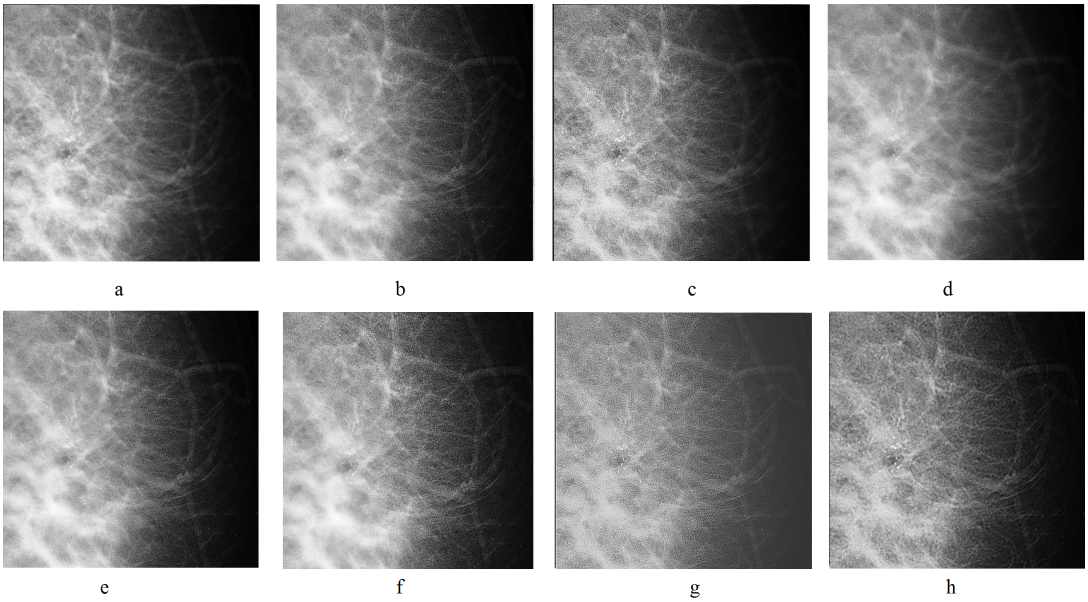

Figure 4.6: Output Images of Enhancement Methods: (a) Original Image (DICOM), (b) Enhanced Image with EWDFT (c) Enhanced Image with EWMStd, (d) Enhanced Image with EWDWT, (e) Enhanced Image with EWKM, (f) Enhanced Image with EWKMMStd, (g) Enhanced Image with EWDWTUM, (h) Enhanced Image with EWNSCT.

Table 4.1: Mean and Standart Deviations of Quality Measures for 33 MIAS Images

Enhancement Method	$\sqrt{(1-DSM)^2+(1-TBC)^2+(1-TBCE)^2}$		Discrete Entropy		Relative Entropy		Mutual Information		Intensity Contrast(GLCM)		Discrete Entropy(GLCM)		Structral Similarity Image Index		Universal Image Quality Index	
	Mean	Standard Deviation	Mean	Standard Deviation	Mean	Standard Deviation	Mean	Standard Deviation	Mean	Standard Deviation	Mean	Standard Deviation	Mean	Standard Deviation	Mean	Standard Deviation
EWFFT	**1.01**	**0.35**	**6.62**	**0.48**	**0.24**	**0.32**	**2.28**	**0.59**	**84.7**	**39.4**	**11.5**	**0.52**	**0.79**	**0.07**	**0.9955**	**0.02**
EWMStd	**1.01**	**0.34**	**6.70**	**0.45**	**0.48**	**0.54**	**1.90**	**0.50**	**148.3**	**57.6**	**11.95**	**0.50**	**0.68**	**0.06**	**0.9904**	**0.03**
EWDWT	**1.17**	**0.23**	**6.65**	**0.48**	**0.21**	**0.18**	**2.16**	**0.51**	**95.5**	**44.1**	**11.7**	**0.50**	**0.76**	**0.02**	**0.9967**	**0.01**
EWFFTKM	**0.97**	**0.28**	**6.82**	**0.44**	**0.77**	**0.60**	**1.68**	**0.47**	**214.4**	**77.5**	**12.37**	**0.52**	**0.59**	**0.06**	**0.9960**	**0.02**
EWMStdKM	**1.01**	**0.28**	**6.82**	**0.41**	**0.82**	**0.71**	**1.69**	**0.52**	**205.4**	**64.00**	**12.37**	**0.43**	**0.59**	**0.07**	**0.9969**	**0.02**
EWDWTUM	**1.16**	**0.28**	**6.70**	**0.46**	**0.81**	**0.29**	**2.08**	**0.50**	**160.3**	**43.26**	**11.8**	**0.49**	**0.73**	**0.03**	**0.9958**	**0.02**
EWNSCT	**1.06**	**0.29**	**6.75**	**0.42**	**0.53**	**0.49**	**1.90**	**0.52**	**117.6**	**4.00**	**11.9**	**0.39**	**0.68**	**0.04**	**1.0065**	**0.05**

Table 4.2: Mean and Standart Deviations of Quality Measures for 30 DICOM Images

Enhancement Method	$\sqrt{(1-DSM)^2+(1-TBC)^2+(1-TBCE)^2}$		Discrete Entropy		Relative Entropy		Mutual Information		Intensity Contrast(GLCM)		Discrete Entropy(GLCM)		Structral Similarity Image Index		Universal Image Quality Index	
	Mean	Standard Deviation	Mean	Standard Deviation	Mean	Standard Deviation	Mean	Standard Deviation	Mean	Standard Deviation	Mean	Standard Deviation	Mean	Standard Deviation	Mean	Standard Deviation
EWFFT	**1.0**	**0.64**	**7.18**	**0.35**	**0.20**	**0.32**	**2.76**	**0.82**	**196.8**	**136.1**	**12.3**	**0.96**	**0.87**	**0.035**	**0.83**	**0.04**
EWMStd	**0.95**	**0.57**	**7.18**	**0.36**	**0.46**	**0.57**	**2.57**	**0.72**	**239.2**	**159.3**	**12.4**	**1.05**	**0.81**	**0.061**	**0.78**	**0.07**
EWDWT	**0.95**	**0.73**	**7.09**	**0.28**	**0.72**	**0.49**	**1.44**	**0.63**	**759.7**	**370.8**	**13.3**	**1.05**	**0.61**	**0.044**	**0.58**	**0.06**
EWFFTKM	**1.13**	**0.61**	**7.20**	**0.35**	**0.36**	**0.46**	**3.12**	**0.77**	**164.2**	**120.3**	**12.3**	**0.90**	**0.87**	**0.073**	**0.84**	**0.07**
EWMStdKM	**1.12**	**0.68**	**7.33**	**0.33**	**0.45**	**0.60**	**1.61**	**0.58**	**433.3**	**142.8**	**13.4**	**0.13**	**0.57**	**0.258**	**0.49**	**0.36**
EWDWTUM	**1.0**	**0.65**	**7.21**	**0.12**	**0.54**	**0.32**	**1.22**	**0.46**	**891.4**	**260.4**	**13.7**	**0.22**	**0.62**	**0.036**	**0.60**	**0.05**
EWNSCT	**0.83**	**0.71**	**7.14**	**0.36**	**0.38**	**0.42**	**2.77**	**0.89**	**209.8**	**79.6**	**12.6**	**0.79**	**0.89**	**0.045**	**0.86**	**0.07**

Even the quality measures provides information about the performance of enhancement methods, it is important that the enhanced image is meaningful for diagnosis. In this study, the enhanced images were evaluated by a radiologist to chose enhancement method which provides clinically significant images. Following this, two methods were chosen for classification step. Tables 4.4-4.5 shows the evaluation of enhancement method by a radiologist for MIAS and DICOM images, respectively. The preferred enhancement for each image is labeled with $+$. For MIAS Images , EWMStd and EWDWT were chosen . For DICOM images , EWMStd and EWNSCT were chosen.

The comparison of the results of the quantitative measures and evaluation of the radiologist provides us how quantitative measures are effective to evaluate the performance of the enhancement methods. For MIAS images EWKM outperforms the other enhancement methods according to quality measures. However, a radiologist found the images which are enhanced by EWKM over enhanced . While the microcalcifications are more brighter and visible than their surrounding tissues, the pattern of the surrounding tissues changes too much. For DICOM images, it can be said that the results of quality metrics match with the assessment of the radiologist. In DICOM images, microcalcifications are carried by middle frequencies if the breast tissue is dense or microcalcifications are in a lesion. For these types of breast tissues, EWNSCT outperforms the detail enhancement methods by looking at quantitative measures .For a radiologist EWNSCT is more preferable, since microcalcifications are more detectable compared to other methods. For fatty tissues detail enhancement methods, EWFFT, EWMStd and EWDWT are preferable according to the assessment of the radiologist. Among these three enhancement methods EWMStd is more preferable than others. While EWFFT and EWDWT uses the frequency information for clustering, EWMStd uses the mean and standard deviation which is less complex than obtaining frequency information.

Table 4.3: Evaluation of Enhancement Methods for MIAS Images By a Radiologist

Image	DFT	MStd	DWT	KM	MStdKM	DWTUM	NSCT
mdb01			+				
mdb021			+				
mdb027	+		+				
mdb079							
mdb090							
mdb110	+		+				
mdb128	+						
mdb133			+				
mdb137			+				
mdb138	+		+				
mdb141	+	+	+				
mdb166			+				
mdb186			+				
mdb188	+	+	+				
mdb209			+				
mdb211	+	+	+				
mdb213	+	+	+				
mdb218			+				
mdb219	+						
mdb222			+				
mdb223	+	+	+				
mdb226		+	+				
mdb227		+	+				
mdb231	+	+					
mdb236		+	+				
mdb238		+	+				
mdb239		+	+				
mdb241		+	+				
mdb245	+	+	+				
mdb247		+					
mdb249		+	+				
mdb252	+	+	+				
mdb253		+					
mdb294		+					
mdb314	+	+	+				
TOTAL:	15	19	27				

Table 4.4: Evaluation of Enhancement Methods for DICOM Images By a Radiologist

Image:	DFT	MStd	DWT	KM	MStd_KM	DWT_UM	NSCT
1			+				
2	+						
3	+	+					
4	+						
5							+
6							+
7				+			
8							+
9							+
10							+
11							+
12			+				+
13							+
14			+				+
15	+	+	+				
16							
17	+						
18							
19							
20							+
21		+					
22		+					
23		+					
24		+					
25		+					
26		+					
27		+					
28	+						
29		+					
30		+					
TOTAL:	6	11	4				10

CHAPTER 5

FEATURE EXTRACTION AND CLASSIFICATION OF MICROCALCIFICATIONS

Feature extraction is needed for classification of microcalcification clusters as benign and suspicious for malignancy. The existing feature extraction methods based on statistical approaches, multichannel filtering, multiresolution analysis and filtering with special kernels. In this chapter , the feature extraction methods proposed for our study are expressed.

5.1 First Order Statistics (FOS)

First Order Statistics (FOS) shows the characteristics of the histogram of the enhanced ROI of the mammogram images. The drawback of FOS is that it does not give any information about relationship between the positions of each pixel. In some cases, noise is unidentified from the histogram, and has an effect on the calculation of FOS [55]. The FOS used in this thesis is given below:

$$Mean = \frac{1}{MN}\sum_{i}^{M}\sum_{j}^{N} p(i,j) \tag{5.1}$$

$$Sigma = \sqrt{\frac{1}{MN}\sum_{i}^{M}\sum_{j}^{N}(p(i,j)-\mu)^2} \tag{5.2}$$

$$Skewness = \sum_{i}^{K}\frac{(pdf(i)-\mu)^3/K}{\sigma^3} \tag{5.3}$$

$$Kurtosis = \sum_{i}^{K}\frac{(pdf(i)-\mu)^4/K}{\sigma^4} \tag{5.4}$$

$$Energy = \sum_{i,j} p(i,j)^2 \tag{5.5}$$

$$Entropy = \sum_{i,j} p_{i,j} Log_2(p_{i,j})) \tag{5.6}$$

In these expressions:

i-) M and N denote the sizes of the image.
ii-) $p(i,j)$ is the intensity value of pixel in the i^{th} row and j^{th} column.
iii-) $pdf(i)$ is the probability density function of gray level i.
iv-) K is the maximum gray level in the image.
v-) σ is the standard deviation of the image.
vi-) μ is the mean of the image.

Among these equations, skewness and kurtosis are related to the histogram of the image. Skewness is a measure based on symmetry. If the left and right of the center point of the histogram are similar, the histogram is symmetric. If the value of skewness is negative, it means that the frequencies of gray levels near black is greater than those near white. Similarly, if the value of skewness is positive, it means that the frequencies of gray levels near white is greater than those near black. For mammogram images which are enriched with microcalcifications, it is expected that skewness has a positive value. On the other hand, kurtosis is a measure whether the distribution of the histogram is peaked or flat. Positive kurtosis value denotes a 'peaked ' distribution while negative kurtosis value denotes 'flat' distribution [56]. Entropy is used in many parts of this thesis, especially in the evaluation of the performance of image enhancement methods. It's a measure of non-uniformity of the pixel values of the image. The entropy with a low value indicates high structural variance, and higher probability of microcalcifications on the image [57].

5.2 Second Order Image Statistics

The features extracted from the gray level co-occurance matrix is known as second order image statistics or Haralicks features. GLCM depicts how frequently two pixels with gray-levels i, j appear in the window separated by a distance d in direction Q [58]. The equations required for the calculation of GLCM for angles $0°$, $45°$, $90°$, and

$135°$, and for a distance d between the pixels are given below:

$$p_{0°,d}(i,j) = \begin{cases} [(k,l)(m,n)] \in D : \\ k-m=0, |l-m| = d \\ I(k,l) = i, I(m,n) = j \end{cases} \tag{5.7}$$

$$p_{45°,d}(i,j) = \begin{cases} [(k,l)(m,n)] \in D : \\ (k-m=d, |l-m| = -d) \\ (k-m=-d, |l-m| = d) \\ I(k,l) = i, I(m,n) = j \end{cases} \tag{5.8}$$

$$p_{90°,d}(i,j) = \begin{cases} [(k,l)(m,n)] \in D : \\ k-m=d, |l-m| = 0 \\ I(k,l) = i, I(m,n) = j \end{cases} \tag{5.9}$$

$$p_{135°,d}(i,j) = \begin{cases} [(k,l)(m,n)] \in D : \\ (k-m=d, |l-m| = d) \\ (k-m=-d, |l-m| = -d) \\ I(k,l) = i, I(m,n) = j \end{cases} \tag{5.10}$$

where $I(k,l)$ and $I(m,n)$ denote the intensities at pixel position (k,l) and (k,l), respectively.

For feature extraction, the contrast, correlation energy, and homogeneity values are calculated from each GLCM. The length of the feature vector is 16. Contrast is a measure of the differences between intensity of a pixel and its adjacent pixels on the whole image. Its value equals to 0 when the GLCM is constant and its maximum value for contrast is $(K-1)^2$ where K is the maximum intensity value in the image. Correlation is a measure of connection with a pixel and its neighbor on the whole image. It takes values between [-1,1] and it is undefined when the standard deviations

0	0	1	1
0	0	1	1
0	2	2	2
2	2	3	3

Figure 5.1: Example image with 4 gray levels [9].

0°	0	1	2	3
0	2	2	1	0
1	0	2	0	0
2	0	0	3	1
3	0	0	0	1

45°	0	1	2	3
0	2	1	0	0
1	0	1	0	0
2	0	2	2	0
3	0	0	1	0

90°	0	1	2	3
0	3	0	2	0
1	0	2	2	0
2	0	0	1	2
3	0	0	0	0

135°	0	1	2	3
0	1	1	2	0
1	0	1	0	0
2	0	0	0	2
3	0	0	0	0

Figure 5.2: GLCM with angles $0°$, $45°$, $90°$, and $135°$ and $d = 1$.

σ_i and σ_j are equal to 0. Homogeneity is a measure of the spatial affinity of the distribution of GLCM. When GLCM is a diagonal matrix, it is equal to 1 which is the maximum value [51].

$$Contrast = \sum_{i,j}^{K} |i-j|^2 p(i,j) \tag{5.11}$$

$$Correlation = \sum_{i,j}^{K} \frac{(i-\mu_i)(j-\mu_j)p(i,j)}{\sigma_i \sigma_j} \tag{5.12}$$

$$Energy = \sum_{i,j} p(i,j)^2 \tag{5.13}$$

$$Homogenity = \sum_{i,j} \frac{p(i,j)}{1+|i-j|} \tag{5.14}$$

5.3 Feature Extraction by using Laws Texture Energy Measures

Another approach for feature extraction is to calculate the Laws texture energy measures which consist of 25 local kernels proposed by Laws [59]. These kernels are computed from the vectors given in Table 5.2. The name of the vectors are mnemonics of their purposes. For instance, E5 is a vector of size 5 and used for detection of edges. There are 25 kernel obtained from these vectors. 23 of these kernels are high pass filters. For texture extraction, an image is convolved with masks. The information obtained from convolution of the same kernels is given in Table 5.1.

Table 5.1: 1D Laws Kernels.

Level	L5=[1 4 6 4 1]
Edge	E5=[-1 -2 0 2 1]
Ripple	R5=[1 -4 6 -4 1]
Spot	S5=[-1 0 2 0 -1]
Wave	W5=[-1 2 0 -2 1]

Table 5.2: Same 5×5 Laws Kernels Used for Texture Analysis

Kernel	Kernel aquistication using 1D kernels	Information extracted from texture
L5L5	$L5^{T}L5$	Gray level intensity of 5 adjacent pixels in both horizontal and vertical direction
L5E5	$L5^{T}E5$	Edge detection in horizontal direction Gray level intensity in vertical direction
L5S5	$L5^{T}S5$	Spot detection in horizontal direction Gray level intensity in vertical direction
E5L5	$E5^{T}L5$	Gray level intensity in horizontal direction Edge detection in vertical direction
E5E5	$E5^{T}E5$	Edge detection in both horizontal and vertical direction
E5S5	$E5^{T}S5$	Edge detection in vertical direction Edge detection in vertical direction
S5L5	$S5^{T}L5$	Gray level intensity in horizontal direction Spot detection in vertical direction
S5E5	$S5^{T}E5$	Edge detection in horizontal direction Spot detection in vertical direction
S5S5	$S5^{T}S5$	Spot detection in both horizontal and vertical direction

For feature extraction mean, standard variation, skewness and kurtosis values are calculated from Laws texture energy mask filtered images. The length of the feature vector is 100. The features are normalized between 0 and 1 for classification.

5.4 Feature Extraction by using Gabor Filter Bank

The 2D Gabor filter bank decomposes an image into components corresponding to different scales and orientation. It can be said that feature extraction by using Gabor filter is a good choice since it provides visual properties like spatial localization, spatial frequency and orientation selectivity [60]. For feature extraction, an image is convolved with 2D Gabor filter mask as given in equation (5.15). This 2D filter consists of a complex exponential centered at a given frequency f and and modulated by

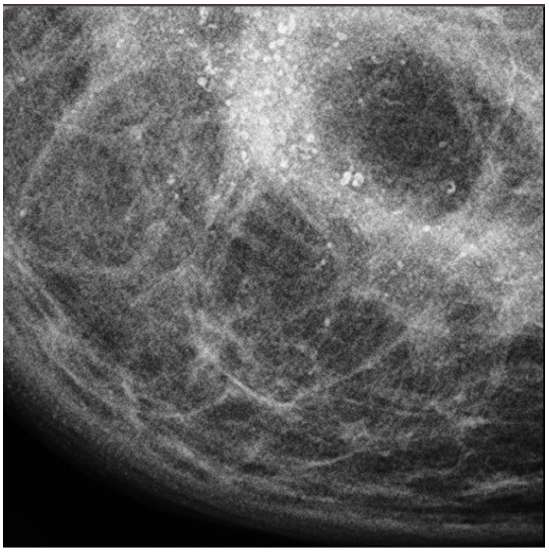

Figure 5.3: A ROI DICOM Image.

Gaussian envelop. f denotes central frequency of the sinusoidal plane wave. θ is the rotation angle of both the Gaussian major axis and the plane wave in interval [0,π). γ and η are parameters for sharpness along the major axis and the minor axis [61].

$$g(x,y) = \frac{f^2}{\pi\gamma\eta} e^{(-\frac{f^2}{\gamma^2}\tilde{x}^2 + \frac{f^2}{\eta^2}\tilde{y}^2)} e^{j2\pi f\tilde{x}} \tag{5.15}$$

$$\tilde{x} = xCos(\theta) + ySin(\theta) \tag{5.16}$$

$$\tilde{y} = -xSin(\theta) + yCos(\theta) \tag{5.17}$$

A Gabor filter bank consists of Gabor filters which are set by individual parameters. These parameters are central frequency, scales and orientation [62]. In general, number of scales is chosen as 5, while the number of orientations is chosen as 8. In this study, 5 scales and 8 orientations are used. This means that Gabor filter bank consists of 40 Gabor filters. The orientations are calculated by equation (5.18). The initial orientation is adjusted as 0°.

$$orientation(i) = \frac{(i-1)\pi}{8}; \quad i = 1, 2, ...8 \tag{5.18}$$

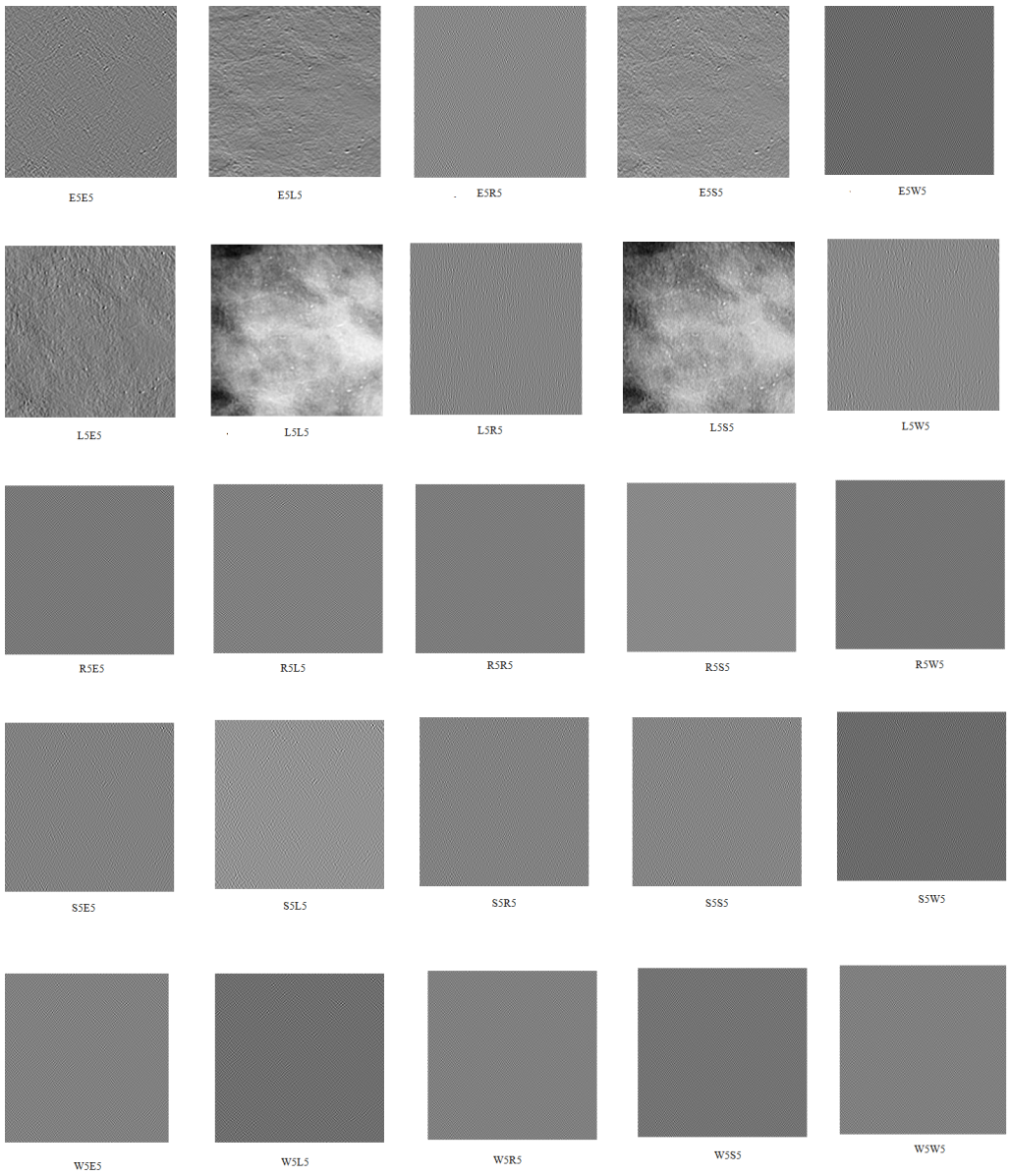

Figure 5.4: Results of Convolution with Laws Texture Energy masks.

The frequencies are adjusted by equation (5.19) and the initial maximum frequency (f_{max}) is chosen as 0.25.

$$frequencies(i) = \frac{f_{max}}{(\sqrt{2})^{i-1}}; i = 1, 2, ..5 \tag{5.19}$$

Since Gabor filter consists of complex exponential, it has both real and imaginary parts. Real part of the Gabor filter bank with 5 scale and 8 orientations are shown in Figure 5.5, the corresponding magnitude images are are given in Figure 5.6.

The ROI of mammogram image from MIAS dataset is depicted in Figure 5.7. The image convolved with this Gabor filter bank and the results of this convolution are given in Figure 5.8 and Fig.5.9. The features used for classification are obtained from the magnitude of the Gabor filters.

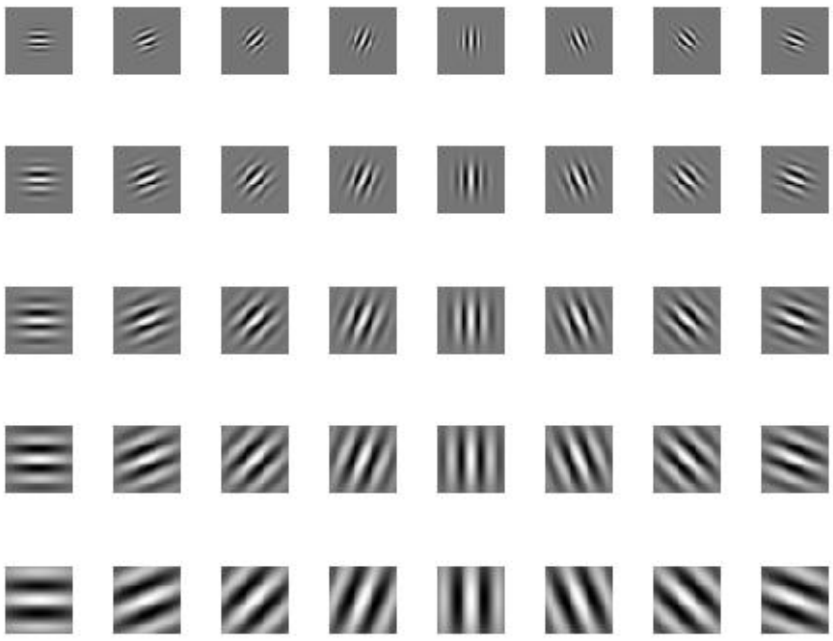

Figure 5.5: Real Parts of the Gabor filters (5 scales and 8 Orientation).

In our study, the Gabor filter bank is convolved with subregions instead of the whole

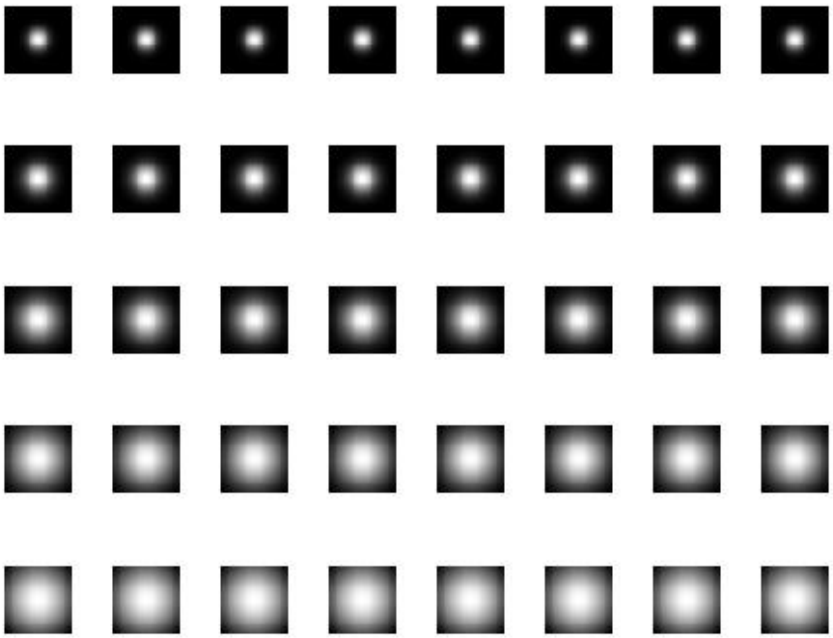

Figure 5.6: Magnitudes of the Gabor filters (5 scales and 8 Orientation).

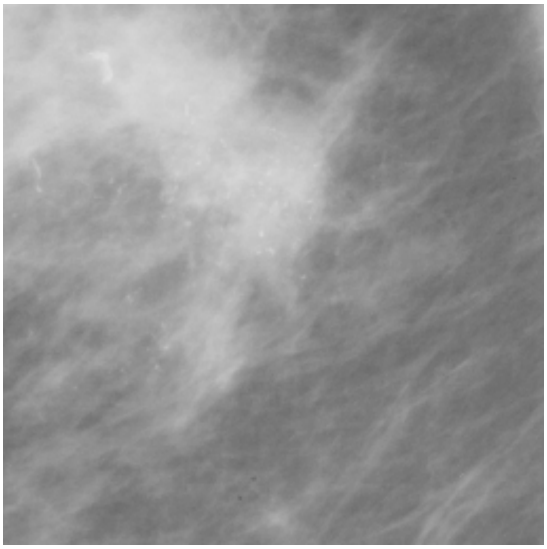

Figure 5.7: ROI of the mammogram image mdb209 from the MIAS database.

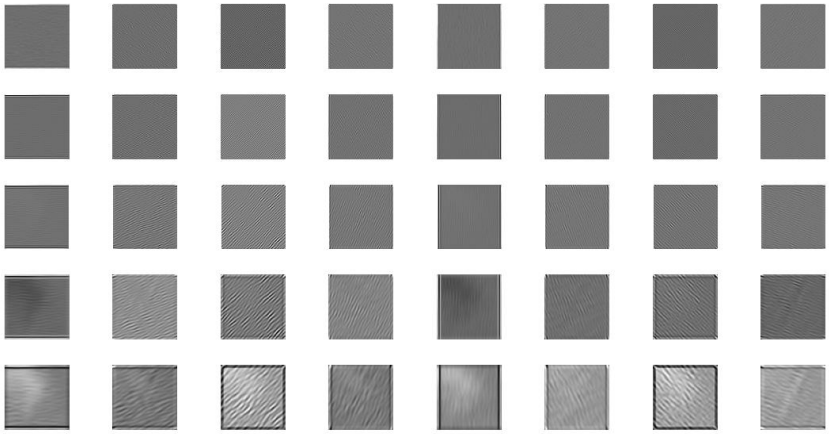

Figure 5.8: Real Parts of the Gabor filtered Image mdb209 (5 scales and 8 Orientation).

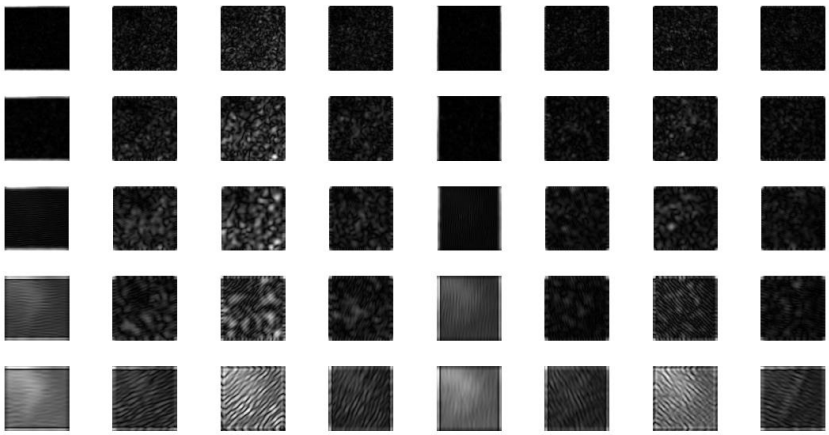

Figure 5.9: Magnitudes of the Gabor Filtered Image mdb209 (5 scales and 8 Orientation).

ROI of mammogram image. The dimension of the ROI of each mammogram image is 512×512. This whole ROI is divided into blocks with size 128×128. Totally 16 blocks are obtained. Then subregions are created by 4 adjacent blocks. 9 subregions are obtained, totally. Illustration of acquisition of these subregions is shown in Figure 5.10. Each area covered with colorful squares represents a subregion. For example last subregion consists of 11^{th}, 12^{th} , 15^{th} and 16^{th} blocks and covered with a yellow square.

Figure 5.10: Illustration of subregion acquisition.

For feature extraction, each subregion is convolved by Gabor filter. Mean, standard deviation, skewness and kurtosis values are obtained from magnitudes of the Gabor filtered subregions. For each subregion, 40 Gabor filtered sub-images are obtained (totally 360). For each sub-images, 4 features are obtained. Length of feature vector for an image is 1440.

5.5 Feature Extraction Based on NSCT

As mentioned in the multi resolution analysis section, the directional decomposition of images provides directional information or energy along a specific direction. Besides image enhancement and image coding, multi resolution analysis is used for

texture analysis due to this property. The method chosen for feature extraction is based on decomposition of the image into directional sub-bands at each scales and calculation of the energy of each subband. For this purpose, firstly the enhanced ROI is decomposed by NSCT at 3 scales. For scale 2, 2 direction is chosen while for scales 3 and 4, 8 directions are chosen. After obtaining subbands by the NSCT decomposition, the energy of each sub-band is calculated. The length of the feature vector that consists of these energy values is 18. The feature vector is normalized between 0 and 1 for classification [26].

5.6 Dimension Reduction Of Features

Dimension reduction is representation of multidimensional data by projecting it on lower dimensions. We need dimension reduction to visualize our data to decide which classifier is suitable for classification, and to reduce the computational cost of the classification operation. For dimension reduction, Fisher Linear Discriminant Analysis(FLDA) is employed in our study. In case, the number of samples is less than the dimension of the feature vector, FLDA will overfit. Principal component analysis (PCA) is applied before FLDA to reduce the dimension of the feature vector to the number of samples-1. Using the PCA before FLDA provides a sort of regularization and prevents overfitting.

FLDA can be used for linear classification. It can also be used for dimension reduction for the feature space. Similar to PCA, it projects high dimensional data onto lower dimension, but it aims to show how the classes are separated from each other. Note that, PCA does not provide class information of the data. It is expected that the distance between the means of the data that belong to each class is as large as possible. In other words, it tries to make class distribution separable.

For data with 2 classes (C_1 and C_2), the mean values of the classes are calculated as follows:

$$M_1 = \frac{1}{N_1} \sum_{x \epsilon C_1} x \tag{5.20}$$

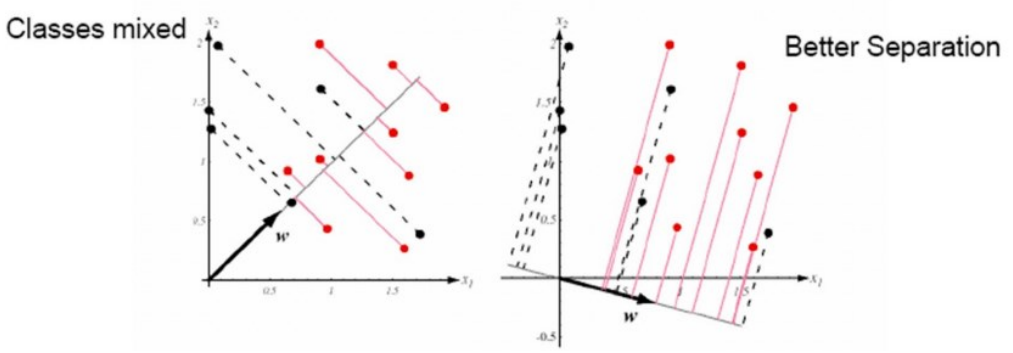

Figure 5.11: Results of the FLDA with the worst projection and the best projections [10].

$$M_2 = \frac{1}{N_2} \sum_{x \epsilon C_2} x \tag{5.21}$$

where N_1 and N_2 are the number of data in class C_1 and C_2, respectively.

The means of projected data on W that belongs to class C_1 and C_2 are:

$$M_1' = \frac{1}{N_1} \sum_{x \epsilon C_1} W^T x \tag{5.22}$$

$$M_2' = \frac{1}{N_2} \sum_{x \epsilon C_2} W^T x \tag{5.23}$$

The distance between the means of the projected classes is obtained by:

$$|M_1' - M_2'|^2 = |W^T M_1 - W^T M_2|^2 \tag{5.24}$$

It is expected that the data points from the same class are very close to each other. There is a measure to show the variability within the class after it is projected on the W space, which is called class scatter or variance in the scatter. It is represented by S_i^2 for class C_i.

$$S_i^2 = \sum_{x \epsilon C_i} (W^T x - M_i)^2 \tag{5.25}$$

Sum of S_1^2 and S_2^2 measures the variability within the 2 classes after the projection.

FLDA tries to find W space that optimize the cost function J which is denoted by

$$J(W) = \frac{|M_1' - M'2|^2}{S_1^2 + S_1^2} J(W) = \frac{(W^T M_1 - W^T M_2)^2}{W^T (S_1 + S_2 W} \tag{5.26}$$

Function $J(W)$ can be modified as:

$$J(W) = \frac{(W^T S_B W)}{W^T S_W W} \tag{5.27}$$

where S_B is the *between class scatter matrix* and S_W is the *within class scatter matrix*.

The derivative of $J(W)$ is equal to 0 when W is maximum. The equation obtained from the derivative of J(W) is:

$$S_W^{-1} S_B W - J(W) W = 0 \tag{5.28}$$

$$S_W^{-1} S_B W = \lambda W \text{where} \lambda = J(W) \tag{5.29}$$

$$W^* = \arg\max_W J(W) = \arg\max_W \frac{W^t S_W W}{W^t S_W W} = S W^{-1} (M_1 - M_2) \tag{5.30}$$

By projecting the feature data on W^* one obtains a low dimensional data with a separable class.

5.7 Classification with Support Vector Machines (SVM)

SVM is the most powerful supervised learning technique that can be used as both linear and non-linear classifier. Hyperplane is the decision surface for classification. SVM attempts to find a hyperplane with a maximum margin. Margin is the distance between the hyperplane and half spaces that are the nearest labeled vectors [63].

The hyperplane $f(x)$ is formulated by:

$$f(x) = Wx + b = 0 \tag{5.31}$$

where W is the normal vector, X is the training data and b is the offset. The half spaces are determined according to this hyperplane. The optimum hyperplane can be found by minimizing the following cost function J.

$$J(W) = \|W\|^2/2 \tag{5.32}$$

subject to

$$W^T x_i + b \geq 1, \text{for } y_i = 1 \tag{5.33}$$

$$W^T x_i + b \geq -1, \text{for } \; y_i = -1 \; ; i = 1, 2, ..., n \tag{5.34}$$

$$y_i(W^T x_i + b) \geq 1; i = 1, 2, ..l. \tag{5.35}$$

where $\|W\|$ is the length of the weight vector and y_i is the label of classes that can get value -1 or 1. l is the number of training sample. To eliminate the misclassification non zero slack variable vector ξ that consists of slack variables ξ_i is added to equation (5.35):

$$y_i(W^T x_i + b) \geq 1 - \xi_i; \xi_i \geq 0; i = 1, 2, ..l. \tag{5.36}$$

The cost function will change according to ξ_i:

$$J(W, \xi) = \frac{\|W\|^2}{2} + C \sum_{i}^{l} \xi_i \tag{5.37}$$

where C is positive regularization parameter that is assigned by the user. It is called as soft margin.

If the data in R^d is non separable, the feature spaces are taken to be the non-linear projection of the input data to the higher dimensional space by a kernel function. ϕ denote the non-linear operator to map the input data x_i into the higher dimensional space.

The hyperplane for non-linear cases is formulated as:

$$f(x) = W^T \phi(x) + b \tag{5.38}$$

where $\phi(x)$ is the transformed data. The cost function to decide hyperplane is different from that of the linearly separable cases is:

$$minJ(w, \xi) = \frac{\|W\|^2}{2} + C \sum_{i=1}^{L} \xi_i \tag{5.39}$$

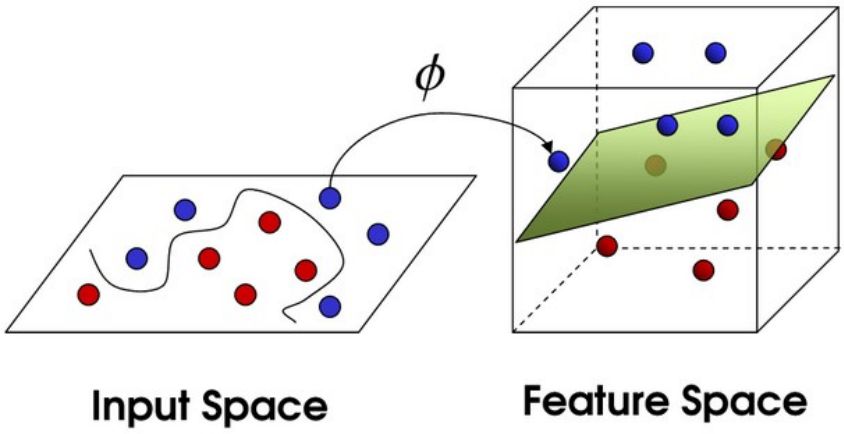

Figure 5.12: Non-linear mapping: The 2D input space is projected on 3D space by the ϕ transform

subject to

$$y_i(W^T\phi(X_i) + b) \geq (1 - \xi_i)\ \xi_i \geq 0; i = 1, 2, ...l \tag{5.40}$$

To minimize the cost function $J(w, \xi)$ Langrange multipliers are used. According to this, the weight vector W is formulated by :

$$W = \sum_{i=1}^{l} \alpha_i y_i \phi(x_i) \tag{5.41}$$

where $\alpha_i \geq 0$, i=1,2..,l are the Lagrange multipliers. The equation for the hyperplane can be rewritten as

$$f(x) = \sum_{i=1}^{l} \alpha_i y_i \phi^T(x_i)\phi(x_i) + b \tag{5.42}$$

In this equation, $\phi^T(x_i)\phi(x_i)$ is replaced with $K(x_i, x)$.

$$K(x, z) = \phi^T(x)\phi(z) \tag{5.43}$$

The Lagrange multipliers α_i are calculated by :

$$maxW(\alpha_1, \alpha_2, .., \alpha_l) = \sum_{i=1}^{l} \alpha_i - \frac{1}{2}\sum_{i=1}^{l}\sum_{j=1}^{l} \alpha_i\alpha_j y_i y_j K(x_i, x_j) \tag{5.44}$$

subject to

$$\sum_{i=1}^{l} \alpha_i y_i = 0 \tag{5.45}$$

In the formulas above, $W(\alpha_1, \alpha_2, .., \alpha_l)$ is the cost function corresponding α_i.

Finding α_i are interpreted in 3 ways:

Firstly, if α_i equals to 0, it indicates that $y_i f(x_i)$ is grater than 1. The data point x_i is outside the decision margin of the hyperplane. This means that x_i is classified correctly.

Secondly, if α_i takes a value between 0 and C, it indicates that $y_i f(x_i)$ is equal to 1. These shows that the data point x_i is on the decision margin of hyperplane. For this case, x_i is called as the 'support vector'.

Finally, if α_i is equal to C, it indicates that $y_i f(x_i)$ is less than 1. The data point x_i is inside the decision margin. It is not certain that x_i is classified correctly. For this case, x_i is called as 'error'. To simplify the hyperplane function, the support vectors are represented with s_j and non zero Lagrange multipliers are represented with α_i^*. The resultant formula of hyperplane is given as follows:

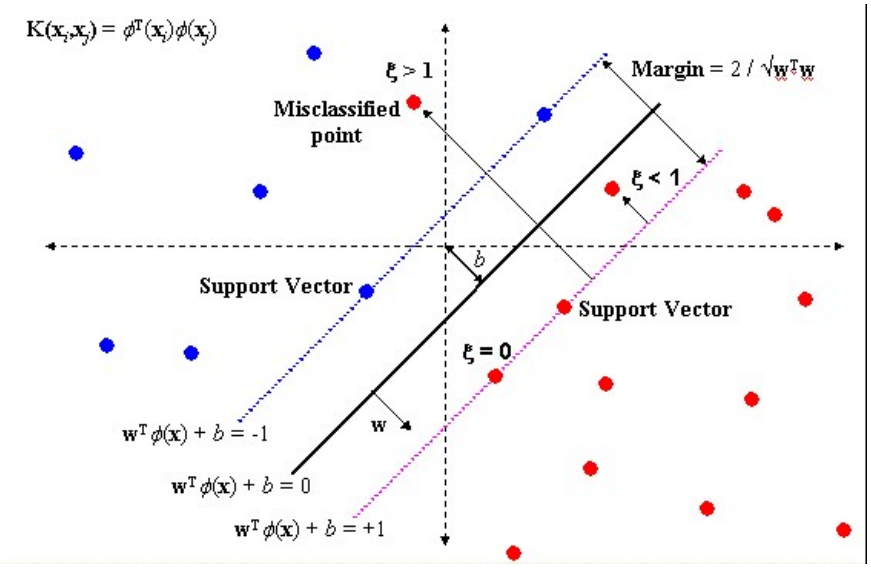

Figure 5.13: SVM Classification Demonstration.

$$f(x) = \sum_{j=1}^{l_s} \alpha_i^* y_i \phi^T(x_i)\phi(x_i) + b \tag{5.46}$$

$$f(x) = \sum_{j=1}^{l_s} \alpha_i^* y_i K(s_j, x) + b \tag{5.47}$$

In this study, as the dimension of feature vector is greater than 2, we are incapable of visualizing the distribution of benign and malignant microcalcification clusters. For this reason we do not know if our data is separable or non separable. In this case, to use the non linear SVM classifiers is suitable. For the non-linear SVM classifiers, the input space is projected into a space with higher dimension by kernel function K derived from non mapping function ϕ as it mentioned previously. We choose Gaussian radial basis kernel function (rbf) as a kernel. For this kernel, a new feature space is a Hilbert space of infinite dimensions. Rbf kernel is defined as:

$$K(x, y) = e^{(-\frac{\|x-y\|^2}{2\sigma^2})} \tag{5.48}$$

where σ is the kernel width and always takes positive value. Sometimes $\frac{1}{2\sigma^2}$ is replaced by γ.

$$K(x, y) = e^{-\|x-y\|^2\gamma} \tag{5.49}$$

The success of classification by using SVM depends on the selection of γ and soft margin C. The optimum γ and C parameters can be find by grid search by assigning exponentially growing values γ and C parameters. Generally range of C parameter values are chosen between 2^{-5} and 2^{15}, while the range of γ values are between 2^{-15} and 2^3. Implementation of SVM with the features mentioned before and its results is discussed Chapter 6.

CHAPTER 6

EXPERIMENTAL RESULTS OF CLASSIFICATION WITH SVM

To observe the effect of enhancement operation on classification of microcalcification, classification is applied on ROI of original images and enhanced images by chosen 2 enhancement methods by a radiologist. Before using database consists of DICOM images obtained from hospitals, the feature extraction and classification operations are applied on mini-MIAS database. 33 images with microcalcification clusters and other types of calcifications from these database are selected. The size of ROI of these images is chosen 256×256. 14 images from these selected images are labeled as 'benign' and the rest of them are labeled as 'suspicious' under the supervision of a radiologist. Some of selected regions with benign and suspicious calcifications for malignancy are shown in Figure 6.1 and Figure 6.2, respectively.

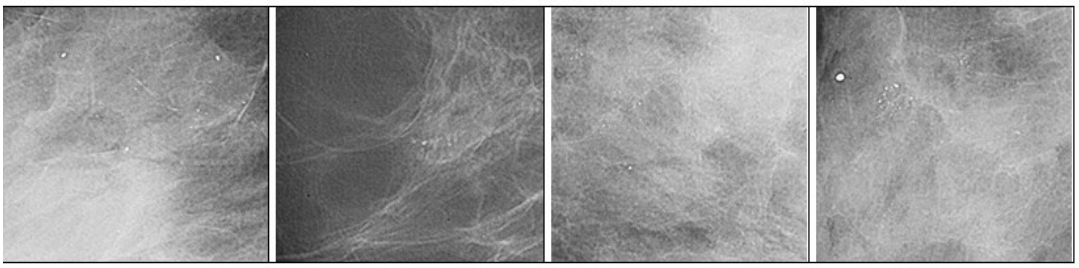

Figure 6.1: Several Images Labelled as Benign

For classification by using all feature types,10 percent of both benign and suspicious samples are chosen for training set and the rest of them are chosen for test set. These

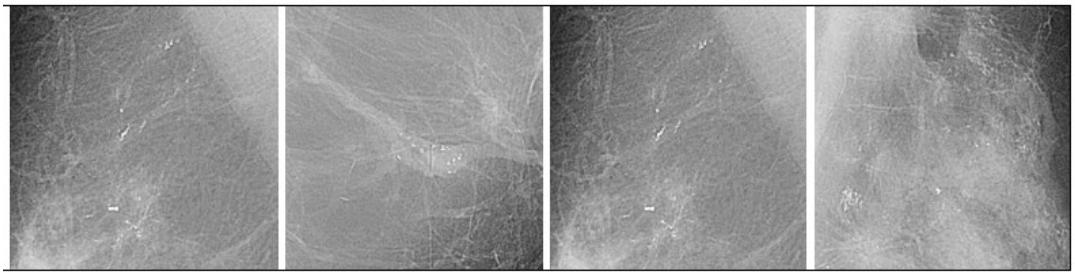

Figure 6.2: Several Images Labelled as Malignant

training and test sets consists of randomly selected samples. The classification operation is iterated 15 times. The average of area under the ROC curve (AUC) is calculated for 15 iterations respect to defined γ and C parameters. Additionally, the average of truth rate(rate of correctly classified samples) is calculated for 15 iterations.

The results of classification with considered features extracted from original images, enhanced images by EWMStd and EWDWT which are chosen by a radiologist are given Figures 6.3-6.8.

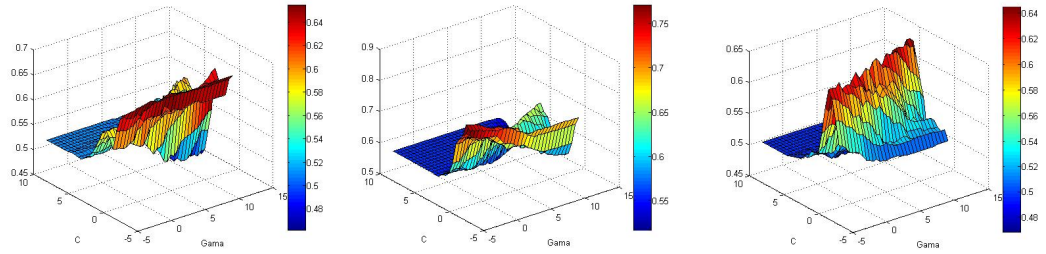

Figure 6.3: Results of classification with FOS : Left: For original images maximum average AUC is 0.65 . Middle: For enhanced images by EWMStd maximum average AUC is 0.77 . Right: For enhanced images by EWDWT maximum average AUC is 0.64.

Following this experiment by using images from mini-MIAS data set, classification of DICOM images with different types of feature set is performed. Totaly 70 regions with microcalcifications and punctate calcifications are used. The size of ROI of these images is chosen 512×512. These samples are labeled according to radiological reports belongs to them. The samples which are diagnosed with BI-RADS 3 are

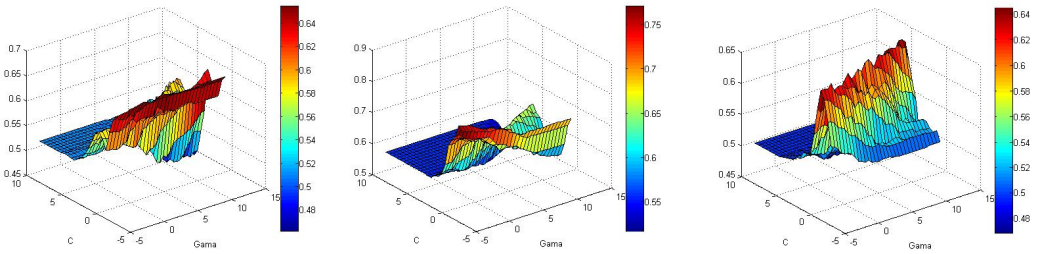

Figure 6.4: Results of classification with FOS : Left: For original Images maximum average truth rate is 0.58. Middle: For enhanced images by EWMStd maximum average truth rate is 0.77. Right: For enhanced images by EWDWT maximum truth rate is 0.67

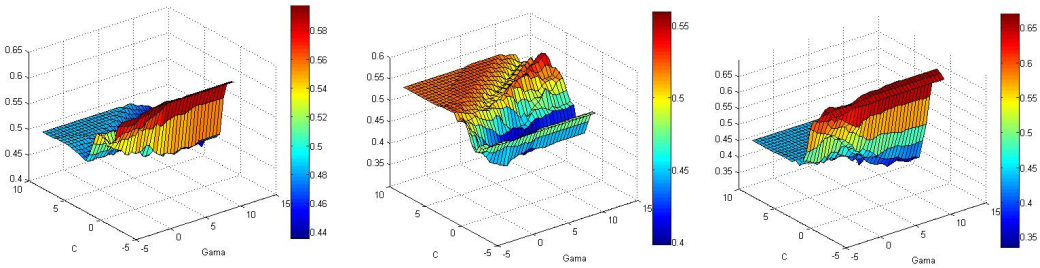

Figure 6.5: Results of classification with GLCM : Left: For original images maximum average AUC is 0.60. Middle: For enhanced images by EWMStd maximum average AUC is 0.56. Right: For enhanced Images by EWDWT maximum average AUC is 0.68

labeled as 0 (benign) and those which are diagnosed with BI-RADS 4 are labeled as 1 (suspicious). There are 29 images labeled as benign and 41 images as labeled malignant.

For classification by using all feature types, 50 percent of both benign and malignant samples are chosen for training set and the rest of them are chosen for test set. These training and test sets consists of randomly selected samples. The classification operation is iterated 30 times. The average of area under the ROC curve (AUC) is calculated for 30 iterations respect to defined γ and C parameters. Additionally, the average of truth rate(rate of correctly classified samples) is calculated for 30 iterations.

First classification is performed with features obtained from FOS. Since the dimension of feature vector is less than number of samples, it does not need to reduce the

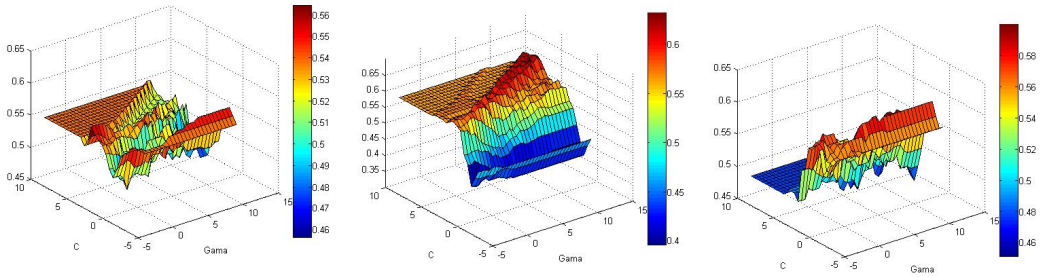

Figure 6.6: Results of classification with GLCM : Left: For original images maximum average truth rate is 0.56. Middle: For enhanced images by EWMStd maximum average truth rate is 0.63. Right: For enhanced images by EWDWT maximum truth rate is 0.60

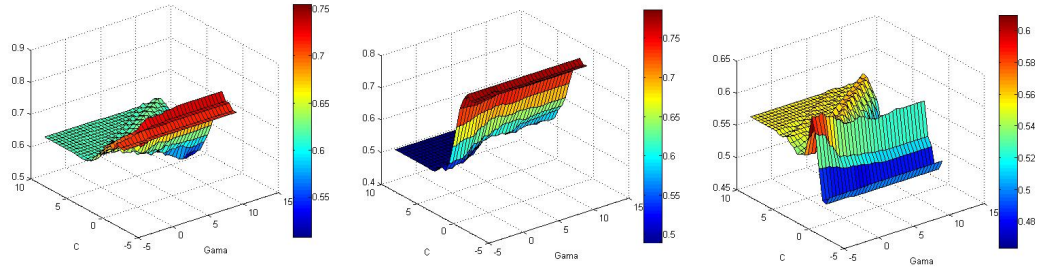

Figure 6.7: Results of classification with energy of NSCT coefficients : Left: For original images maximum average AUC is 0.75 . Middle: For enhanced images by EWMStd maximum average AUC is 0.79. Right: For enhanced images by EWDWT maximum average AUC is 0.61.

dimension of feature vector. The left plot given in Figure 6.9 shows the average of areas under the ROC for 30 iterations for original images, the middle plot hows the average of areas under the ROC for 30 iterations for enhanced images by EWMStd, and the right plot shows the average of areas under the ROC for 30 iterations for enhanced images by EWNSCT, respectively .

The results of classification with using GLCM are given Figures 6.12-6.13.

The results of classification with using Laws texture features are given Figures 6.13-6.14. The number of features are reduced to 7, since it is believed that for a best classification number of samples should be 10 times greater than number of features. To do this, FLDA is applied on training data, the test data is projected on W obtained from FLDA.

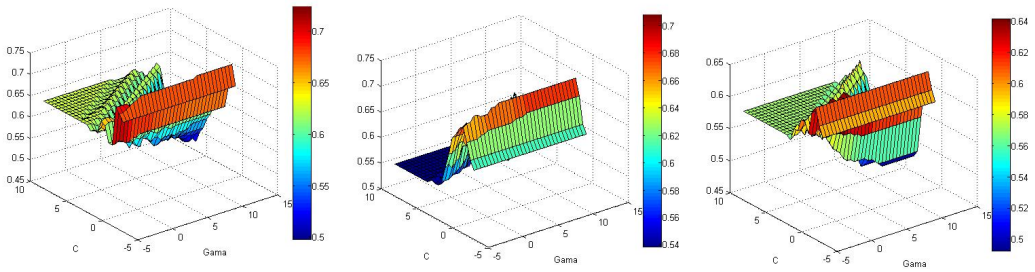

Figure 6.8: Results of classification with energy of NSCT coefficients : Left: For original images maximum average truth rate is 0.65. Middle: For enhanced images by EWMStd maximum average truth rate is 0.68. Right: For enhanced images by EWDWT maximum truth rate is 0.61

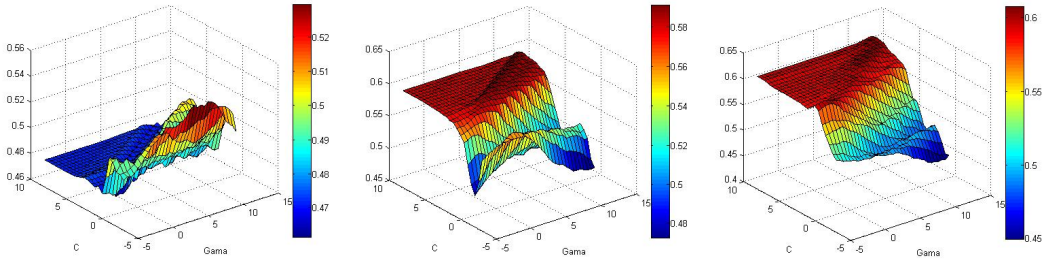

Figure 6.9: Results of classification with FOS : Left: For original images maximum average AUC is 0.53. Middle: For enhanced images by EWMStd maximum average AUC is 0.59. Right: For enhanced images by EWNSCT maximum average AUC is 0.61

The results of classification with using energy of NSCT coefficients are given Figures 6.15-6.16 .

Finally classification is performed with features obtained from Gabor filter bank. The dimension reduction of features to 7 same as classification with using Laws Texture features is applied. Results of classification by using Gabor filter bank is given in Figures 6.17-6.18.

According to these results, it is observed that best classification is obtained by features obtained from Gabor filter banks and enhanced images with EWMStd by 77 percent truth rate (the area under the ROC curve is 0.81) . However there is no dramatic change the performance of classification compared to classification by using ROI of the original images.

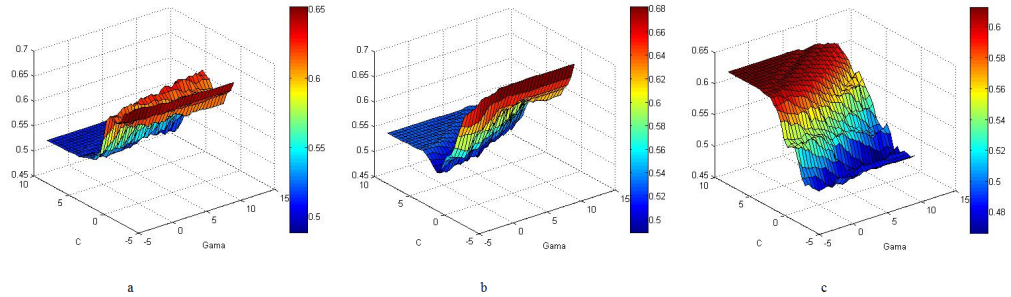

Figure 6.10: Results of classification with FOS : Left: For original images maximum average truth rate is 0.56. Middle: For enhanced images by EWMStd maximum average truth rate is 0.57. Right: For enhanced images by EWNSCT maximum truth rate is 0.59

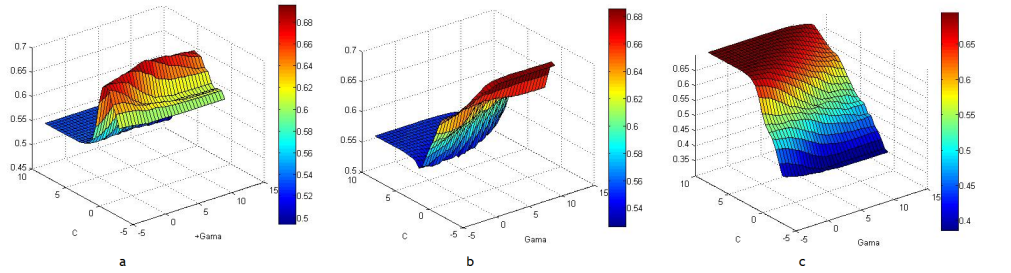

Figure 6.11: Results of classification with GLCM : Left: For original images maximum average AUC is 0.69. Middle: For enhanced images by EWMStd maximum average AUC is 0.69. Right: For enhanced images by EWNSCT maximum average AUC is 0.69

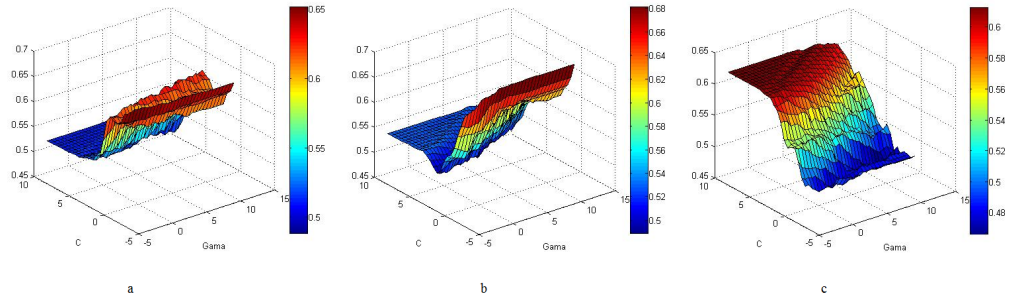

Figure 6.12: Results of classification with GLCM : Left: For original Images maximum average truth rate is 0.65. Middle: For enhanced Images by EWMStd maximum average truth rate is 0.68. Right: For enhanced Images by EWNSCT maximum truth rate is 0.61

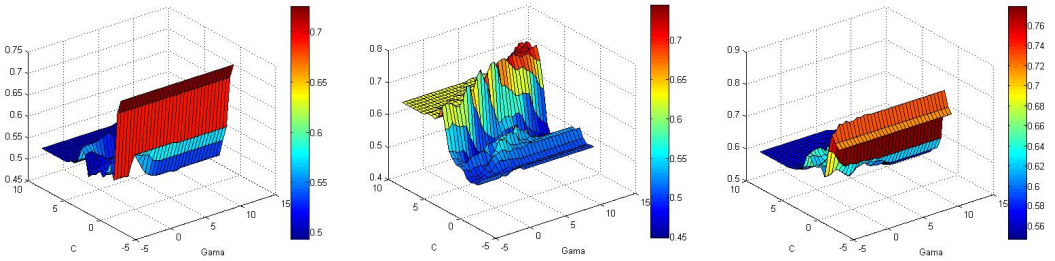

Figure 6.13: Results of classification with Laws texture features : Left: For original images maximum average AUC is 0.72. Middle: For enhanced images by EWMStd maximum average AUC is 0.74. Right: For enhanced images by EWNSCT maximum average AUC is 0.78

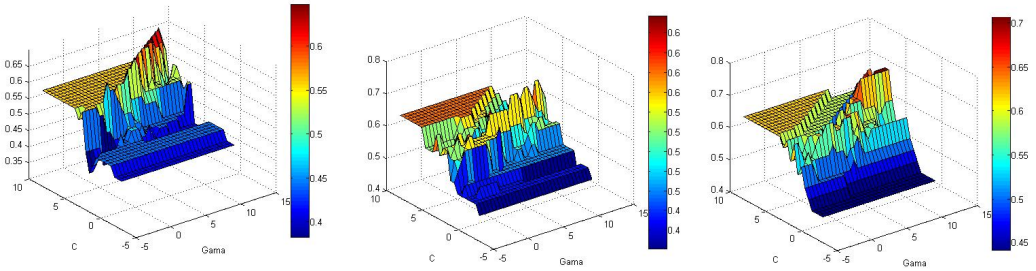

Figure 6.14: Results of classification with Laws texture features: Left: For original images maximum average truth rate is 0.65. Middle: For enhanced images by EWM-Std maximum average truth rate is 0.68. Right: For enhanced images by EWNSCT maximum truth rate is 0.71

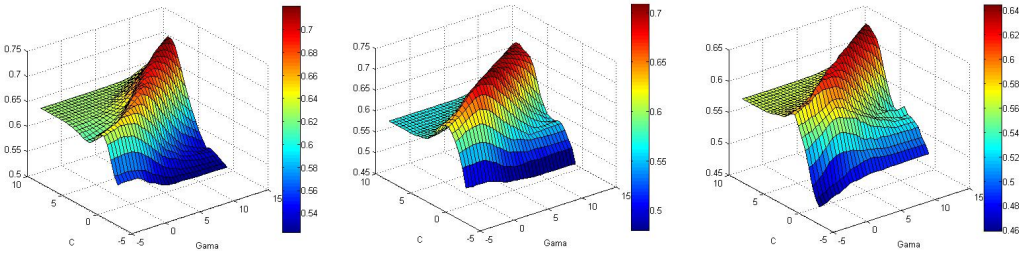

Figure 6.15: Results of classification with energy of NSCT coefficients : Left: For original images maximum average truth rate is 0.64 . Middle: For enhanced images by EWMStd maximum average truth rate is 0.65 . Right: For enhanced images by EWNSCT maximum truth rate is 0.58

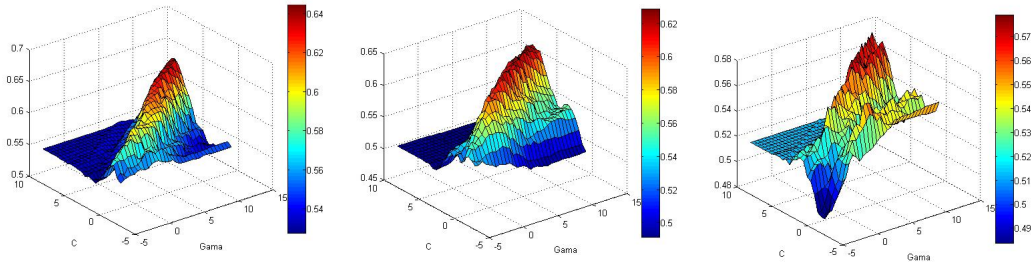

Figure 6.16: Results of classification with energy of NSCT coefficients : Left: For original images maximum average truth rate is 0.72. Middle: For enhanced images by EWMStd maximum average truth rate is 0.74. Right: For enhanced images by EWNSCT maximum average truth rate is 0.78

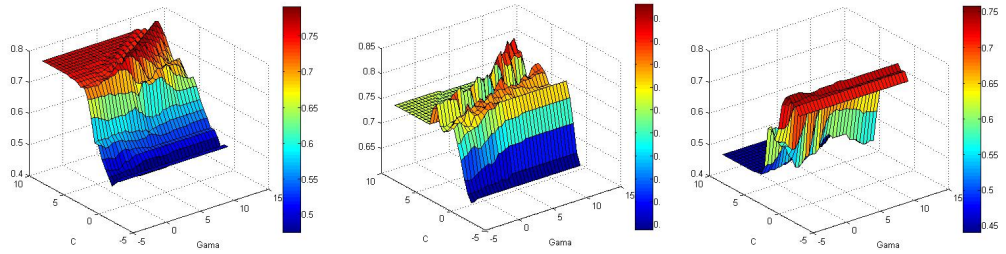

Figure 6.17: Results of classification with Gabor Filter Bank : Left: For original Images maximum average AUC is 0.79. Middle: For enhanced Images by EWMStd maximum average AUC is 0.81. Right: For enhanced Images by EWNSCT maximum average AUC is 0.76

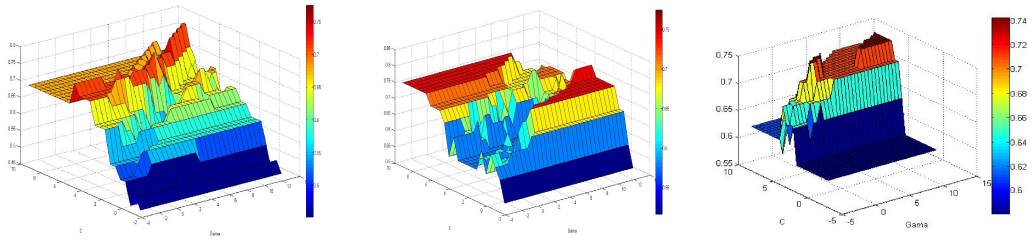

Figure 6.18: Results of classification with Gabor Filter Bank: Left: For original Images maximum average truth rate is 0.77. Middle: For enhanced Images by EWMStd maximum average truth rate is 0.77. Right: For enhanced Images by EWNSCT maximum truth rate is 0.74

To compare feature extraction by Gabor Filter Banks and the other feature extraction methods, features are obtained from Gabor filter bank locally.

CHAPTER 7

CONCLUSION AND FEATURE WORK

Breast cancer is the second leading cause of cancer deaths for women. Early diagnosis of breast cancer is important for treatment of it. Mammography is the most effective technology presently available for breast cancer screening, despite the fact that there are still some limitations of the imaging technique. It is also important to catch small details like microcalcifications, which may be first sign of breast cancer. To identify them, a high spatial resolution is necessary. As the difference between X-ray attenuation of normal and cancerous tissues are quite small, it is difficult to detect microcalcification clusters in some cases. The breasts of younger woman contains more glands and ligaments resulting in dense breast tissue. In heterogeneously dense breast, it is difficult to detect cancerous tissue on mammogram, since the fibrograndular tissue may hides the abnormalities. With aging, the breast tissue become fattier and has fewer glands. In this case, it is more easier to detect cancer related tissues on mammogram images. Insufficient resolution, low local contrast and noise combined with the subtle nature of the usual radiographic findings are other limitations of mammography.

In this study, it is aimed to develop computer aided diagnosis (CAD) system in order to increase the efficiency of the mammographic screening processing order to provide automated detection of microcalcification clusters leading a considerable decrease in misdiagnosis rates.

For this purpose, several image enhancement algorithms on both spatial domain (histogram modeling, morphological operators) and frequency domain(detail enhancement based on frequency, multiresolution analysis etc.) have been implemented on

region of interest (ROI) of real mammogram images which include microcalcification clusters. Among this methods, detail enhancement methods and enhancement methods based on multiresolution analysis are preferred. Both types of enhancement methods are based on identification of the region with microcalcification cluster and determining the specific coefficients to amplify them. Detail enhancement methods are local enhancement methods and enhancement methods based on multiresolution analysis are global methods. It was considered that local enhancement methods provides better enhancement results compared to global approaches. Among detail enhancement methods, DWT provides geometrical information compared to DFT. Wavelet coefficients obtained by DWT achieve to detect point-like objects such as microcalcifications.

To evaluate the performance of enhancement algorithms, quantitative measures have been implemented and assessment of radiologists was considered, since the enhanced image should be meaningful for diagnosis. Two enhancement methods chosen by a radiologist were preferred to observe efficiency of enhancement for classification.

Following enhancement operation, textural features have been extracted from ROI original images and enhanced images by chosen enhancement methods. Different types of textural features are extracted As a next step classification by using SVM were performed. To achieve best classification the different variables of parameters of SVM γ and C which defined by user were selected.For DICOM images, classification operation was iterated 30 times. For each iteration 50 percent of each data was selected as an training set and the rest of it was selected as test set. The samples are labeled as 0 for images diagnosed with BIRADS 3 and 1 for images diagnosed by BIRADS 4. Before classification first PCA and then FLDA were applied to reduce dimension of feature vector, since for number of some features are greater than number of samples and this could cause overfitting.

To evaluate performance of classification with different features, under the area of ROC and truth rate were considered. The average of these values obtained from 30 iterations are calculated.

According to performance of classifications, it is observed that best classification is obtained by features obtained from Gabor filter banks and enhanced images with

EWMStd by 77 percent truth rate (the area under the ROC curve is 0.81). For classifications on all feature types and enhanced images with EWMStd the performance of classification was generally increased. However, there is no dramatic change(2-3 %) the performance of classification compared to classification by using ROI of the original images. To compare feature extraction by other feature extraction methods, features are obtained from Gabor filter bank locally. The chosen ROI was chosen 512×512 which may include more background information for grouped microcalcifications in small area. Decrease in size of ROI causes less spatial resolution.

Shape could be a significant feature for decide type of microcalcification cluster. However, shape analysis is unable for individual microcalcifications because of their small size.

The classification operation could be more effective if it is performed for fatty breast tissues and dense breast tissues individually. Since the number of samples are quite less in comparison with other studies in literature, it could not be implemented on this thesis. As a future work by increasing number of samples, it is believed that performance of classification is found accurately. Novel quasi supervised learning methods based on Bayesian approaches are not preferred for this study .If the number of data reaches 1000 at least, these methods can be tried for classification of microcalcification and they can be modified.

In this study, CAD was developed for only detection and classification of microcalcifications. However, there are more breast abnormalities such as mass, architectural distortion that can be a first sign of breast cancer. Similar CAD would be proposed for automatic detection of these abnormalities and combination of them could be profitable for radiologist to first diagnosis of breast cancer and eliminate unnecessary biopsy operations.

Other future work for this study could be a design of a user interface. As the display range of MATLAB is under the gray level of DICOM images, it needs some adjustments. These adjustments are not enough to display images for best diagnosis. For this reason the user interface conjugated with DICOM viewer could be develop by other programming languages such as IMAGE J framework of JAVA.

REFERENCES

[1] M. Rizzi, M. D'Aloia, and B. Castagnolo, "Review: Health care CAD systems for breast microcalcification cluster detection," *Journal of Medical and Biological . . .*, vol. 32, no. 3, pp. 147–156, 2012.

[2] "Worldwide Cancer Incidence Statistics." : Cancer Research UK. N.p., n.d. Web. 04 Jan. 2015. <http://www.cancerresearchuk.org/cancer-info/cancerstats/world/incidence/>

[3] "Mammography - Canadian Cancer Society." Www.cancer.ca. N.p., n.d. Web. 02 Jan. 2015. <http://www.cancer.ca/en/cancer-information/diagnosis-and-treatment/tests-and-procedures/mammography/?region=on>.

[4] E. Exhibit, V. M. Campos, J. M. S. Martinez, C. B. Carron, J. A. Guirola, and J. A. F. Gomez, "Tracks to face a breast imaging and succeed," pp. 1–44, 2013.

[5] Kim, Hyoung-Joon, et al. "Contrast enhancement using adaptively modified histogram equalization." Advances in Image and Video Technology. Springer Berlin Heidelberg, 2006. 1150-1158.

[6] M. Do and M. Vetterli, "Framing pyramids," *Signal Processing, IEEE Transactions on*, vol. 51, pp. 2329–2342, Sept 2003.

[7] J. Dubois, "Directional decomposition of images:implementation issues including gpu techniques," Master's thesis, Norwegian University, February 2008 .

[8] S. Singh and K. Bovis, "An evaluation of contrast enhancement techniques for mammographic breast masses," *Information Technology in Biomedicine, IEEE Transactions on*, vol. 9, pp. 109–119, March 2005.

[9] G. Lema^, "Texture segmentation : Co-occurrence matrix and Laws ' texture masks methods," tech. rep.

[10] R. Duda, P. Hart, and D. Stork, *Pattern Classification*. Wiley, 2001.

[11] "USF Digital Mammography Home Page." USF Digital Mammography Home Page. N.p., n.d. Web. 02 Jan. 2015. <http://marathon.csee.usf.edu/Mammography/Database.html>.

[12] "The Mini-MIAS Database of Mammograms." The Mini-MIAS Database of Mammograms. N.p., n.d. Web. 02 Feb. 2015. <http://peipa.essex.ac.uk/info/mias.html>.

[13] K. Bowyer, D. Kopans, W. Kegelmeyer, R. Moore, M. Sallam, K. Chang, and K. Woods, "The digital database for screening mammography," in *Third International Workshop on Digital Mammography*, vol. 58, 1996.

[14] Acr, *2013 ACR BI-RADS Atlas: Breast Imaging Reporting and Data System*. American College of Radiology, 2013.

[15] I. N. Bankman, T. Nizialek, I. Simon, O. B. Gatewood, I. N. Weinberg, and W. R. Brody, "Segmentation algorithms for detecting microcalcifications in mammograms.," *IEEE transactions on information technology in biomedicine : a publication of the IEEE Engineering in Medicine and Biology Society*, vol. 1, no. 2, pp. 141–149, 1997.

[16] P. Shanmugavadivu, "Detection of Microcalcification in Mammogram Images using Semi-Automated Texture based GrabCut Segmentation," pp. 198–203, 2012.

[17] A. K. Jumaat, S. S. Yasiran, W. Eny, Z. Wan, A. Rahman, and A. A. Malek, "Boundary Segmentation of Microcalcification using Parametric Active Contours," *Word Academy of Science ,Engineering and Technology*, pp. 909–913, 2012.

[18] M. a. Duarte, a. V. Alvarenga, C. M. Azevedo, a. F. C. Infantosi, and W. C. a. Pereira, "Automatic microcalcifications segmentation procedure based on Otsu's method and morphological filters," *Pan American Health Care Exchanges, PAHCE 2011 - Conference, Workshops, and Exhibits. Cooperation / Linkages: An Independent Forum for Patient Care and Technology Support*, pp. 102–106, 2011.

[19] J. K. Kim and H. W. Park, "Statistical textural features for detection of microcalcifications in digitized mammograms.," *IEEE transactions on medical imaging*, vol. 18, pp. 231–8, Mar. 1999.

[20] a. F. Laine, S. Schuler, J. Fan, and W. Huda, "Mammographic feature enhancement by multiscale analysis.," *IEEE transactions on medical imaging*, vol. 13, pp. 725–40, Jan. 1994.

[21] N. Arikidis, S. Skiadopoulos, F. Sakellaropoulos, G. Panayiotakis, and L. Costaridou, "Microcalcification features extracted from principal component analysis in the wavelet domain.," vol. 204, pp. 730–736, 2006.

[22] L. Shen, R. M. Rangayyan, and J. L. Desautels, "Application of shape analysis to mammographic calcifications.," *IEEE transactions on medical imaging*, vol. 13, pp. 263–74, Jan. 1994.

[23] H. Soltanian-Zadeh, F. Rafiee-Rad, and S. Pourabdollah-Nejad D, "Comparison of multiwavelet, wavelet, Haralick, and shape features for microcalcification

classification in mammograms," *Pattern Recognition*, vol. 37, pp. 1973–1986, Oct. 2004.

[24] C. Manoharan and N. S. R. Lakshmi, "Classification of micro calcifications in mammogram using combined feature set with svm," *International Journal of Computer Applications*, vol. 11, no. 10, pp. 30–34, 2010.

[25] I. I. Andreadis, G. M. Spyrou, and K. S. Nikita, "A comparative study of image features for classification of breast microcalcifications," *Measurement Science and Technology*, vol. 22, p. 114005, Nov. 2011.

[26] J. Jasmine, S. Baskaran, and A. Govardhan, "Nonsubsampled Contourlet Transform Based Classification of Microcalcification in Digital Mammograms," *Procedia Engineering*, vol. 38, pp. 622–631, 2012.

[27] J. Dheeba and S. Selvi, "Classification of malignant and benign microcalcification using svm classifier," in *Emerging Trends in Electrical and Computer Technology (ICETECT), 2011 International Conference on*, pp. 686–690, IEEE, 2011.

[28] S.-N. Yu, K.-Y. Li, and Y.-K. Huang, "Detection of microcalcifications in digital mammograms using wavelet filter and Markov random field model.," *Computerized medical imaging and graphics : the official journal of the Computerized Medical Imaging Society*, vol. 30, pp. 163–73, Apr. 2006.

[29] P. Zhang and K. Agyepong, "A Hybrid Microcalcification Detection Algorithm In Digital Mammograms," *American Journal of Science and Engineering*, vol. 1, no. 1, 2012.

[30] C. Li, K. M. Lam, L. Zhang, C. Hui, and S. Zhang, "Mammogram microcalcification cluster detection by locating key instances in a multi-instance learning framework," in *Signal Processing, Communication and Computing (ICSPCC), 2012 IEEE International Conference on*, pp. 175–179, IEEE, 2012.

[31] P. Kuş and I. Karagöz, "Detection of microcalcification clusters in digitized X-ray mammograms using unsharp masking and image statistics," *Turkish Journal of Electrical Engineering & Computer Sciences*, vol. 21, pp. 2048–2061, 2013.

[32] J. C. Fu, S. K. Lee, S. T. C. Wong, J. Y. Yeh, a. H. Wang, and H. K. Wu, "Image segmentation feature selection and pattern classification for mammographic microcalcifications.," *Computerized medical imaging and graphics : the official journal of the Computerized Medical Imaging Society*, vol. 29, pp. 419–29, Sept. 2005.

[33] D. Onder, S. Sarioglu, and B. Karacali, "Automated labelling of cancer textures in colorectal histopathology slides using quasi-supervised learning.," *Micron (Oxford, England : 1993)*, vol. 47, pp. 33–42, Apr. 2013.

[34] P. Hiremath, P. T. Akkasaligar, and S. Badiger, "Article: Performance comparison of wavelet transform and contourlet transform based methods for despeckling medical ultrasound images," *International Journal of Computer Applications*, vol. 26, pp. 34–41, July 2011. Full text available.

[35] T. Arici, S. Dikbas, and Y. Altunbasak, "A histogram modification framework and its application for image contrast enhancement," *Image Processing, IEEE Transactions on*, vol. 18, pp. 1921–1935, Sept 2009.

[36] A. E. Turan, "Analysis and comparison of the contrast enhancement techniques for infrared images," Master's thesis, Middle East Technical University,February 2012.

[37] S. M. Pizer, E. P. Amburn, J. D. Austin, R. Cromartie, A. Geselowitz, T. Greer, B. ter Haar Romeny, J. B. Zimmerman, and K. Zuiderveld, "Adaptive histogram equalization and its variations," *Computer Vision, Graphics, and Image Processing*, vol. 39, no. 3, pp. 355 – 368, 1987.

[38] Da, Celia Feritas, Cruz. "Automatic Analysis of Mammography Images:Enhancement and Segmentation Techniques." Thesis. University of Porto, 2011.

[39] R. Szeliski, *Computer Vision: Algorithms and Applications*. New York, NY, USA: Springer-Verlag New York, Inc., 1st ed., 2010.

[40] X. Bai and F. Zhou, "Analysis of new top-hat transformation and the application for infrared dim small target detection," *Pattern Recognition*, vol. 43, pp. 2145–2156, June 2010.

[41] A. Karali, O. Okman, and T. Aytac, "Adaptive enhancement of infrared images containing sea surface targets," in *Signal Processing and Communications Applications Conference (SIU), 2010 IEEE 18th*, pp. 605–608, April 2010.

[42] Quintanilla-Dominguez, Joel, et al. "Microcalcification detection applying artificial neural networks and mathematical morphology in digital mammograms." World Automation Congress (WAC), 2010. IEEE, 2010.

[43] M. Mustra, M. Grgic, and K. Delac, "Enhancement of microcalcifications in digital mammograms," in *Systems, Signals and Image Processing (IWSSIP), 2012 19th International Conference on*, pp. 248–251, April 2012.

[44] T. C. Wang and N. B. Karayiannis, "Detection of microcalcifications in digital mammograms using wavelets," *Medical Imaging, IEEE Transactions on*, vol. 17, no. 4, pp. 498–509, 1998.

[45] M. Do and M. Vetterli, "The contourlet transform: an efficient directional multiresolution image representation," *Image Processing, IEEE Transactions on*, vol. 14, pp. 2091–2106, Dec 2005.

[46] Do, Minh N., and Martin Vetterli. "Pyramidal directional filter banks and curvelets." Image Processing, 2001. Proceedings. 2001 International Conference on. Vol. 3. IEEE, 2001.

[47] Zhou, Jianping, Arthur L. Cunha, and Minh N. Do. "Nonsubsampled contourlet transform: construction and application in enhancement." Image Processing, 2005. ICIP 2005. IEEE International Conference on. Vol. 1. IEEE, 2005.

[48] J. M. M. Muñoz, H. d. J. O. Domínguez, O. O. V. Villegas, V. G. C. Sánchez, and L. O. Maynez, "The nonsubsampled contourlet transform for enhancement of microcalcifications in digital mammograms," in *MICAI 2009: Advances in Artificial Intelligence*, pp. 292–302, Springer, 2009.

[49] "Nonsubsampled contourlet toolbox, in http://www.mathworks.com/."

[50] S. Agaian, K. Panetta, and A. Grigoryan, "Transform-based image enhancement algorithms with performance measure," *Image Processing, IEEE Transactions on*, vol. 10, pp. 367–382, Mar 2001.

[51] R. C. Gonzalez and R. E. Woods, *Digital Image Processing (3rd Edition)*. Upper Saddle River, NJ, USA: Prentice-Hall, Inc., 2006.

[52] Z. Ye, H. Mohamadian, and H. Majlesein, "Adaptive enhancement of gray level and true color images with quantitative measurement using entropy and relative entropy," in *System Theory, 2008. SSST 2008. 40th Southeastern Symposium on*, pp. 127–131, March 2008.

[53] S.-D. Chen and A. Ramli, "Minimum mean brightness error bi-histogram equalization in contrast enhancement," *Consumer Electronics, IEEE Transactions on*, vol. 49, pp. 1310–1319, Nov 2003.

[54] Z. Wang, A. Bovik, H. Sheikh, and E. Simoncelli, "Image quality assessment: from error visibility to structural similarity," *Image Processing, IEEE Transactions on*, vol. 13, pp. 600–612, April 2004.

[55] G. N. Srinivasan and G. Shobha, "Statistical Texture Analysis," vol. 36, no. December, pp. 1264–1269, 2008.

[56] "Measures of Skewness and Kurtosis." National Institute of Standards and Technology's Web Site. , Web. 2 Jan. 2015.

[57] A. Dhawan, Y. Chitre, and C. Kaiser-Bonasso, "Analysis of mammographic microcalcifications using gray-level image structure features," *Medical Imaging, IEEE Transactions on*, vol. 15, pp. 246–259, Jun 1996.

[58] R. Haralick, K. Shanmugam, and I. Dinstein, "Textural features for image classification," *Systems, Man and Cybernetics, IEEE Transactions on*, vol. SMC-3, pp. 610–621, Nov 1973.

[59] Laws, Kenneth I. "Rapid texture identification." 24th Annual Technical Symposium. International Society for Optics and Photonics, 1980.

[60] S. Lahmiri and M. Boukadoum, “Hybrid Discrete Wavelet Transform and Gabor Filter Banks Processing for Features Extraction from Biomedical Images,” *Journal of Medical Engineering*, vol. 2013, pp. 1–13, 2013.

[61] Y.-h. Liu, M. Muftah, T. Das, L. Bai, K. Robson, and D. Auer, “Classification of mr tumor images based on gabor wavelet analysis,” *Journal of Medical and Biological Engineering*, vol. 32, no. 1, pp. 22–28, 2012.

[62] M. Yeşilkaya, “A mass detection algorithm for mammogram images,” Master’s thesis, Middle East Technical University, September 2014.

[63] I. Andreadis, K. Nikita, G. Giannakopoulou, D. Koulocheri, G. Zografos, A. Antaraki, P. Ligomenides, and G. Spyrou, “Computer aided insights on obscure cases of breast cancer diagnosis,” in *Imaging Systems and Techniques, 2008. IST 2008. IEEE International Workshop on*, pp. 237–242, Sept 2008.